Determination of phase diagrams via computer simulation: methodology and applications to water, electrolytes and proteins

2008 J. Phys.: Condens. Matter 20 153101

(http://iopscience.iop.org/0953-8984/20/15/153101)

IOP PUBLISHING JOURNAL OF PHYSICS: CONDENSED MATTER

J. Phys.: Condens. Matter **20** (2008) 153101 (38pp) doi:10.1088/0953-8984/20/15/153101

TOPICAL REVIEW

Determination of phase diagrams via computer simulation: methodology and applications to water, electrolytes and proteins

C Vega[1], **E Sanz, J L F Abascal and E G Noya**

Departamento de Química Física, Facultad de Ciencias Químicas, Universidad Complutense, 28040 Madrid, Spain

Received 31 October 2007, in final form 23 January 2008
Published 4 March 2008
Online at stacks.iop.org/JPhysCM/20/153101

Abstract

In this review we focus on the determination of phase diagrams by computer simulation, with particular attention to the fluid–solid and solid–solid equilibria. The methodology to compute the free energy of solid phases will be discussed. In particular, the Einstein crystal and Einstein molecule methodologies are described in a comprehensive way. It is shown that both methodologies yield the same free energies and that free energies of solid phases present noticeable finite size effects. In fact, this is the case for hard spheres in the solid phase. Finite size corrections can be introduced, although in an approximate way, to correct for the dependence of the free energy on the size of the system. The computation of free energies of solid phases can be extended to molecular fluids. The procedure to compute free energies of solid phases of water (ices) will be described in detail. The free energies of ices Ih, II, III, IV, V, VI, VII, VIII, IX, XI and XII will be presented for the SPC/E and TIP4P models of water. Initial coexistence points leading to the determination of the phase diagram of water for these two models will be provided. Other methods to estimate the melting point of a solid, such as the direct fluid–solid coexistence or simulations of the free surface of the solid, will be discussed. It will be shown that the melting points of ice Ih for several water models, obtained from free energy calculations, direct coexistence simulations and free surface simulations agree within their statistical uncertainty. Phase diagram calculations can indeed help to improve potential models of molecular fluids. For instance, for water, the potential model TIP4P/2005 can be regarded as an improved version of TIP4P. Here we will review some recent work on the phase diagram of the simplest ionic model, the restricted primitive model. Although originally devised to describe ionic liquids, the model is becoming quite popular to describe the behavior of charged colloids. Moreover, the possibility of obtaining fluid–solid equilibria for simple protein models will be discussed. In these primitive models, the protein is described by a spherical potential with certain anisotropic bonding sites (patchy sites).

(Some figures in this article are in colour only in the electronic version)

Contents

[1] Author to whom any correspondence should be addressed.

1. Introduction

One of the first findings of computer simulation was the discovery of a fluid–solid transition for a system of hard spheres [1, 2]. At that time the idea of a solid phase without the presence of attractive forces was not easily accepted. It took some time to accept it, and it was definitively proved after the work of Hoover and Ree [3], in which the location of the transition was determined beyond any doubt and, even more recently, when it was experimentally found for colloidal systems [4]. Certainly the study of phase transitions has always been a hot topic within the area of computer simulation. However, fluid–fluid phase transitions (liquid immiscibility, vapor–liquid) have received far more attention than fluid–solid equilibria [5]. The appearance of the Gibbs ensemble [6, 7] in the late 1980s provoked an explosion of papers dealing with vapor–liquid equilibria. The method has been applied to determine vapor–solid equilibria [8], but not for studying fluid–solid equilibria.

An interesting approach to the problem of the fluid–solid equilibrium was provided by Wilding and co-workers, who, in 1997, proposed the phase switch Monte Carlo method [9, 10]. This method was first applied to the study of the free energy difference between fcc and hcp close-packed structures of hard spheres [9, 11]. Three years later, Wilding and Bruce showed that the method could be applied to obtain fluid–solid equilibrium, and the fluid–solid equilibria of hard spheres was determined for different system sizes [12, 13]. Quite recently, Wilding and co-workers and Errington independently illustrated how the method could also be applied to Lennard-Jones (LJ) particles [14, 15]. In our view, the phase switch Monte Carlo is closely related to the 'Gibbs ensemble method' for fluid–solid equilibria, because, as in the Gibbs ensemble method, phase equilibria are computed without free energy calculations. In the phase switch methodology, trial moves are introduced within the Monte Carlo program, in which configurations obtained from simulations of the liquid are tested for the solid phase and vice versa (phase switch). For a certain thermodynamic condition (p and T) the relative probability of the system being in the liquid or solid phase is evaluated, and this allows one to estimate free energy differences. In the phase switch methodology the system jumps suddenly from the liquid to the solid in just one step. This method has been reviewed recently by Bruce and Wilding [10], and has proved to be quite successful for hard spheres and LJ systems. It is likely that the methodology can also be applied to molecular systems although results have not been presented so far. It is not obvious whether the methodology can be used to determine solid–solid equilibria in complex systems.

Another alternative route has emerged in recent years. Grochola [16] proposed to establish a thermodynamic path connecting the liquid with the solid phase. Of course, phase transitions should not occur along the path. If this is the case then it is possible to compute the free energy difference between the two phases. It is fair to say that Lovett [17] was the first to suggest such a path, although it was Grochola who developed it into a practical method. The system goes from the liquid to the solid not in one step (as in the

phase switching methodology) but in a gradual way. Several variations have been proposed so far and the method has been applied successfully to LJ, electrolytes, aluminum [16, 18, 19] and also molecular systems, such as benzene [20]. At this stage it is not obvious whether it could also be applied to study solid–solid equilibria.

Another approach to get free energies of solids is to use lattice dynamic methods [21]. By diagonalizing the quadratic form of the Hamiltonian the system may be transformed into a collection of independent harmonic oscillators for which the free energy is easily obtained. This procedure allows one to estimate free energies at low temperatures and fails for discontinuous potentials and when anharmonic contributions become important (close to the melting point). The method has been used by Tanaka *et al* [22, 23] to get the melting point of several water models.

In this review we focus on the determination of phase equilibria between two phases, where at least one of them is a solid phase. Therefore, the goal is not just fluid–solid equilibria but also solid–solid equilibria. Free energy calculations allow in fact the determination of the global phase diagram of a system (fluid–solid and solid–solid). In this methodology the free energy is determined for the two coexisting phases and the coexistence point is obtained by imposing the conditions of equal pressure, temperature and chemical potential. Usually the chemical potential of the liquid is obtained via thermodynamic integration. Different methods are used to determine the chemical potential of the solid. In their pioneering work, Hoover and Ree used the so called cell occupancy method [24, 3]. In this method each molecule is restricted to its Wigner–Seitz cell, and the solid is expanded up to low densities [3]. One of the problems of this method is the appearance of a phase transition in the integration path (from the solid to the gas). The method has also been applied to the LJ system [25, 26].

In 1984, Frenkel and Ladd proposed an alternative method, the Einstein crystal method [27]. In this method, that has become the standard method for determining free energies of solids, the change in free energy from the real crystal to an ideal Einstein crystal (in which there are no intermolecular interactions and where each molecule vibrates around its lattice point via a harmonic potential) is computed. Since the free energy of the reference ideal Einstein crystal is known analytically, it is possible to compute the free energy of the solid. If the equation of state (EOS) and free energies of both phases are known it is then possible to determine the conditions for the equilibrium between the two phases. Repeating the calculation at different thermodynamic conditions, it is then possible to determine the phase diagram for a certain potential model. This route has often been used in the past for a number of simple models including hard ellipsoids [28], the Gay Berne model [29], the hard Gaussian [30], hard dumbbells [31–34], hard spherocylinders [35–37], diatomic LJ models [38–40], quadrupolar hard dumbells [41], hard flexible chains [42, 43], linear rigid chains [44, 45], chiral systems [46], quantum hard spheres [47], primitive models of water [48], electrolytes [49, 50], benzene [51, 52], propane [53] and idealized models of colloidal particles [54–56, 50, 57, 58]. Some of the main findings of this research (up to 2000) have been reviewed by Monson and Kofke [5]. Forty years after the first determination of fluid–solid equilibria (for hard spheres [2]), the number of models for which it has been determined is still small. The situation is even worse if one considers studies of phase diagram calculations (including both fluid–solid and solid–solid calculations) for models describing real molecules. Then the number of considered systems is quite small, comprising nitrogen [59], alkanes [60], fullerenes [61], ionic salts [62, 63] and just in the last few years carbon [64], silicon [65], silica [66, 67] and hydrates [68].

As can be seen, water was missing, and this is surprising taking into account its importance as solvent and as the medium where life occurs [69]. Although water has been studied in thousands of simulation studies since the pioneering works of Barker and Watts [70] and Rahman and Stillinger [71], the study of its phase diagram by computer simulation has not received much attention. Interest has focused mainly on the possible existence of a liquid–liquid equilibrium [72–79]. The interest in the solid phases of water has been rather limited, although one observes a clear revival in the last decade [80–104]. The only attempt previous to our work to determine the phase diagram of water was performed by Baez and Clancy in 1995 [105, 106]. Estimates of the melting point of TIP4P were provided by Tanaka *et al* [22, 23], Vlot *et al* [107] and Haymet *et al* [108, 109]. Motivated by this, our group has undertaken the task of determining the phase diagram for a number of water models [110, 111]. The study of water revealed that phase diagram calculations are indeed feasible for molecular systems and that they constitute a severe test for potential models. It is clear that the phase diagram contains information about the intermolecular interactions [112–114].

The determination of a phase diagram is not, in principle, a difficult task. However, it is cumbersome, and somewhat tricky. In this work we will illustrate the details leading to the determination of the phase diagram of water. They can indeed be useful for those interested in water and its phase diagram. But the described methodology can be applied to other substances/models as well. We believe that by describing the calculations for water we are also describing how to do it for any other type of molecule. Problems where the determination of the fluid–solid equilibria by molecular simulation can indeed bring new light are, among others, the design of model potentials for water and other molecules [69, 115, 116, 20], the study of nucleation [117–121] (where the equilibrium conditions should be known in advance), the study of the fluid–solid equilibria in colloidal systems and also the very interesting problem of protein crystallization. Our goal here is to describe all the details to encourage the reader to implement phase diagram calculations (including at least one solid phase) either to gain new insight on appealing problems or to improve currently available potential models.

2. Basic definitions

For a pure substance, two phases (labeled as I and II) are in equilibrium when their pressures, temperatures and chemical potentials are equal. A phase diagram is just a plot (for instance in the p, T plane) of the coexistence points between the different phases of the system (gas, liquid or solid). In this paper we shall focus on determining the phase equilibria for rigid molecules. Two ensembles are particularly useful to study phase equilibria: the canonical ensemble (NVT) and the isobaric–isothermal ensemble (NpT). In the canonical ensemble the Helmholtz free energy A is given by the following expression [122, 26]:

$$A = -k_{\mathrm{B}}T \ln(Q(N, V, T)) = -k_{\mathrm{B}}T \ln\left(\frac{q^N}{N!} \times \int \exp[-\beta U(\mathbf{r}_1, \omega_1, \ldots, \mathbf{r}_N, \omega_N)]\, \mathrm{d}1 \ldots \mathrm{d}N\right) \quad (1)$$

where $\beta = 1/(k_{\mathrm{B}}T)$, U is the intermolecular energy of the whole system, q is the molecular partition function and di stands for $\mathrm{d}\mathbf{r}_i\, \mathrm{d}\omega_i$, where $\mathrm{d}\mathbf{r}_i = \mathrm{d}x_i\, \mathrm{d}y_i\, \mathrm{d}z_i$. The location of molecule i is given by the Cartesian coordinates x_i, y_i, z_i of the reference point and a normalized set of angles defining the orientation of the molecule (ω_i). By normalized we mean that $\int \mathrm{d}\omega_i = 1$. For instance a reasonable choice for ω_i is $\omega_i = \mathbf{\Omega}_i / V_\Omega$, where $\mathbf{\Omega}_i$ are the Euler angles [123] defining the orientation of the molecule and $V_\Omega = \int \mathrm{d}\mathbf{\Omega}_i = 8\pi^2$. For a non-linear molecule the partition function can be written as [122]

$$q = q_{t'} q_{\mathrm{r}} q_{\mathrm{v}} q_{\mathrm{e}}$$

$$q = \left[\left(\frac{2\pi m k_{\mathrm{B}}T}{h^2}\right)^{3/2}\right]\left[\frac{(2\pi k_{\mathrm{B}}T)^{3/2} V_\Omega (I_1 I_2 I_3)^{1/2}}{s' h^3}\right] \times \left[\prod_j \frac{\exp(-\beta h \nu_j/2)}{1 - \exp(\beta h \nu_j)}\right]\left[g\mathrm{e}^{-\beta D_e}\right]. \quad (2)$$

In the previous equation translational and rotational degrees of freedom are treated classically (except for the symmetry number s' and for the factor h), and vibrational and electronic degrees of freedom are described by the quantum partition function. $q_{t'} = q_{\mathrm{t}}/V$ is the translational partition function (divided by the volume), and q_{r}, q_{v} and q_{e} are the rotational, vibrational and electronic partition functions, respectively. The rotational, vibrational and electronic partition functions are dimensionless. We shall assume that the rotational, vibrational and electronic partition functions are identical in two coexistence phases. For this reason their precise value does not affect phase equilibria and we shall simply assume that their value is unity (we do not pretend to determine absolute free energies but rather phase equilibria). The first factor $q_{t'}$ has units of inverse volume or inverse cubic length. It is usually denoted as the inverse of the cubic de Broglie wavelength [122] (i.e. $1/\Lambda^3$). Therefore, in this work $q_{t'}$ is given by

$$q_{t'} = \frac{1}{\Lambda^3} = \frac{1}{(h^2/(2\pi m k_{\mathrm{B}}T))^{3/2}}. \quad (3)$$

In the NpT ensemble the Gibbs free energy G can be obtained as $G = -k_{\mathrm{B}}T \ln(Q(N, p, T))$, where $Q(N, p, T)$ is given by

$$Q(N, p, T) = \frac{q^N \beta p}{N!} \int \exp(-\beta p V)\, \mathrm{d}V \times \int \exp[-\beta U(\omega_1, \mathbf{s}_1, \ldots, \mathbf{s}_N, \omega_N; \mathbf{H})] V^N \times \mathrm{d}\mathbf{s}_1\, \mathrm{d}\omega_1\, \mathrm{d}\mathbf{s}_N\, \mathrm{d}\omega_N \quad (4)$$

where $\mathbf{s}_i$ stands for the coordinates of the reference point of molecule i in simulation box units. The conversion from simulation box units $\mathbf{s}_i$ to Cartesian coordinates $\mathbf{r}_i$ can be performed via the $\mathbf{H}$ matrix $\mathbf{r}_i = \mathbf{H}\mathbf{s}_i$ (the volume of the system is just the determinant of the $\mathbf{H}$ matrix). When performing Monte Carlo (MC) simulations of solid phases it is important that changes in the shape of the simulation box are allowed (i.e. changes in $\mathbf{H}$). This is usually denoted as anisotropic NpT simulations. They were first introduced within MD simulations by Parrinello and Rahman [124, 125], and extended to MC simulations by Yashonath and Rao [126]. In anisotropic NpT Monte Carlo the elements of the $\mathbf{H}$ matrix undergo random displacements, and this provokes a change both in the volume of the system and in the shape of the simulation box. Further details of the methodology can be found elsewhere [126, 127]. The use of the anisotropic version of the NpT ensemble is absolutely required to simulate solid phases. It guarantees that the shape of the simulation box (and therefore that of the unit cell of the solid) is the equilibrium one. It also guarantees that the solid is under hydrostatic pressure and free of stress (the pressure tensor will then be diagonal, with the three components being identical to the thermodynamic pressure).

3. Fluid–solid equilibrium from NpT simulations?

A possible way to determine the fluid–solid equilibria is by performing simulations at constant pressure and cooling the liquid until it freezes. However, it is very difficult to observe in computer simulations the formation of a crystal, and this is especially true for molecular fluids [82, 83, 128]. The nucleation of the solid is an activated process and it may be difficult to observe within the timescale of the simulation. In fact even in real experiments super-cooled liquids are often found [128]. The other possibility is to heat the solid until it melts. Experimentally, when a solid is heated at constant pressure it always melts at the melting temperature (with only a few exceptions to this rule). In fact, Bridgman [129] stated in 1912 'It is impossible to superheat a crystalline phase with respect to the liquid'. Unfortunately in computer simulations (in contrast to real experiments) one may superheat the solid before it melts. This is well known for hard spheres [130] (with pressure being the thermodynamic variable in question) and for Lennard-Jones particles [131]. The same is true for other systems, such as water. For water models it has been found that in NpT runs ices melt at a temperature about 90 K above the equilibrium melting point [132, 133]. Similar results have been obtained for nitromethane [134] or NaCl [19]. In this respect NpT simulations provide an upper limit of the melting point.

Introducing defects within the solid reduces considerably the amount of superheating [135, 136].

The difference between the results of NpT simulations and those found in experiments (summarized in the Bridgman's statement) is striking. The explanation to this puzzle is that in experiments melting occurs typically via heterogeneous nucleation starting at interfaces (real solids do always have interfaces), whereas in NpT simulations it must occur via homogeneous nucleation (due to the absence of the interface), requiring a rather long time [131, 137, 138]. Therefore new strategies must be proposed to obtain fluid–solid (or solid–solid) equilibria from simulations. The first possibility is to compute separately the free energy of the liquid and of the solid and determine the condition of chemical equilibrium. The second is to introduce a liquid nucleus in contact with the solid (i.e. a seed), since this will eliminate the superheating. These two possibilities will be discussed in this paper.

4. Thermodynamic integration: a general scheme to obtain free energies

In thermodynamic integration the free energy difference between two states/systems is obtained by integrating a certain thermodynamic function along the path connecting both states/systems [139]. The path connecting the two systems or states must be reversible. No first order phase transition should be found along the path. We shall distinguish (somewhat arbitrarily) two types of thermodynamic integration. In the first one the two states connected by the path possess the same Hamiltonian (i.e. interaction potential) and they just differ in the thermodynamic conditions (i.e. T, p ...). We shall denote this type of integration as thermodynamic integration. In the second one, the thermodynamic conditions are the same for the final and initial conditions (i.e. the same p and T or same density and T), but the Hamiltonian (i.e. the intermolecular potential) will be different for the initial and final systems. This type of integration will be denoted as Hamiltonian thermodynamic integration.

4.1. Thermodynamic integration

Assuming that the free energy at a certain thermodynamic state is known, the free energy at another thermodynamic state is determined by establishing a reversible path connecting both states. For a closed system, with a fixed number of particles, two thermodynamic variables are needed to determine the state of the system (for instance p and T or V and T). In practice, it is convenient to keep one of the thermodynamic variables constant while performing the integration.

4.1.1. Keeping T constant (integration along isotherms). Once the Helmholtz free energy at a certain reference density $\rho_1 = N/V_1$ is known, the free energy at another density $\rho_2 = N/V_2$ (T being the same in both cases) can be obtained as

$$\frac{A(\rho_2, T)}{Nk_BT} = \frac{A(\rho_1, T)}{Nk_BT} + \int_{\rho_1}^{\rho_2} \frac{p(\rho)}{k_BT\rho^2}\,d\rho. \tag{5}$$

The integrand can be obtained in a simple way from NpT runs, isotropic for the fluid and anisotropic for solid phases [124–126] (so that the equilibrium density is obtained for different pressures).

4.1.2. Keeping p constant (integration along isobars). In this integration the temperature of the system is modified while keeping constant the value of the pressure. In this way the Gibbs free energy G is obtained for any temperature along the isobar starting from an initial known value. The working expression is

$$\frac{G(T_2, p)}{Nk_BT_2} = \frac{G(T_1, p)}{Nk_BT_1} - \int_{T_1}^{T_2} \frac{H(T)}{Nk_BT^2}\,dT \tag{6}$$

where H is the enthalpy. In practice, several NpT simulations (anisotropic NpT for solids) are performed at different temperatures and the integrand is determined from the simulations.

4.1.3. Keeping the density constant (integration along isochores). In this case the density is constant and the temperature is modified. The working expression is

$$\frac{A(T_2, V)}{Nk_BT_2} = \frac{A(T_1, V)}{Nk_BT_1} - \int_{T_1}^{T_2} \frac{U(T)}{Nk_BT^2}\,dT. \tag{7}$$

For fluids the integrand is easily obtained from NVT simulations. Although equation (7) is quite useful for fluid phases, it is not so useful for solid phases. The reason is that for solids the density should be constant along the integration but the shape of the simulation box should not (except for cubic solids). In fact, the equilibrium shape of the unit cell (simulation box shape) changes when the temperature is modified at constant density.

4.2. Hamiltonian integration

In this type of integration the Hamiltonian of the system changes between the initial ($\lambda = 0$) and the final state ($\lambda = 1$). This can be accomplished by introducing a coupling parameter (λ) into the interaction energy of the system. The interaction energy becomes then a function of this coupling parameter ($U(\lambda)$). The free energy of the system will be a function not only of the thermodynamic variables but also of λ:

$$A(N, V, T, \lambda) = -k_BT \ln\left[\frac{q^N}{N!}\int \exp[-\beta U(\lambda)]d1 \ldots dN\right]. \tag{8}$$

By performing the derivative with respect to λ in equation (8) one obtains

$$\frac{\partial A(N, V, T, \lambda)}{\partial \lambda} = \left\langle \frac{\partial U(\lambda)}{\partial \lambda} \right\rangle_{N,V,T,\lambda}. \tag{9}$$

By integrating this differential equation one obtains

$$A(N, V, T, \lambda = 1) = A(N, V, T, \lambda = 0) + \int_{\lambda=0}^{\lambda=1} \left\langle \frac{\partial U(\lambda)}{\partial \lambda} \right\rangle_{N,V,T,\lambda} d\lambda. \tag{10}$$

This equation gives the difference in free energy between two states with the same temperature and density but with different

Hamiltonians (intermolecular potentials). A similar equation can be obtained within the isobaric–isothermal ensemble. In this case the difference in Gibbs free energy between two systems with the same temperature and pressure and different Hamiltonians is given by

$$G(N, p, T, \lambda = 1) = G(N, p, T, \lambda = 0) + \int_{\lambda=0}^{\lambda=1} \left\langle \frac{\partial U(\lambda)}{\partial \lambda} \right\rangle_{N,p,T,\lambda} \mathrm{d}\lambda. \quad (11)$$

5. The machinery in action. I. Obtaining the free energy of the liquid phase

Here we shall briefly describe three possibilities to obtain the free energy of the liquid phase (there are other possibilities). The three routes considered are: thermodynamic integration, Hamiltonian thermodynamic integration and the Widom test particle method.

5.1. Thermodynamic integration

When the density of a fluid tends to zero, the particles are far apart so that intermolecular interactions are irrelevant, and the system tends to an ideal gas. Therefore the free energy of the real fluid at a certain density ρ and temperature is given by

$$\frac{A(\rho, T)}{Nk_{\mathrm{B}}T} = \ln(\rho\Lambda^3) - 1 + \frac{\ln(2\pi N)}{2N} + \int_0^{\rho} \left[\frac{p}{k_{\mathrm{B}}T\rho'^2} - \frac{1}{\rho'} \right] \mathrm{d}\rho' \quad (12)$$

where the first three terms on the right-hand side represent the ideal gas contribution to the free energy (a logarithmic correction to the Stirling's approximation was included) and the last term is the residual part (a residual property is defined as the difference between that of the system and that of an ideal gas at the same temperature and density). To derive equation (12) the rotational, vibrational and electronic contributions to the partition function, equation (2), were set to one. The integrand in equation (12) tends at low densities to the second virial coefficient. The first term on the right-hand side of equation (12) is just a reduced density and of course is dimensionless (although its numerical value depends on the value of Λ). To avoid phase transitions the integration along the isotherm should be performed at supercritical temperatures. Once the density of the liquid is achieved, one can integrate along an isochore to low temperatures.

5.2. Free energy of liquids by Hamiltonian thermodynamic integration

Let us label as A the system for which the free energy is known in the fluid phase, and B the system for which the free energy is unknown. By introducing a coupling parameter one can change from the Hamiltonian of A to the Hamiltonian of B:

$$U(\lambda) = (1 - \lambda)U_{\mathrm{A}} + \lambda U_{\mathrm{B}} \quad (13)$$

where λ is a parameter ranging from zero (system A) to unity (system B).

According to equation (10), the free energy difference between A and B is given by

$$A_{\mathrm{B}}(N, V, T) = A_{\mathrm{A}}(N, V, T) + \int_0^1 \langle U_{\mathrm{B}} - U_{\mathrm{A}} \rangle_{N,V,T,\lambda} \, \mathrm{d}\lambda \quad (14)$$

where $\langle U_{\mathrm{B}} - U_{\mathrm{A}} \rangle_{N,V,T,\lambda}$ can be obtained by performing NVT simulations for a certain value of λ. The value of the integral is then obtained numerically.

5.3. Widom test particle method

The chemical potential can be obtained by the procedure proposed by Widom in 1963 [140], which yields

$$\mu^{\mathrm{res}} = -k_{\mathrm{B}}T \ln \langle \exp(-\beta U_{\mathrm{test}}) \rangle_{N,V,T} . \quad (15)$$

This formula states that the residual value of the chemical potential μ^{res} is just the average of the Boltzmann factor of the interaction energy (U_{test}) of a test particle. Although this formula is quite useful, its practical implementation may be problematic when the density of the system is high (so that inserting a particle becomes difficult). This is especially true for molecular systems and even more dramatic for systems with important orientational dependence in the pair potential. This is the case of water, for which it is quite difficult to obtain reliable chemical potentials by using the test particle method [141].

6. The machinery in action. II. Free energy of solids

The Einstein crystal method was proposed by Frenkel and Ladd in 1984 [27] and, since then, it has become the standard method to compute the free energy of solids [32, 41, 42, 142, 29, 143, 62, 44, 144, 63]. In this method an ideal Einstein crystal is used as the reference system to compute the free energy of a solid. An ideal Einstein crystal is a solid (the word ideal pointing out the absence of intermolecular interactions) in which the particles (atoms or molecules) are bounded to their lattice positions and orientations by a harmonic potential and in which there are no interparticle interactions. The free energy of an ideal Einstein crystal can be computed analytically for atomic solids and numerically for molecular solids.

For practical reasons, that will be clarified later, it is convenient to use an Einstein crystal where a certain reference point of the whole crystal is fixed. Two choices are possible.

- Fixing the position of the center of mass. This was the original choice of Frenkel and Ladd [27]. We shall denote the reference system as an ideal Einstein crystal with fixed center of mass and the technique will be referred to as the Einstein crystal approach.
- The second choice is to fix the position of just one of the molecules of the system, for instance molecule 1. In this second case we shall denote the reference system as an ideal Einstein molecule with fixed molecule 1. This methodology has been proposed quite recently [145] and will be denoted as the Einstein molecule approach.

Since the determination of free energy for solids is rather involved and not many examples can be found in the literature describing the details, we shall describe both methodologies in detail. Obviously both approaches are quite similar and indeed provide identical values of the free energy of the solid phase.

6.1. *The Einstein crystal method*

In the Einstein crystal approach the reference system is an ideal Einstein crystal with fixed center of mass. Let us describe briefly the notation that will be used in this section. The superscript CM indicates that the center of mass is fixed. The subscript specifies the interactions present in the system. In particular, the subscript Ein-id stands for ideal Einstein crystal (without intermolecular interactions), the subscript Ein-sol means that both the harmonic springs and the intermolecular interactions are present and the subscript sol indicates that only the intermolecular interactions are present (without the harmonic springs).

The whole path from the reference ideal Einstein crystal with fixed center of mass to the crystal of interest can be described as

$$A_{\rm sol} = A^{\rm CM}_{\rm Ein\text{-}id} + [(A^{\rm CM}_{\rm Ein\text{-}sol} - A^{\rm CM}_{\rm Ein\text{-}id}) + (A^{\rm CM}_{\rm sol} - A^{\rm CM}_{\rm Ein\text{-}sol})] + (A_{\rm sol} - A^{\rm CM}_{\rm sol}). \quad (16)$$

Here $A^{\rm CM}_{\rm Ein\text{-}id}$ is the free energy of the reference system (i.e. the ideal Einstein crystal with fixed center of mass). The first step is the computation of the free energy difference between the ideal Einstein crystal and the interacting Einstein crystal both with center of mass fixed ($A^{\rm CM}_{\rm Ein\text{-}sol} - A^{\rm CM}_{\rm Ein\text{-}id}$). In the second step ($A^{\rm CM}_{\rm sol} - A^{\rm CM}_{\rm Ein\text{-}sol}$), the springs of the interacting Einstein crystal are gradually turned off to obtain the crystal of interest (both systems with fixed center of mass). Finally, the solid with fixed center of mass is transformed into a solid with no fixed center of mass ($A_{\rm sol} - A^{\rm CM}_{\rm sol}$). Equation (16) can be written in a simpler way as

$$A_{\rm sol} = A^{\rm CM}_{\rm Ein\text{-}id} + [\Delta A_1 + \Delta A_2] + \Delta A_3. \quad (17)$$

By comparing equation (17) with equation (16) the meaning of the terms ΔA_1, ΔA_2 and ΔA_3 is clarified. Basically, obtaining $A_{\rm sol}$ is a four step process, since we need to obtain $A^{\rm CM}_{\rm Ein\text{-}id}$ (step 0), ΔA_1 (step 1), ΔA_2 (step 2) and ΔA_3 (step 3). This integration path is schematically shown in figure 1(a).

6.1.1. Step 0. Obtaining the free energy of the ideal Einstein crystal with fixed center of mass: $A^{\rm CM}_{\rm Ein\text{-}id}$. As mentioned above, an ideal Einstein crystal is a solid in which the molecules are bounded to their lattice positions and orientations by harmonic springs. We will focus on rigid non-linear molecular solids. Although the translational field is always applied in the same form, the expression of the orientational field depends on the geometry of the considered molecule. We shall describe here the procedure for a molecule with point group C_{2v}, for instance water. The appropriate expression of the orientational field for other geometries will be given later on.

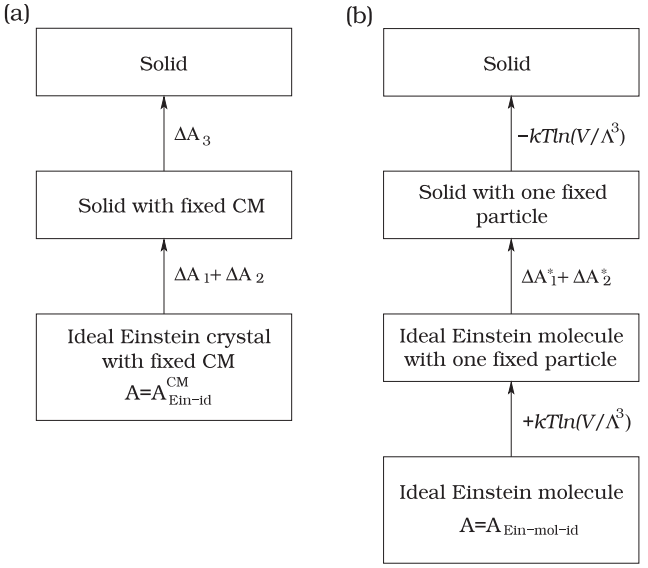

Figure 1. Thermodynamic path used in (a) the Einstein crystal method (Frenkel and Ladd [27] and Polson *et al* [142]) and (b) the Einstein molecule approach [145].

The energy of the ideal Einstein crystal is given by

$$U_{\rm Ein\text{-}id} = U_{\rm Ein\text{-}id,t} + U_{\rm Ein,or} \quad (18)$$

$$U_{\rm Ein\text{-}id,t} = \sum_{i=1}^{N} \left[\Lambda_E (\mathbf{r}_i - \mathbf{r}_{i0})^2\right] \quad (19)$$

$$U_{\rm Ein,or}(C_{2v}) = \sum_{i=1}^{N} u_{{\rm Ein,or},i} = \sum_{i=1}^{N} \left[\Lambda_{E,a} \sin^2(\psi_{a,i}) + \Lambda_{E,b} \left(\frac{\psi_{b,i}}{\pi}\right)^2\right]. \quad (20)$$

In the preceding equation $\mathbf{r}_i$ represents the instantaneous location of the reference point of molecule i, and $\mathbf{r}_{i0}$ is the equilibrium position of this reference point of molecule i in the crystal (i.e. $\mathbf{r}_i$ will fluctuate along the simulation run but $\mathbf{r}_{i0}$ will not). A possible choice for the reference point (which defines the location of the molecule) is the molecular center of mass. In fact, the rotational partition function of the molecule $q_{\rm r}$ is computed by using the principal moments of inertia (I_1, I_2 and I_3) with respect to a body frame with origin at the center of mass of the molecule. One could also use the center of mass of the molecule as the reference point to compute configurational properties. However, it should be pointed out that configurational properties do not depend on the choice of the reference point. For this reason, to compute configurational properties, there is a certain degree of freedom in choosing the reference point of the molecule. For free energy calculations it is very convenient (the reasons will be clarified later) if the reference point is chosen so that all elements of symmetry pass through it. This requirement is satisfied by the center of mass, but it may also be satisfied by other points. For instance, in the case of water, all elements of symmetry pass through the oxygen atom so that its choice as reference point is also quite convenient. Alternatively, one could argue that the

oxygen would become the center of mass of the molecule if the hydrogen atoms would have zero mass. Since the phase diagram of a water model does not depend on the masses of the atoms forming the molecule, setting the masses of the hydrogen atoms to zero would not affect the phase equilibria. In this work we shall use the oxygen as the reference point of the water molecule and this choice will not affect the phase equilibria (take the reason you prefer: either because configurational properties do not depend on the choice of the reference point, or because there is a certain combination of masses of the atoms of the molecule that render the center of mass on the oxygen atom). The term $U_{\text{Ein-id,t}}$ in equation (19) is a harmonic field that tends to keep the particles at their lattice positions ($\mathbf{r}_{i0}$), while $U_{\text{Ein,or}}$ forces the particles to have the right orientation. Λ_E, $\Lambda_{E,a}$ and $\Lambda_{E,b}$ are the coupling parameters of the springs (not to be confused with the thermal de Broglie wavelength Λ). Notice that $\Lambda_{E,a}$ and $\Lambda_{E,b}$ have energy units whereas Λ_E has units of energy over a squared length. The angles $\psi_{a,i}$ and $\psi_{b,i}$ are defined in terms of two unit vectors, $\vec{a}$ and $\vec{b}$, that specify the orientation of the molecule. $\psi_{a,i}$ is the angle formed by the unit vector $\vec{a}$ of molecule i in a given configuration ($\vec{a}_i$) and the unit vector ($\vec{a}_{i0}$) of this molecule in the reference lattice. The angle $\psi_{b,i}$ is defined analogously but with vector $\vec{b}$. The definition of vectors $\vec{a}$ and $\vec{b}$ for a rigid triatomic molecule is shown in figure 2. This form of the orientational field (equation (20)) was used by Vega and Monson [48] to get the free energy of a primitive model of water [146]. The vector $\vec{a}$ is calculated as the subtraction of the bond vectors $\vec{a} = (\vec{l}_2 - \vec{l}_1)/|\vec{l}_2 - \vec{l}_1|$, while $\vec{b} = (\vec{l}_2 + \vec{l}_1)/|\vec{l}_2 + \vec{l}_1|$. The angles $\psi_{a,i}$ and $\psi_{b,i}$ can be obtained simply from the scalar product of vectors $\vec{a}_i$ and $\vec{a}_{i0}$ (both of them being unitary vectors) and $\vec{b}_i$ and $\vec{b}_{i0}$ (both of them being unitary vectors) respectively as

$$\begin{aligned} \psi_{a,i} &= a\cos(\vec{a}_i \cdot \vec{a}_{i0}) \\ \psi_{b,i} &= a\cos(\vec{b}_i \cdot \vec{b}_{i0}) \end{aligned} \tag{21}$$

so that $\psi_{a,i}$ and $\psi_{b,i}$ will adopt values between zero and π. Notice that in the orientational field along the $\vec{b}$ direction (see equation (20)) the angle $\psi_{b,i}$ is divided by a factor of π. In this way, this term $(\psi_{b,i}/\pi)^2$ also takes values between zero (when $\vec{b}$ is parallel to $\vec{b}_{i0}$) and unity (when $\vec{b}_i$ and $\vec{b}_{i0}$ form an angle of π radians), and both orientational fields have the same strength (the $\sin^2(\psi_a)$ field changes from zero when $\psi_a = 0$ or $\psi_a = \pi$ to unity when $\psi_a = \pi/2$).

The partition function of the ideal Einstein crystal in the canonical ensemble (after integrating over the rotational momenta) is given by

$$\begin{aligned} Q_{\text{Ein-id}} = {} & \frac{1}{N!}\frac{1}{h^{3N}}(q_{\text{r}}q_{\text{v}}q_{\text{e}})^N \\ & \times \int \exp\left[-\beta \sum_{i=1}^{N} \frac{\mathbf{p}_i^2}{2m_i}\right] \mathrm{d}\mathbf{p}_1 \ldots \mathrm{d}\mathbf{p}_N \\ & \times \int \exp\left[-\beta U_{\text{Ein-id}}\right] \mathrm{d}1 \ldots \mathrm{d}N, \end{aligned} \tag{22}$$

where $\mathbf{p}_i = (p_{xi}, p_{yi}, p_{zi})$ represents the momentum of molecule i and $\mathrm{d}i = \mathrm{d}\mathbf{r}_i\,\mathrm{d}\boldsymbol{\omega}_i$, with $\mathbf{r}_i$ the position vector of the reference point of molecule i and $\boldsymbol{\omega}_i$ its normalized angular

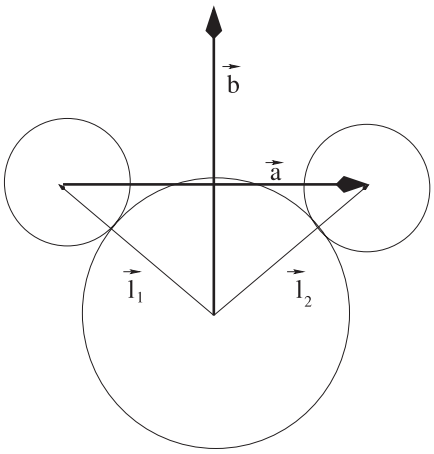

Figure 2. Definition of the vectors $\vec{a}$ and $\vec{b}$ in a triatomic rigid molecule with a twofold symmetry axis. The vectors $\vec{a}$ and $\vec{b}$ should be normalized to have modulus one.

coordinates. Consistent with our choice for the fluid phase, $q_{\text{r}}, q_{\text{v}}, q_{\text{e}}$ will be set arbitrarily to unity (they will be omitted in what follows). Now a subtle issue appears. In the Einstein crystal approach each molecule (via the reference point) is attached to a lattice point. One can compute the free energy for a solid where each molecule is attached to one and only one lattice point. However, one should not forget that there are $N!$ possible permutations. Therefore, the true free energy of the system is that obtained for a certain field where each molecule is attached to one lattice site multiplied by the number of possible permutations (i.e., $N!$). For this reason the partition function is

$$\begin{aligned} Q_{\text{Ein-id}} = {} & \frac{1}{h^{3N}} \int \exp\left[-\beta \sum_{i=1}^{N} \frac{\mathbf{p}_i^2}{2m_i}\right] \mathrm{d}\mathbf{p}_1 \ldots \mathrm{d}\mathbf{p}_N \\ & \times \int_{\text{one permutation}} \exp\left[-\beta U_{\text{Ein-id}}\right] \mathrm{d}1 \ldots \mathrm{d}N, \end{aligned} \tag{23}$$

where the integral over coordinates is now computed for just one permutation (and hence the label one permutation in the integral over coordinates). The expression one permutation in equation (23) reminds us that each molecule is attached (via $U_{\text{Ein-id}}$) to one and only one lattice point. Let us now impose mathematically the condition of fixed center of mass of the reference points. For water we are fixing the center of mass of the oxygen atoms (the O will act as the reference point of the molecule) rather than fixing the center of mass of the whole system (including the hydrogens). It is simpler and more convenient for molecular fluids to fix the center of mass of the reference points, rather than fixing the center of mass of all the atoms of the system. In the configurational space, the restriction implies that

$$\begin{aligned} \mathbf{R}_{\text{CM}}(\mathbf{r}_1, \mathbf{r}_2 \ldots \mathbf{r}_N) - \mathbf{R}_{\text{CM}}^0 &= 0 \\ \sum_{i=1}^{N} \mu_i(\mathbf{r}_i - \mathbf{r}_{i0}) &= 0 \end{aligned} \tag{24}$$

where, if the mass assigned to all reference points (one per molecule) is the same, $\mu_i = 1/N$, $i = 1, \ldots, N$. In the

previous equation $\mathbf{R}_{\mathrm{CM}}$ is the center of mass of the reference points of the system (there is one reference point per molecule) in an instantaneous configuration and $\mathbf{R}^0_{\mathrm{CM}}$ is the center of mass of the reference points of the system when the molecules stand on the lattice positions of the Einstein crystal field. $\mathbf{R}_{\mathrm{CM}}$ is a function of the coordinates of the particles of the system whereas $\mathbf{R}^0_{\mathrm{CM}}$ is one parameter. Due to thermal vibration, in general $\mathbf{R}_{\mathrm{CM}}$ will be different from $\mathbf{R}^0_{\mathrm{CM}}$. The constraint given by equation (24) means that from all possible configurations of the particles of the system only those satisfying $\mathbf{R}_{\mathrm{CM}} = \mathbf{R}^0_{\mathrm{CM}}$ will be allowed.

A comment is in order here. The value of the molecular mass does not affect the phase equilibria (i.e., the molecular mass is irrelevant to determine phase transitions). For instance, for an LJ system, the triple point does not depend on the particular value of the mass of the system (for Ar and Kr the melting point is different, not because of their mass but because of the different values of the parameters of the LJ potential). For this reason, for phase diagram calculations it is quite convenient to assign the same mass to all molecules of the system (regardless of whether this is true or not in real experiments). For instance, for NaCl, it is possible to assign the same mass to Na and Cl without affecting the phase equilibria of the model. In fact, we have used this strategy to determine its melting point [147]. Therefore, the simple choice $\mu_i = 1/N$, $i = 1, \ldots, N$ (i.e., assigning the same mass to all particles of the system or similarly to all reference points) can be used to determine phase equilibria without affecting the results. We strongly recommend this choice. Of course, dynamic properties depend on the mass, but not phase equilibria, which is the main focus of this paper.

As a consequence of the centre of mass constraint, the space of momenta is constrained to

$$\sum_{i=1}^{N} \mathbf{p}_i = 0. \tag{25}$$

The partition function of an ideal Einstein crystal with fixed center of mass $Q^{\mathrm{CM}}_{\mathrm{Ein\text{-}id}}$ can be written as

$$Q^{\mathrm{CM}}_{\mathrm{Ein\text{-}id}} = Q^{\mathrm{CM}}_{\mathrm{Ein,t}} Q_{\mathrm{Ein,or}}. \tag{26}$$

Then the free energy is simply obtained as

$$\begin{aligned} A^{\mathrm{CM}}_{\mathrm{Ein\text{-}id}} &= A^{\mathrm{CM}}_{\mathrm{Ein,t}} + A_{\mathrm{Ein,or}} \\ &= -k_{\mathrm{B}}T \ln Q^{\mathrm{CM}}_{\mathrm{Ein,t}} - k_{\mathrm{B}}T \ln Q_{\mathrm{Ein,or}}. \end{aligned} \tag{27}$$

The orientational term $Q_{\mathrm{Ein,or}}$ will be computed by evaluating numerically the following integral:

$$Q_{\mathrm{Ein,or}} = \left[\frac{1}{8\pi^2}\int \exp\left(-\beta u_{\mathrm{Ein,or}}\right) \sin\theta \mathrm{d}\phi\, \mathrm{d}\theta\, \mathrm{d}\gamma\right]^N \tag{28}$$

where ϕ, θ and γ stand for the Euler angles defining the orientation of the molecule and $u_{\mathrm{Ein,or}}$ is the orientational Einstein field for just one molecule (see equation (20)). We have chosen to use the definition of Gray and Gubbins of the Euler angles [123]. In the particular case of a molecule with C_{2v} symmetry (for instance water) it reads

$$\begin{aligned} Q_{\mathrm{Ein,or}} = \Bigg[\frac{1}{8\pi^2}\int \exp\Bigg(&-\beta\Lambda_{E,a}\sin^2(\psi_a) \\ &- \beta\Lambda_{E,b}\left(\frac{\psi_b}{\pi}\right)^2\Bigg) \sin\theta \mathrm{d}\phi\, \mathrm{d}\theta\, \mathrm{d}\gamma\Bigg]^N. \end{aligned} \tag{29}$$

Notice that ψ_a and ψ_b are functions of the Euler angles. The integral given by equation (28) or (29) can be evaluated numerically (for instance using a Monte Carlo numerical integration methodology). An approximate analytical expression [48] has been provided for C_{2v} which is valid in the limit of large coupling constants ($\Lambda_{E,a}, \Lambda_{E,b}$). The translational term $Q^{\mathrm{CM}}_{\mathrm{Ein,t}}$ is given by the following expression:

$$\begin{aligned} Q^{\mathrm{CM}}_{\mathrm{Ein,t}} = {} & \frac{1}{h^{3(N-1)}}\int \exp\left[-\beta\sum_{i=1}^{N}\frac{\mathbf{p}_i^2}{2m_i}\right]\delta\left(\sum_{i=1}^{N}\mathbf{p}_i\right)\mathrm{d}\mathbf{p}_1\ldots\mathrm{d}\mathbf{p}_N \\ & \times \int \exp\left[-\beta\Lambda_E\sum_{i=1}^{N}(\mathbf{r}_i - \mathbf{r}_{i0})^2\right] \\ & \times \delta\left(\sum_{i=1}^{N}\frac{1}{N}(\mathbf{r}_i - \mathbf{r}_{i0})\right)\mathrm{d}\mathbf{r}_1\ldots\mathrm{d}\mathbf{r}_N. \end{aligned} \tag{30}$$

Notice that to simplify the notation we have dropped the subindex 'one permutation' in the integration over coordinates, since it is sufficiently clear that this is indeed the case when each molecule is attached by harmonic springs to just one lattice point. This integral (equation (30)) can be solved analytically [142] (see appendix A for the details) and the result is

$$Q^{\mathrm{CM}}_{\mathrm{Ein,t}} = P^{\mathrm{CM}}\left(\frac{\pi}{\beta\Lambda_E}\right)^{3(N-1)/2}(N)^{3/2}. \tag{31}$$

The factor P^{CM} accounts for the contribution of the integral over the space of momenta. Its value is not given explicitly, because we will see later that it cancels out with another similar term.

6.1.2. Step 1. Free energy change between an interacting Einstein crystal and a non-interacting Einstein crystal (both with fixed center of mass): evaluating ΔA_1. The free energy difference between two arbitrary systems 1 and 2 is given by

$$A_2 - A_1 = -k_{\mathrm{B}}T \ln \frac{\int \exp(-\beta U_2)\mathrm{d}1\ldots\mathrm{d}N}{\int \exp(-\beta U_1)\mathrm{d}1\ldots\mathrm{d}N}. \tag{32}$$

Multiplying and dividing the numerator of the integrand by the factor $\exp(-\beta U_1)$, it is obtained that

$$A_2 - A_1 = -k_{\mathrm{B}}T \ln \langle \exp\left[-\beta(U_2 - U_1)\right]\rangle_1 \tag{33}$$

where $\langle \exp[-\beta(U_2 - U_1)]\rangle_1$ is an average over the configurations visited by system 1. Taking $U_2 = U_{\mathrm{Ein\text{-}id}} + U_{\mathrm{sol}}$ and $U_1 = U_{\mathrm{Ein\text{-}id}}$ (with U_{sol} the intermolecular potential of the solid), the previous expression can be written

$$A^{\mathrm{CM}}_{\mathrm{Ein\text{-}sol}} - A^{\mathrm{CM}}_{\mathrm{Ein\text{-}id}} = -k_{\mathrm{B}}T \ln \langle \exp\left[-\beta(U_{\mathrm{sol}})\right]\rangle_{\mathrm{Ein\text{-}id}}. \tag{34}$$

Therefore, the free energy change can be computed simply as the ensemble average of the factor $\exp[-\beta(U_{\mathrm{sol}})]$ along a simulation of the ideal Einstein crystal with fixed center

of mass. This average is evaluated in an NVT MC simulation [41, 48, 57, 50]. Note that this calculation must be done with the center of mass fixed. Often it is not possible to evaluate the free energy change as expressed in equation (34), because the exponential $\exp(-\beta U_{\rm sol})$ takes values larger than those that can be handled by a computer. This problem can be avoided if the expression is rewritten in such a way that the exponent does not take large values, for example, adding and subtracting from the energy of the solid $U_{\rm sol}$ the constant lattice energy $U_{\rm lattice}$:

$$\Delta A_1 = A^{\rm CM}_{\text{Ein-sol}} - A^{\rm CM}_{\text{Ein-id}} = U_{\rm lattice} - k_{\rm B}T \times \ln \langle \exp\left[-\beta(U_{\rm sol} - U_{\rm lattice})\right]\rangle_{\text{Ein-id}}\,. \tag{35}$$

One of the parameters that needs to be fixed when implementing the Einstein crystal method is the value of the spring constant (we will choose $\Lambda_E = \Lambda_{E,a} = \Lambda_{E,b}$). A convenient choice for Λ_E is one that guarantees a small value (of about 0.02 $Nk_{\rm B}T$) for the second term on the right-hand side of equation (35). When this is the case, ΔA_1 is quite close to the lattice energy $U_{\rm lattice}$, defined as the intermolecular energy of the system when the molecules stand on the positions and orientations of the external Einstein field.

6.1.3. Step 2. Free energy change between the solid and the interacting Einstein crystal (both with fixed center of mass): evaluating ΔA_2. The free energy change between the solid and the interacting Einstein crystal (both with fixed center of mass) will be computed by Hamiltonian thermodynamic integration. The harmonic springs are turned off gradually, and the total potential energy can be given by

$$U(\lambda) = \lambda U_{\rm sol} + (1-\lambda)(U_{\text{Ein-id}} + U_{\rm sol}). \tag{36}$$

The parameter λ is defined between zero and unity, so that when $\lambda = 0$ one has the Einstein solid and when $\lambda = 1$ one obtains the solid of interest. The free energy change along this path will be given by

$$\begin{aligned}\Delta A_2 &= A(N,V,T,\lambda=1) - A(N,V,T,\lambda=0)\\ &= \int_{\lambda=0}^{\lambda=1} \left\langle \frac{\partial U(\lambda)}{\partial \lambda}\right\rangle_{N,V,T,\lambda} {\rm d}\lambda\\ &= -\int_{\lambda=0}^{\lambda=1} \langle U_{\text{Ein-id}}\rangle_{N,V,T,\lambda}\,{\rm d}\lambda.\end{aligned} \tag{37}$$

It is a good idea to use the same values for Λ_E, $\Lambda_{E,a}$, $\Lambda_{E,b}$. Then the spring constants along the integration are given by $\lambda\Lambda_E$, $\lambda\Lambda_{E,a}$ and $\lambda\Lambda_{E,b}$ (all of them being equal). It is convenient to perform a change in the independent variable from λ to $\lambda\Lambda_E$ so that the integral of equation (37) can be rewritten as

$$\Delta A_2 = A^{\rm CM}_{\rm sol} - A^{\rm CM}_{\text{Ein-sol}} = -\int_0^{\Lambda_E} \frac{\langle U_{\text{Ein-id}}\rangle_{N,V,T,\lambda}}{\Lambda_E}\,{\rm d}(\lambda\Lambda_E). \tag{38}$$

Since the integrand changes by several orders of magnitude it is convenient to perform a new change of variable [27, 139] $\lambda\Lambda_E$ to $\ln(\lambda\Lambda_E + c)$, where c is a constant:

$$\begin{aligned}\Delta A_2 &= A^{\rm CM}_{\rm sol} - A^{\rm CM}_{\text{Ein-sol}} = \Delta A_2\\ &= -\int_{\ln(c)}^{\ln(\Lambda_E+c)} \frac{\langle U_{\text{Ein-id}}\rangle_{N,V,T,\lambda}\,(\lambda\Lambda_E + c)}{\Lambda_E}\\ &\quad\times {\rm d}(\ln(\lambda\Lambda_E + c)).\end{aligned} \tag{39}$$

The integrand is now a smooth function of the variable $\ln(\lambda\Lambda_E + c)$. A value [27] of $c = \exp(3.5)$ provides a good estimate of the integral (although the optimum value of c may depend on the particular considered problem). The integral of this smoother function can be accurately computed using, for example, the Gauss–Legendre quadrature formula [148]. It is usual to use between ten and 20 points to evaluate the integral. Fixing the position of the center of mass avoids the quasi-divergence of the integrand of equation (38) when the coupling parameter λ tends to zero. Without this constraint, the integrand would increase sharply in this limit (although it would remain finite), making the evaluation of the integral (equation (38)) numerically involved, and making the accurate evaluation of the integrand at low values of the coupling parameter somewhat difficult. For this reason, it is numerically convenient to avoid the translation of the crystal as a whole for low values of λ and this is achieved either by fixing the center of mass, as in the Einstein crystal technique, or by fixing the position of one molecule of the system, as in the Einstein molecule approach to be described below. In appendix B, the procedure to implement the somewhat unpleasant condition of fixed center of mass within a Monte Carlo simulation is described. This is important since the calculations leading to ΔA_1 and ΔA_2 should be done with the center of mass fixed.

6.1.4. Step 3. Free energy change between an unconstrained solid and the solid with fixed center of mass: evaluating ΔA_3. As we have seen before—see equation (32)—the free energy change between two systems can be obtained as

$$\Delta A_3 = A_{\rm sol} - A^{\rm CM}_{\rm sol} = -k_{\rm B}T \ln \frac{Q_{\rm sol}}{Q^{\rm CM}_{\rm sol}} = k_{\rm B}T \ln \frac{Q^{\rm CM}_{\rm sol}}{Q_{\rm sol}} \tag{40}$$

where $Q^{\rm CM}_{\rm sol}$ is given (after integration over rotational momenta) by

$$\begin{aligned}Q^{\rm CM}_{\rm sol} &= \frac{(q_{\rm r}q_{\rm v}q_{\rm e})^N}{N!h^{3(N-1)}}\\ &\quad\times \int \exp\left[-\beta\sum_{i=1}^{N}\frac{\mathbf{p}_i^2}{2m_i}\right]\delta\left(\sum_{i=1}^{N}\mathbf{p}_i\right){\rm d}\mathbf{p}_1\ldots{\rm d}\mathbf{p}_N\\ &\quad\times \int \exp\left[-\beta U_{\rm sol}(\mathbf{r}_1,\omega_1\ldots\mathbf{r}_N,\omega_N)\right]\\ &\quad\times \delta\left(\sum_{i=1}^{N}\mu_i(\mathbf{r}_i - \mathbf{r}_{i0})\right){\rm d}\mathbf{r}_1\,{\rm d}\omega_1\ldots{\rm d}\mathbf{r}_N\,{\rm d}\omega_N\end{aligned} \tag{41}$$

and $Q_{\rm sol}$ is given by an expression similar to that of $Q^{\rm CM}_{\rm sol}$ but without the delta functions (and with h^{3N} in the denominator instead of $h^{3(N-1)}$). Notice that the factor $N!$ cancels out when computing the free energy change (it appears both in $Q_{\rm sol}$ and $Q^{\rm CM}_{\rm sol}$). The integration over the space of momenta of the unconstrained solid is simply the integral of a product of Gaussian functions, whose solution is (when all molecules have the same mass)

$$P = \left(\frac{2\pi m k_{\rm B}T}{h^2}\right)^{(3N)/2} = \left(\frac{1}{\Lambda}\right)^{3N}. \tag{42}$$

The integral over the space of momenta of the solid with fixed center of mass is equal to the integral of momenta of

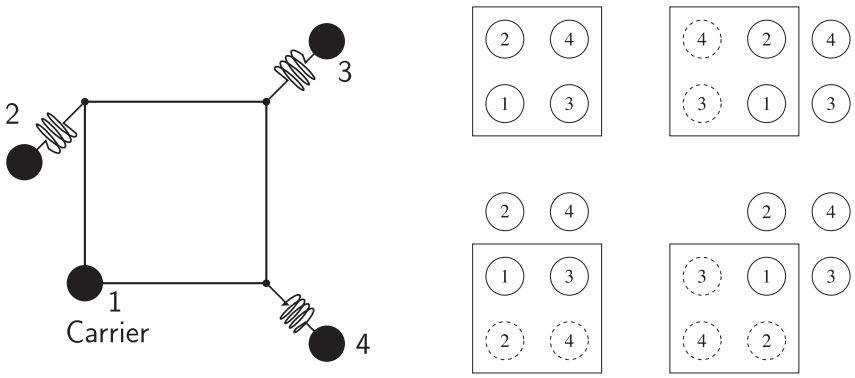

Figure 3. Left: schematic representation of the Einstein molecule, in which particle 1 is fixed and acts as the carrier of the lattice. The movement of all the remaining particles is given relative to the position of particle 1. Right: permutations generated through periodical boundary conditions by the motion of particle 1.

the ideal Einstein crystal with fixed center of mass, which was denoted as P^{CM}. Substituting the partition functions in equation (40), we arrive at the following expression:

$$\begin{aligned}\Delta A_3 = A_{\mathrm{sol}} - A_{\mathrm{sol}}^{\mathrm{CM}} = k_{\mathrm{B}}T \ln\left(\frac{P^{\mathrm{CM}}}{P}\right)\\ + k_{\mathrm{B}}T \ln\Bigg\{\int \exp\left[-\beta U_{\mathrm{sol}}(\mathbf{r}_1, \omega_1 \ldots \mathbf{r}_N, \omega_N)\right]\\ \times \delta\left(\sum_{i=1}^{N}(1/N)(\mathbf{r}_i - \mathbf{r}_{i0})\right)\mathrm{d}\mathbf{r}_1\omega_1 \ldots \mathrm{d}\mathbf{r}_N\omega_N\Bigg\}\\ \times \Bigg\{\int \exp\left[-\beta U_{\mathrm{sol}}(\mathbf{r}_1, \omega_1, \ldots \mathbf{r}_N, \omega_N)\right]\\ \times \mathrm{d}\mathbf{r}_1\,\mathrm{d}\omega_1 \ldots \mathrm{d}\mathbf{r}_N\,\mathrm{d}\omega_N\Bigg\}^{-1}. \qquad (43)\end{aligned}$$

The energy of a system is not modified if the system is translated (while keeping the relative orientation of the molecules). The mathematical consequence of this is that $U_{\mathrm{sol}}(\mathbf{r}_1, \omega_1, \ldots, \mathbf{r}_N, \omega_N)$ can be rewritten as $U_{\mathrm{sol}}(\omega_1, \mathbf{r}'_2, \omega_2, \ldots, \mathbf{r}'_N\omega_N)$, where $\mathbf{r}'_i = \mathbf{r}_i - \mathbf{r}_1$. Let us locate the center of mass of the lattice point at the origin of the coordinate system so that $\sum(1/N)\mathbf{r}_{i0} = \mathbf{R}^0_{\mathrm{CM}} = 0$. Let us perform a change of variables from $\mathbf{r}_1, \mathbf{r}_2, \ldots, \mathbf{r}_N$ to $\mathbf{r}'_2, \ldots, \mathbf{R}_{\mathrm{CM}}$ where $\mathbf{R}_{\mathrm{CM}}$ is the position of the center of mass of the reference points. The Jacobian of this transformation is N. With these changes one obtains for the second term on the right-hand side of equation (43)

$$\begin{aligned}k_{\mathrm{B}}T \ln\Bigg\{\int \exp(-\beta U_{\mathrm{sol}}(\omega_1, \mathbf{r}'_2, \omega_2, \mathbf{r}'_3, \ldots, \mathbf{r}'_N, \omega_N))\\ \times \delta(\mathbf{R}_{\mathrm{CM}})N\,\mathrm{d}\omega_1\,\mathrm{d}\mathbf{r}'_2\,\mathrm{d}\omega_2\,\mathrm{d}\mathbf{r}'_3 \ldots \mathrm{d}\mathbf{r}'_N\,\mathrm{d}\omega_N\,\mathrm{d}\mathbf{R}_{\mathrm{CM}}\Bigg\}\\ \times \Bigg\{\int \exp(-\beta U_{\mathrm{sol}}(\omega_1, \mathbf{r}'_2, \omega_2, \mathbf{r}'_3, \ldots, \mathbf{r}'_N, \omega_N))\\ \times N\,\mathrm{d}\omega_1\,\mathrm{d}\mathbf{r}'_2\,\mathrm{d}\omega_2\,\mathrm{d}\mathbf{r}'_3 \ldots \mathrm{d}\mathbf{r}'_N\,\mathrm{d}\omega_N\,\mathrm{d}\mathbf{R}_{\mathrm{CM}}\Bigg\}^{-1}. \qquad (44)\end{aligned}$$

After integrating with respect to $\omega_1\mathbf{r}'_2\omega_2 \ldots \mathbf{r}'_N\omega_N$ one obtains

$$k_{\mathrm{B}}T \ln\frac{\int \delta(\mathbf{R}_{\mathrm{CM}})\,\mathrm{d}\mathbf{R}_{\mathrm{CM}}}{\int \mathrm{d}\mathbf{R}_{\mathrm{CM}}} = k_{\mathrm{B}}T \ln\frac{1}{\int \mathrm{d}\mathbf{R}_{\mathrm{CM}}}. \qquad (45)$$

Since the Dirac Delta is normalised to one. Now there is a quite subtle issue. The integral in the denominator of equation (45) is just the volume available to the center of mass. What is the value of this volume? An interesting comment made explicitly by Wilding [11, 13, 15, 10] is that the translation of a crystal as a whole under periodical boundary conditions generates N permutations between the particles. This is illustrated in figure 3 for a two dimensional model. When counting the number of possible configurations we used the value $N!$ when going from equations (22) to (23). Therefore, we counted all possible permutations, so the integral in the denominator of equation (45) is the volume available to the center of mass within one given permutation. This value is simply V/N. Using V instead of (V/N) in the denominator of equation (45) is incorrect if the value $N!$ was used to count the number of permutations. In this case certain permutations would be counted twice, the first time in the factor $N!$ and the second via the translation of the whole crystal (in the volume V). Therefore,

$$\Delta A_3 = A_{\mathrm{sol}} - A_{\mathrm{sol}}^{\mathrm{CM}} = k_{\mathrm{B}}T\left[\ln(P^{\mathrm{CM}}/P) - \ln(V/N)\right]. \qquad (46)$$

As can be seen the expression for ΔA_3 is general and does not depend on the particular form of the intermolecular potential U_{sol}. Notice that correct results would also be obtained if one used V in the denominator of equation (45) (so that the center of mass moves in the whole simulation box) but used $(N-1)!$ when counting the number of permutations (i.e. count all permutations between particles except those obtained via the translation of the whole crystal through the periodical boundary conditions). In equation (23) one then would obtain a term $(N-1)!/N!$, which provides an $1/N$ factor that could be joined with the $\ln(1/V)$ term of equation (45) to give a contribution $-kT\ln(V/N)$ which is identical to that given in equation (46). Thus ΔA_3 will have a term of the form $-kT\ln(V/N)$ if $N!$ permutations were included in $A^{\mathrm{CM}}_{\mathrm{Eins\text{-}id}}$ (as done by Polson *et al* [142], and described here) or will have a term of the form $-kT\ln(V)$ if $(N-1)!$ permutations were included in $A^{\mathrm{CM}}_{\mathrm{Eins\text{-}id}}$. Both choices are possible and provide the same total free energy. However, when presenting results it is important to state clearly the choice, not to confuse the reader. A sentence like the following could be useful.

- All permutations were included in the reference ideal Einstein crystal. This would indicate that a term $N!$ was used, and therefore ΔA_3 contains a term of the form $-kT\ln(V/N)$.
- All permutations except those obtained by translation of the crystal under periodical boundary conditions were included in the reference ideal Einstein crystal. This would indicate that a term $(N-1)!$ was used, and therefore ΔA_3 contains a term of the form $-kT\ln(V)$.

However, when presenting results we recommend joining $A^{\mathrm{CM}}_{\mathrm{Eins\text{-}id}}$ and ΔA_3 into a unique term since the sum of both terms is unique and does not depend on the choice of the number of permutations included in $A^{\mathrm{CM}}_{\mathrm{Eins\text{-}id}}$. It is fair to say that Wilding [12] was the first to point out explicitly that N permutations were generated by translation under periodical boundary conditions. This has been taken into account implicitly by Polson *et al* [142], since they used a term of the form $-kT\ln(V/N)$ for ΔA_3.

6.1.5. Final expression. The final expression of the free energy of the solid is

$$A_{\mathrm{sol}} = (A^{\mathrm{CM}}_{\mathrm{Ein\text{-}id}} + \Delta A_3) + \Delta A_1 + \Delta A_2 = A_0 + \Delta A_1 + \Delta A_2 \tag{47}$$

where we have defined A_0 as $A_0 = A^{\mathrm{CM}}_{\mathrm{Ein\text{-}id}} + \Delta A_3$. Taking into account all the contributions to the free energy, the free energy of a molecular solid can be computed using the following expression:

$$\frac{A_{\mathrm{sol}}}{Nk_{\mathrm{B}}T} = -\frac{1}{N}\ln\left[\left(\frac{1}{\Lambda}\right)^{3N}\left(\frac{\pi}{\beta\Lambda_E}\right)^{3(N-1)/2}(N)^{3/2}\frac{V}{N}\right] + \frac{A_{\mathrm{Ein,or}}}{Nk_{\mathrm{B}}T} + \left[\frac{U_{\mathrm{lattice}}}{Nk_{\mathrm{B}}T} - \frac{1}{N}\ln\langle\exp[-\beta(U_{\mathrm{sol}} - U_{\mathrm{lattice}})]\rangle_{\mathrm{Ein\text{-}id}}\right] - \int_{\lambda=0}^{\lambda=1}\left\langle\frac{U_{\mathrm{Ein\text{-}id}}}{Nk_{\mathrm{B}}T}\right\rangle_{N,V,T,\lambda}\mathrm{d}\lambda. \tag{48}$$

Notice that P^{CM} does not appear in the final expression (so that its value is irrelevant for free energy calculations). The first two terms in equation (48) correspond to A_0. The last two terms of equation (48) are ΔA_1 and ΔA_2 respectively. The argument of the logarithm in the first term on the right-hand side (embraced by brackets) is adimensional. In fact it has three factors, the first factor having dimensions of L^{-3N}, the second factor having dimensions of $L^{3(N-1)}$ and the last factor having dimensions of L^3. In any computer program a unit of length l is selected. It is quite convenient to set the thermal de Broglie wavelength to $\Lambda = l$, and this choice should be used for the solid (in equation (48)) and for the liquid (in equation (12)). Then the volume of the simulation box V (in equation (48)) should be given in l^3 units and the value of the translational spring Λ_E should be given in energy/(l^2) units. Notice that assigning an arbitrary value to Λ affects the absolute value of the free energies but it does not affect the coexistence properties.

An important final comment is in order. Free energy calculations are usually performed in the NVT ensemble (with temperature and density fixed). It is quite important that the shape of the simulation box used in free energy calculations corresponds to that adopted by the system at equilibrium. It is not valid to impose (for instance from experiment) the shape of the simulation box since this will give free energies higher than the correct ones (the equilibrium shape minimizes the free energy of the system for a certain density). Rather, one should first perform NpT anisotropic Monte Carlo simulations [124–126], and determine the shape at equilibrium of the simulation box at a certain p, T and Hamiltonian (the density will be obtained as an average of the run) and then to perform free energy calculations in the NVT ensemble using the density and equilibrium shape of the simulation box obtained from the NpT runs. This remark is important for solids belonging to any crystalline class but cubic. A convenient choice for the vectors $\mathbf{r}_{i0}$, $\vec{a}_{i,0}$ and $\vec{b}_{i,0}$ that define the Einstein crystal field (equations (18)–(20)) is to use the equilibrium positions (to determine $\mathbf{r}_{i0}$) and orientations (to determine $\vec{a}_{i,0}$ and $\vec{b}_{i,0}$) of the molecules of the system. Other choices are also possible (for instance fields driving the molecules into configurations slightly distorted from the equilibrium one). However, the choice of the equilibrium configuration has the advantage that a lower value of the external field Λ_E is needed to obtain reliable results. Obviously, the free energy of the solid should not depend on the particular choice of the vectors $\mathbf{r}_{i0}$, $\vec{a}_{i,0}$ and $\vec{b}_{i,0}$ that define the Einstein crystal field.

6.2. The Einstein molecule approach

Quite recently Vega and Noya have proposed [145] a slightly different version of the Frenkel–Ladd method. The method has been denoted as the Einstein molecule approach. The idea behind the Einstein molecule approach is to fix the position of one molecule of the system (say molecule 1) instead of fixing the center of mass. More precisely, by fixing the position of molecule 1, we mean that we fix the position of its reference point. The molecule can still rotate as long as its reference point remains fixed. Therefore, we fix the position of molecule 1 (as given by the reference point) but we do not fix the orientation of molecule 1. Of course for a simple fluid (HS, LJ) there are no orientational degrees of freedom, so that in the Einstein molecule approach atom 1 is fixed. Fixing the position of one molecule avoids the quasi-divergence of the integrand of equation (38) when the coupling parameter λ tends to zero. The computational implementation of the method as well as the derivation of the main equations is fairly simple.

6.2.1. The ideal Einstein molecule: definition and free energy. The partition function in the canonical ensemble (after integrating over the space of momenta) is given by the following expression:

$$Q = \frac{(q_{\mathrm{r}}q_{\mathrm{v}}q_{\mathrm{e}})^N}{N!\Lambda^{3N}}\int\exp[-\beta U(\mathbf{r}_1,\omega_1,\ldots,\mathbf{r}_N,\omega_N)] \times \mathrm{d}\mathbf{r}_1\,\mathrm{d}\omega_1\ldots\mathrm{d}\mathbf{r}_N\,\mathrm{d}\omega_N. \tag{49}$$

We shall assign $q_{\mathrm{r}}, q_{\mathrm{v}}, q_{\mathrm{e}}$ the arbitrary value of one. This expression can be written in a more convenient way by

exploiting the fact that the potential energy of the system U depends only on the relative positions of the particles, and not on their absolute positions; i.e., it is invariant under translations of the whole system (while keeping the orientations of all the molecules in the translation). We will perform a change of variables from $(\mathbf{r}_1, \mathbf{r}_2, \ldots, \mathbf{r}_N)$ to $(\mathbf{r}_1, \mathbf{r}_2{}' = \mathbf{r}_2 - \mathbf{r}_1, \ldots, \mathbf{r}_N{}' = \mathbf{r}_N - \mathbf{r}_1)$. Under periodic boundary conditions and the minimum image convention, this change of variables leaves the limits of the integrals unchanged, because the maximum distance between two particles in any of the three directions of the space is always less than the length of the simulation box. Therefore,

$$\begin{aligned} Q &= \frac{1}{N!\Lambda^{3N}} \int \mathrm{d}\mathbf{r}_1 \int \exp\left[-\beta U(\omega_1, \mathbf{r}'_2, \omega_2, \ldots, \mathbf{r}'_N, \omega_N)\right] \\ &\quad \times \mathrm{d}\omega_1\, \mathrm{d}\mathbf{r}'_2\, \mathrm{d}\omega_2 \ldots \mathrm{d}\mathbf{r}'_N\, \mathrm{d}\omega_N \\ &= \frac{1}{N!\Lambda^{3N}} \int \mathrm{d}\mathbf{r}_1\, \kappa. \end{aligned} \tag{50}$$

The value of the integral κ is independent of the value of $\mathbf{r}_1$ and, therefore, we can integrate over $\mathbf{r}_1$:

$$Q = \frac{1}{N!\Lambda^{3N}} V\, \kappa. \tag{51}$$

The whole partition function (κ) can be computed by multiplying the integral corresponding to one permutation (κ') by the number of possible permutations, which, for a given fixed position of particle 1, is equal to $(N-1)!$. Therefore, the partition function can be written as

$$Q = \frac{1}{N!\Lambda^{3N}} V(N-1)! \quad \kappa' = \frac{1}{N\Lambda^{3N}} V\, \kappa'. \tag{52}$$

Let us now define the ideal Einstein molecule. The ideal Einstein molecule is an ideal system (without intermolecular interactions) where the reference point of one of the molecules (e.g. molecule 1) does not vibrate and acts as reference, while the rest of the molecules of the system (i.e. molecules $2, 3, \ldots, N$) vibrate around their equilibrium configurations (see figure 3 for a schematic representation). The reference point of molecule 1 is called the carrier, because this point transports the lattice. Notice that, in the Einstein molecule, molecule 1 can undergo orientational vibrations, as long as its reference point remains in a fixed position (obviously for a simple fluid there is no such rotation, and the carrier is just the position of atom 1). The lattice (crystal) is uniquely determined by the position of the carrier. The Einstein molecule can move as a whole, and this motion is represented by the motion of the carrier, which is able to move and occupy any position in the simulation box. The expression of the energy of the ideal Einstein molecule is

$$\begin{aligned} U_{\text{Ein-mol-id}} &= U_{\text{Eins-mol-id,t}} + U_{\text{Ein,or}} \\ U_{\text{Ein-mol-id,t}} &= \sum_{i=2}^{N} \left[\Lambda_E (\mathbf{r}_i - \mathbf{r}_{i0})^2\right]. \end{aligned} \tag{53}$$

Notice that the main difference from equation (19) is the absence of a harmonic term for the reference point of molecule 1. The orientational part of the potential is identical in the Einstein crystal and in the Einstein molecule approach. The partition function of the ideal Einstein molecule can be obtained by performing the integral κ' for this particular case and substituting the value in equation (52). The translational integral is particularly simple since is just a set of $3(N-1)$ oscillators. The orientational contribution is obtained as in the Einstein crystal approach. Therefore, the Helmholtz free energy $A_{\text{Ein-mol-id}}$ of the ideal Einstein molecule is given by

$$\begin{aligned} \frac{\beta A_{\text{Ein-mol-id}}}{N} &= -\frac{1}{N}\ln(Q) = \frac{1}{N}\ln\left(\frac{N\Lambda^3}{V}\right) \\ &\quad + \frac{3}{2}\left(1 - \frac{1}{N}\right)\ln\left(\frac{\Lambda^2 \beta \Lambda_E}{\pi}\right) - \frac{1}{N}\ln(Q_{\text{Ein,or}}). \end{aligned} \tag{54}$$

In the case where the carrier molecule (molecule 1) is fixed, the free energy will be equal to the free energy of the ideal Einstein molecule plus a term $kT\ln(V/\Lambda^3)$ (where the term V comes from the constraint on the position of molecule 1, and the term Λ^3 comes from the constraint on the momentum).

6.2.2. Integration path and computation of the free energy in each step. In the ideal Einstein molecule approach, the free energy of a given solid will be computed from integration to the ideal Einstein molecule. This integral is performed in several steps, that are summarized in the scheme shown in figure 1. First the ideal Einstein molecule is transformed into an ideal Einstein molecule with one molecule fixed (what we mean by particle fixed is that its reference point remains fixed). Then the ideal Einstein molecule with one particle fixed is transformed into the real solid with one particle fixed. In the last step this fixed particle is allowed to move to obtain the real solid. As is shown in the scheme, the factor $kT\ln(V/\Lambda^3)$ that appears as a result of fixing one molecule in the ideal Einstein molecule cancels out with the free energy contribution of allowing molecule 1 to move to recover the real solid. As a result, the free energy of a solid can be computed simply by adding to the free energy of the ideal Einstein molecule the free energy change between an ideal Einstein molecule with one fixed atom and the solid with one fixed atom (given by $\Delta A_1^* + \Delta A_2^*$):

$$A_{\text{sol}} = A_{\text{Ein-mol-id}} + \Delta A_1^* + \Delta A_2^* = A_0^* + \Delta A_1^* + \Delta A_2^* \tag{55}$$

where the asterisk in ΔA_1^* and ΔA_2^* serves to remind us that the integral should be performed while keeping the position of the reference point of molecule 1 fixed (and A_0^* is just $A_{\text{Ein-mol-id}}$). The computation of the free energy change between the solid and the ideal Einstein molecule keeping one particle fixed is completely analogous to the computation of the free energy change between the solid and the ideal Einstein crystal keeping the center of mass of the system fixed. As in the Einstein crystal method, this free energy change will be calculated in two steps, represented by the terms ΔA_1^* and ΔA_2^*. In particular, in the first step (ΔA_1^*) we will compute the free energy change between the interacting Einstein molecule with one fixed particle and the ideal Einstein molecule with one fixed particle. This free energy change is evaluated using the same procedure as in the Einstein crystal method with the

Table 1. Free energy of the fcc hard sphere solid at a density $\rho^* = 1.040\,86$. The values of the different terms that contribute to the free energy in the Einstein molecule and in the Einstein crystal methods are also shown. All free energies are given in Nk_BT units. The thermal de Broglie wavelength was set to $\Lambda = \sigma$, the hard sphere diameter.

		Einstein molecule				Einstein crystal			
N	$\Lambda_E/(kT/\sigma^2)$	ΔA_1^*	ΔA_2^*	A_0^*	A_{sol}	ΔA_1	ΔA_2	A_0	A_{sol}
108	632.026	0.0172	−3.0046	7.8830	4.896	0.0175	−2.9400	7.8180	4.895
256	632.026	0.0174	−3.0116	7.9254	4.931	0.0175	−2.9797	7.8929	4.931
1372	1000.00	0.0018	−3.6862	8.6383	4.955	0.0018	−3.6802	8.6304	4.952
2048	1000.00	0.0018	−3.6866	8.6403	4.955	0.0015	−3.6819	8.6347	4.954

difference that, instead of fixing the center of mass, the position of molecule 1 is kept fixed:

$$\Delta A_1^* = U_{\text{lattice}} - k_BT \ln \langle \exp[-\beta(U_{\text{sol}} - U_{\text{lattice}})] \rangle_{\text{Ein-mol-id}} \tag{56}$$

which is formally identical to equation (35) except for the fact that averages should be computed over the ideal Einstein molecule system, rather than over the ideal Einstein crystal, and that molecule 1 will be fixed instead of the center of mass.

In the second step, the free energy change between the interacting Einstein molecule with one fixed particle and the solid with one fixed particle is computed (ΔA_2^*). This will be done by slowly switching off the springs of the interacting Einstein molecule:

$$U(\lambda) = \lambda U_{\text{sol}} + (1-\lambda)(U_{\text{Ein-mol-id}} + U_{\text{sol}}). \tag{57}$$

The parameter λ is defined between zero and unity, so that when $\lambda = 0$ one has the interacting Einstein molecule, and when $\lambda = 1$ one obtains the solid of interest (both with the position of molecule 1 fixed). U_{sol} is the potential of the system under consideration. This equation is equivalent to equation (36) for the Einstein crystal. The free energy change in this first step will be calculated from the following expression:

$$\Delta A_2^* = -\int_0^{\Lambda_E} \frac{\langle U_{\text{Ein-mol-id}} \rangle_{N,V,T,\lambda}}{\Lambda_E} \, \mathrm{d}(\lambda \Lambda_E) \tag{58}$$

which is identical to equation (38) except for the replacement of $U_{\text{Ein-id}}$ by $U_{\text{Ein-mol-id}}$. The asterisk indicates that the reference point of molecule 1 is fixed in the integration. Notice that this integral does not diverge at low values of λ, because the translations of the system as a whole are prevented by fixing the reference point of molecule 1.

6.3. *Calculations for the hard sphere solid*

Let us now present some results for the free energy of an fcc solid of hard spheres at a density $\rho^* = 1.040\,86$. We shall compute the free energy using both the Einstein crystal methodology [27, 142] described extensively in this paper and the Einstein molecule approach. Results are presented in table 1. The first point to be noted is that ΔA_1 and ΔA_1^* (and ΔA_2 and ΔA_2^*) are similar but not identical (reflecting the fact that it is not exactly the same fixing the center of mass as fixing molecule 1). However, the sum of all terms contributing to A_{sol} gives the same value, so that the estimated free energy is the same (within statistical errors) with both methodologies. Obviously, the free energy of a well defined state should not depend on the procedure chosen to compute it. Since ΔA_1 and ΔA_1^* are quite similar, and the free energy of the system must be the same computed by both routes (fixing the center of mass or fixing molecule 1), then ΔA_2 and ΔA_2^* must differ by about $3\ln(N)/(2N)$, which is the analytical difference between A_0^* and A_0. This is indeed the case as it can be seen in table 1. The third aspect to be considered from the results of table 1 is that the total free energy presents a strong size dependence. Notice that this is not a problem of the methodology chosen to compute the free energy, but it is an intrinsic property of the HS solid (and likely of other solids as well). In other words, the free energy of solids presents important finite size effects. This is further illustrated in figure 4, where the free energy is plotted as a function of $1/N$. The estimated value of $A/(Nk_BT)$ in the thermodynamic limit from our results is 4.9590(2), which is in good agreement with the estimates of Polson *et al* [142] (4.9589), Chang and Sandler [149] (4.9591), Almarza [150] (4.9589) and de Miguel *et al* (4.9586) [151] (all obtained from free energy calculations, although with different implementations). Therefore, the value of the free energy of hard spheres in the thermodynamic limit for the density $\rho^* = 1.040\,86$ seems to be firmly established.

A consequence of the strong N dependence of the solid free energy is that the coexistence pressure p^* also presents a strong N dependence as illustrated in figure 4. It is of interest to estimate the properties at coexistence in the thermodynamic limit. We found [145] $p^* = p/(k_BT/\sigma^3) = 11.54(4)$, $\rho_s^* = \rho_s\sigma^3 = 1.0372$, $\rho_l^* = \rho_l\sigma^3 = 0.9387$ and $\mu^* = \mu/(k_BT) = 16.04$. The coexistence pressure is in agreement with estimates by Frenkel and Smit [139] (11.567), Wilding [12] (11.50(9)), Speedy [152] (11.55(11)) and Davidchack and Laird [153] (11.55). The Hoover and Ree estimate (11.70) seems now to be a little bit high. The chemical potential at coexistence obtained here is consistent with the value reported by Sweatman [154] ($\mu^* = 15.99$–16.08) obtained using the self-referential methodology to compute fluid–solid equilibria.

Although finite size effects are present both in fluid and solid phases, they seem to be more pronounced in the solid (probably due to the coupling between the periodical boundary conditions and the geometry of the solid). In principle, one is interested in properties of the system in the thermodynamic limit rather than for a finite size system. To estimate free energies in the thermodynamic limit one should repeat the free energy calculations for several system sizes and extrapolate

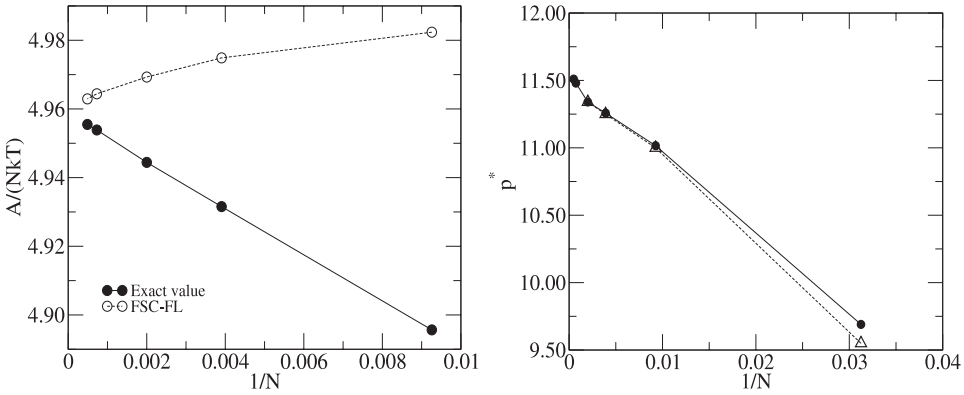

Figure 4. Left: free energies of HS in the fcc solid for $\rho^* = 1.040\,86$ as a function of system size (filled circles). The open circles represent the free energies after including the Frenkel–Ladd finite size corrections (i.e. adding $(2/N)\ln N$ to the free energies of the solid). For all values of N the free energies obtained here (black circles) are in excellent agreement with those reported by Polson *et al* [142] and de Miguel *et al* [151]. Right: coexistence pressure of the fluid–solid equilibria of hard spheres as a function of the system size as obtained from free energy calculations (filled circles) or from phase switching simulations as reported by Wilding [12] and Errington [14] (open triangles).

to the thermodynamic limit. This is quite involved and time consuming. For this reason it is of practical interest to introduce finite size corrections (FSCs) that allow the estimation (although in an approximate way) of large system free energies, by performing simulations of small systems (something similar to the $g(r) = 1$ approximation [130] used to correct for the introduction of the cut-off). Several recipes have been proposed recently [145]. Here we shall describe one of them, namely the Frenkel–Ladd FSC.

6.4. Finite size corrections: the Frenkel–Ladd approach

In the original paper of 1984, Frenkel and Ladd (FL) provided an expression for the free energy of the solid $(2/N)\ln N$ higher than the correct free energy. This was first pointed out by Polson *et al* [142]. In appendix C the reasons for the appearance of the extra term $(2/N)\ln N$ will be described. Thus the FL free energy $A_{\rm sol}^{\rm FL}/(Nk_{\rm B}T)$ is given by

$$A_{\rm sol}^{\rm FL}/(Nk_{\rm B}T) = A_{\rm sol}/(Nk_{\rm B}T) + (2/N)\ln N. \qquad (59)$$

Notice that the term $(2/N)\ln(N)$ tends to zero in the thermodynamic limit, and therefore the FL expression is valid in this limit. However, for finite systems the FL expression gives a free energy higher than the true free energy of the system. For a typical system size $N = 350$ the difference between both values is of the order of $0.03\ Nk_{\rm B}T$. The interesting issue is that the FL free energies, although incorrect (for a certain value of N), are relatively close to the value of the free energy in the thermodynamic limit. This is illustrated in figure 4 for the HS system. For this reason, one may simply view the FL expression as containing an approximate prescription for the finite size corrections, providing free energies closer to the thermodynamic limit than the correct free energies of the system of finite size. Other approximate expressions for the FSCs have been proposed recently [145].

6.5. The symmetry of the orientational field in Einstein crystal calculations

For molecular fluids, the choice of the orientational external field used within the Einstein crystal (or Einstein molecule) simulations should be made with care since this can be a source of methodological errors. The position of the molecule is given by the position of the reference point. Things become simpler if the reference point is chosen in such a way that all elements of symmetry of the molecule contain this point. For instance, a convenient choice for H_2O, NH_3, benzene and N_2 are the O, the N, the center of the hexagon and the geometrical center of the N_2, respectively. Now two orthogonal unit vectors $\vec{a}$ and $\vec{b}$ are attached to the reference point, and these two vectors are sufficient to define the orientation of the molecule (in fact two degrees of freedom are needed to locate the orientation of a unit vector $\vec{a}$, and just one degree of freedom to locate the vector $\vec{b}$, which is perpendicular to $\vec{a}$). Therefore, the unit vectors $\vec{a}$ and $\vec{b}$ are a useful way of defining the orientation of the molecule (the Euler angles could be used as well but it is more convenient to use $\vec{a}$ and $\vec{b}$). For convenience, the vector $\vec{b}$ is chosen along the principal symmetry axis of the molecule (the C_n with the highest value of n). When the molecule i stands on its equilibrium position and orientation in the crystal then the vectors $\vec{a}_i$ and $\vec{b}_i$ adopt the values $\vec{a}_{i0}$ and $\vec{b}_{i0}$ respectively. Thus the subindex 0 will refer to the orientation of the molecule in the equilibrium lattice position. Let us denote as $\psi_{a,i}$ the angle between the vectors $\vec{a}_i$ and $\vec{a}_{i0}$ and as $\psi_{b,i}$ the angle between the vectors $\vec{b}_i$ and $\vec{b}_{i0}$ in an instantaneous configuration. Which expression should be used for the orientational field? The translational part will always be given as in equation (19) for the Einstein crystal approach or as in equation (53) for the Einstein molecule approach. The orientational part will be the same for the Einstein crystal or Einstein molecule approaches. We have already given a convenient expression for the orientational field of a molecule with point group C_{2v} (for example water). Let us now give a convenient expression for other symmetries. For a molecule with a point group of type C_{nv} a convenient expression for

$U_{\text{Ein-id,or}}$ is

$$U_{\text{Ein,or}} = \sum_{i=1}^{N} \left[\Lambda_{E,a} \sin^2 \left(\frac{n\psi_{a,i}}{2} \right) + \Lambda_{E,b} \left(\frac{\psi_{b,i}}{\pi} \right)^2 \right]. \quad (60)$$

For a molecule with a point group of type D_{nh} a convenient expression for $U_{\text{Ein-id,or}}$ is

$$U_{\text{Ein,or}} = \sum_{i=1}^{N} \left[\Lambda_{E,a} \sin^2 \left(\frac{n\psi_{a,i}}{2} \right) + \Lambda_{E,b} \sin^2 \left(\psi_{b,i} \right) \right]. \quad (61)$$

For a molecule with point group O_h, a convenient expression [57] for $U_{\text{Ein-id,or}}$ is

$$U_{\text{Ein,or}} = \sum_{i=1}^{N} \left[\Lambda_{E,a} \sin^2 \left(\psi_{a,i,\text{min}} \right) + \Lambda_{E,b} \sin^2 \left(\psi_{b,i,\text{min}} \right) \right] \quad (62)$$

where $\psi_{b,i,\text{min}}$ stands for the minimum angle between $\vec{b}_{i0}$ and the six vectors connecting the reference point of the molecule with the six octahedral atoms/sites and an analogous definition for $\psi_{a,i,\text{min}}$.

For a linear molecule only one vector (i.e. vector $\vec{b}_i$) is needed and the applied field should be of the form, for a $D_{\infty,h}$,

$$U_{\text{Ein,or}} = \sum_{i=1}^{N} \left[\Lambda_{E,b} \sin^2 \left(\psi_{b,i} \right) \right]. \quad (63)$$

For a $C_{\infty,v}$ molecule a convenient choice is

$$U_{\text{Ein,or}} = \sum_{i=1}^{N} \left[\Lambda_{E,b} \left(\frac{\psi_{b,i}}{\pi} \right)^2 \right]. \quad (64)$$

When performing an MC run, it is convenient to introduce two different types of moves, translations and rotations. In a translation move the molecule moves as a whole and there is no change in the orientation of the molecule. Only the change in the translational energy with respect to the reference Einstein crystal (or molecule) needs to be computed. In a second type of move the molecule is rotated in a random direction and angle with respect to an axis passing through the reference point of the molecule. Since the reference point does not change the position under such a rotation, only the orientational energy with respect to the reference Einstein crystal (or molecule) needs to be computed.

The choice of an orientational field adapted to the symmetry of the molecule such as the ones proposed here is highly recommended. When this is done the energy with the external field is invariant to any of the symmetry operations of the molecule. Thus, a standard MC or MD program will provide correct values of the orientational contribution to the free energy. One interesting question is whether it is possible to use an external orientational field that does not reflect the symmetry of the molecule. The answer is, in principle, yes, but a special MC or MD code should be written for this purpose. Special moves should be added where the symmetry operations of the molecule are implemented. For instance, for water one should incorporate the C_2 operation that exchanges the positions of the two H atoms. Of course the energy of the molecule with the rest of the system is not affected by this operation. However, the energy of the molecule with the external orientational field may change when the external orientational field does not reflect the symmetry of the molecule (see the interesting paper by Schroer and Monson [51] illustrating this problem for benzene).

For this reason, it is far more convenient and simpler to use an orientational field that respects the symmetry of the molecule (examples for C_{nv}, D_{nh}, O_h and linear molecules have been given here). This subtle issue of the symmetry of the orientational field may have been an important source of errors in free energy calculations for molecular fluids. Let us just finish by saying that although we found it convenient to have the vectors $\vec{a}$ and $\vec{b}$ orthogonal other choices (as long as they are not collinear) are also valid and correct.

6.6. Einstein crystal calculations for disordered systems

Let us now discuss briefly the case of disordered solids. When implementing the Einstein crystal, harmonic springs are incorporated to fix the position (as given by the reference point) and the orientation of the molecules of the system to the equilibrium configuration. In a disordered solid, there may be many possible 'equilibrium configurations' differing in a significant way (not just differing in the labeling of the molecules). Let us just give three examples.

Plastic crystals. Molecules with an almost spherical shape tend to form plastic crystals when freezing. In these plastic crystals the reference points of the molecules form a true lattice but the other atoms of the molecule are able to rotate (either with a free or with a hindered rotation) around the reference points. In principle the Einstein crystal methodology described in the previous section can also be applied to determine free energies for plastic crystals [28, 31–33, 36, 37, 57]. In addition to the translational field, an orientational field is included, forcing the molecules to adopt an orientationally ordered solid for large values of the orientational field. Some issues should be taken into account when evaluating the free energy for a plastic crystal phase. At low values of the orientational field very long runs should be performed to guarantee that the molecules are able to rotate. Many values (20–30) of the coupling parameter Λ_E should be used to compute the integral of equations (38) or (58) (the orientational contribution to the integrand increases quite rapidly for low values of the orientational field). Finally, the absence of phase transitions along the integration path should be checked (the external field should lead the system from an orientationally disordered solid at low values of coupling parameter to an orientationally ordered solid for large values of the coupling parameter without undergoing any phase transition).

Water. In the case of solid water (say ice Ih), while the oxygens are ordered (i.e., they form a lattice) the hydrogens are disordered. However, Bernal and Fowler [155] and Pauling [156] suggested that configurations satisfying the so called Bernal–Fowler rules have the same statistical weight and that configurations violating the Bernal–Fowler rules can be

neglected. The correct estimate of the experimental residual entropy of ice at 0 K by using these two assumptions was a major achievement. Therefore, the free energy of ice is approximated by

$$A = -k_B T \ln(\Omega A_{\text{configuration}}) = -k_B T \ln(\Omega) - k_B T \ln(A_{\text{configuration}}) \quad (65)$$

where $A_{\text{configuration}}$ is the free energy (obtained via the Einstein crystal methodology for a certain configuration satisfying the Bernal–Fowler rules) and Ω is the degeneracy. Pauling estimates $-k_B T \ln(\Omega)$ as $-k_B T \ln((3/2)^N)$. Therefore, for ices one computes the free energy for a certain configuration and then adds the Pauling contribution to the free energy. This entropy can also be computed numerically (see for instance the work by Berg and Yang [157]). Notice that when MC or MD runs are performed for a certain configuration of ice satisfying the Bernal–Fowler rules the system remains in this configuration along the run. This is because the time required by the system to jump from one configuration to another (both satisfying the Bernal–Fowler rules) is beyond the typical time of a simulation run. Equation (65) is useful not only for ice but for other disordered solids as well. In fact, it can be applied successfully [158, 159, 32, 160, 38] to tangent dimers, formed by two tangent spheres, where Nagle [161] has estimated Ω, and for fully flexible hard sphere chains [42] (where Flory and Huggins [162, 163] have estimated Ω).

Partially disordered phases. In certain cases the system possesses disorder, but still certain configurations are more likely than others. Getting the free energy in such a situation is especially difficult. Firstly it is important to sample the configurational space properly to obtain equilibrium configurations of the system representative of the partial disorder. Secondly these configurations will differ in statistical weight, so it does not seem a good idea to perform Einstein crystal calculations for just one configuration, since its statistical weight is unknown. In this case thermodynamic integration can be a more adequate route. An example of a partially disordered phase is the fcc disordered structure of the RPM model (see discussion on this later on).

7. The machinery in action. III. Obtaining coexistence lines: the Gibbs–Duhem integration

Once the free energy of the liquid and the solid has been obtained for a reference state it is relatively straightforward to perform thermodynamic integration to obtain it for other thermodynamic states and locate a coexistence point between two phases (in case where it exists). The Gibbs–Duhem integration allows the determination of the coexistence lines once an initial coexistence point is known.

7.1. Gibbs–Duhem integration

In 1993 Kofke realized that the Clapeyron equation can be integrated to determine coexistence lines [164–166]. The Clapeyron equation between two coexistence phases (labeled as I and II) can be written as

$$\frac{\mathrm{d}p}{\mathrm{d}T} = \frac{s_{\text{II}} - s_{\text{I}}}{v_{\text{II}} - v_{\text{I}}} = \frac{h_{\text{II}} - h_{\text{I}}}{T(v_{\text{II}} - v_{\text{I}})} \quad (66)$$

where we use lower case for thermodynamic properties per particle. Since the difference in enthalpy and volume between two phases can be determined easily (at a certain T and p), the equation can be integrated numerically. When implementing the Gibbs–Duhem integration one obtains the coexistence pressure for the selected temperatures (the temperature acting as the independent variable). This is quite convenient when the coexistence line does not present a large slope in the p–T plane. When the slope of the coexistence line is large within a p–T representation then it may be more convenient to integrate the Clapeyron equation in a different way: $\frac{\mathrm{d}T}{\mathrm{d}p} = \frac{T\Delta v}{\Delta h}$. In this case the coexistence temperatures are determined for a set of selected pressures (the pressure acting as the independent variable). A fourth order Runge–Kutta algorithm is quite useful to integrate the differential equation. It is important to stress that anisotropic NpT simulations should be used for the solid phase within Gibbs–Duhem calculations. Isotropic NpT simulations could be used for fluid phases and for solids of cubic symmetry.

7.2. Hamiltonian Gibbs–Duhem integration

When a coupling parameter λ is introduced within the expression of the potential energy of the system, then a set of generalized Clapeyron equations can be derived [31, 167, 168]. For two phases at coexistence,

$$g_{\text{I}}(T, p, \lambda) = g_{\text{II}}(T, p, \lambda). \quad (67)$$

If the system is perturbed slightly while preserving the coexistence it must hold that

$$v_{\text{I}}\,\mathrm{d}p - s_{\text{I}}\,\mathrm{d}T + \left(\frac{\partial g_{\text{I}}}{\partial \lambda}\right)\mathrm{d}\lambda = v_{\text{II}}\,\mathrm{d}p - s_{\text{II}}\,\mathrm{d}T + \left(\frac{\partial g_{\text{II}}}{\partial \lambda}\right)\mathrm{d}\lambda; \quad (68)$$

the last terms appearing in equation (68) are due to the presence of the new intensive thermodynamic variable λ. If λ is constant when performing the perturbation then one recovers the traditional Clapeyron equation. If the pressure remains constant when the perturbation is performed (so that T and λ are changed) then one obtains

$$\frac{\mathrm{d}T}{\mathrm{d}\lambda} = \frac{T[(\partial g_{\text{II}}/\partial\lambda) - (\partial g_{\text{I}}/\partial\lambda)]}{h_{\text{II}} - h_{\text{I}}}. \quad (69)$$

It is simple to show (within the NpT ensemble) that $\partial g/\partial\lambda$ is nothing but $\frac{\partial g}{\partial \lambda} = \langle \frac{\partial u(\lambda)}{\partial \lambda} \rangle_{N,p,T,\lambda}$, which can be determined within an NpT simulation. The final working expression of the generalized Clapeyron equation (for perturbations of T and λ while keeping p constant) is

$$\frac{\mathrm{d}T}{\mathrm{d}\lambda} = \frac{T(\langle \partial u_{\text{II}}(\lambda)/\partial\lambda \rangle_{N,p,T,\lambda} - \langle \partial u_{\text{I}}(\lambda)/\partial\lambda \rangle_{N,p,T,\lambda})}{h_{\text{II}} - h_{\text{I}}}. \quad (70)$$

This generalized Clapeyron equation can be integrated numerically, yielding the change in coexistence temperature (at

a certain pressure) due to a perturbation of the Hamiltonian of the system (i.e. of the potential energy). A similar expression can be obtained for the case in which the system is perturbed at constant T (changing the pressure and λ). In this case one obtains

$$\frac{\mathrm{d}p}{\mathrm{d}\lambda} = -\frac{\langle \partial u_{\mathrm{II}}(\lambda)/\partial\lambda\rangle_{N,p,T,\lambda} - \langle \partial u_{\mathrm{I}}(\lambda)/\partial\lambda\rangle_{N,p,T,\lambda}}{v_{\mathrm{II}} - v_{\mathrm{I}}}. \quad (71)$$

The change in the coexistence pressure (at a certain temperature) due to a change in the Hamiltonian of the system (potential energy) is then obtained. Equations (71) and (70) will be denoted as Hamiltonian Gibbs–Duhem integration. Hamiltonian Gibbs–Duhem integration is a very powerful technique since it allows one to analyze the influence of the parameters of the potential on the coexistence properties. It also allows one to change the parameters of the potential to improve phase diagram predictions. These two possible applications will be illustrated later on for the case of water.

In the particular case in which λ is used as a coupling parameter taking the system from a certain potential to another (by changing λ from zero to one),

$$U(\lambda) = \lambda U_{\mathrm{B}} + (1-\lambda)U_{\mathrm{A}}. \quad (72)$$

Then the generalized Clapeyron equations can be written as

$$\frac{\mathrm{d}T}{\mathrm{d}\lambda} = \frac{T(\langle u_{\mathrm{B}} - u_{\mathrm{A}}\rangle^{\mathrm{II}}_{N,p,T,\lambda} - \langle u_{\mathrm{B}} - u_{\mathrm{A}}\rangle^{\mathrm{I}}_{N,p,T,\lambda})}{h_{\mathrm{II}} - h_{\mathrm{I}}} \quad (73)$$

$$\frac{\mathrm{d}p}{\mathrm{d}\lambda} = -\frac{\langle u_{\mathrm{B}} - u_{\mathrm{A}}\rangle^{\mathrm{II}}_{N,p,T,\lambda} - \langle u_{\mathrm{B}} - u_{\mathrm{A}}\rangle^{\mathrm{I}}_{N,p,T,\lambda}}{v_{\mathrm{II}} - v_{\mathrm{I}}} \quad (74)$$

where u_{B} is the internal energy per molecule when the interaction between particles is described by U_{B} (with a similar definition for u_{A}). If a coexistence point is known for the system with potential A, then it is possible to determine the coexistence conditions for the system with potential B (it is just sufficient to integrate the previous equations changing λ from zero to unity). In this way the task of determining the phase diagram of system B (unknown) from the phase diagram of system A (known) is simplified considerably.

8. Coexistence by interfaces

8.1. Direct fluid–solid coexistence

In 1978 Ladd and Woodcock devised a method to obtain fluid–solid equilibria without free energy calculations, the direct coexistence method [169–171]. In this method, the fluid and the solid phases are introduced into the simulation box, and simulations are performed (NVE MD) to achieve equilibrium between the two coexistence phases. The coexistence conditions can then be obtained easily. Although the initial results for LJ and inverse 12 power were not very successful (probably due to the small size of the systems and to the short length of the runs), the method has become more popular in the last few years. In fact, it has been applied to simple fluids [172–175, 153, 176], metals [177–180], silicon [181], ionic systems [182, 183], hard dumbells [184], nitromethane [135] and water [108, 109, 185–191]. Two simulation boxes, having an equilibrated solid and liquid respectively, are joined along the z axis (the direction perpendicular to the plane of the interface). This could generate overlapping at the interface, and this overlapping should be relaxed/removed. The coexistence conditions (i.e. pressure, temperature) will be independent of the plane selected for the interface, but the dynamic behavior (and of course the interface properties) will be different for different planes [192, 193, 190].

The direct coexistence method can be implemented either within molecular dynamics or Monte Carlo simulations. Both are equally valid, although if dynamical properties are of interest (for instance crystal growth rates) then MD is the only choice. The direct coexistence method was firstly used in the NVE ensemble, but other ensembles such as NVT, NpH, NpT and Np_zT can be applied. Each ensemble will have its advantages and disadvantages, and the election of one ensemble or another depends on the information that one wants to obtain. Broadly speaking there are two kinds of ensembles, those at which it is possible to reach equilibrium having two coexistence phases at equilibrium and those for which it is not possible to have two phases at equilibrium. Obviously, for the study of interface properties only those ensembles that lead to equilibrium should be used.

8.1.1. NVE ensemble. This is the simplest approach. The idea behind the method is that the system will evolve to the equilibrium temperature and pressure by moving the interface (so that either the amount of solid or the amount of liquid increases). If the system is above the melting temperature, the solid will melt, provoking (at constant E) a decrease of temperature. If the system is below the melting temperature, the fluid will freeze, provoking (at constant E) an increase of temperature. In NVE runs the initial configuration should not be too far from equilibrium to guarantee some portion of liquid and solid in the final configuration. The equilibrium temperature and pressure are obtained in NVE simulations at the end of the run. The knowledge of the coexistence pressure only at the end of the run is a serious problem. In fact, the lattice parameter used in the xy plane (which remains fixed along the run) may not correspond to the equilibrium value for the solid at the coexistence pressure. In other words, stress was introduced, and this may affect the free energy of the solid and, therefore, the melting point. This can be adjusted by trial and error [172, 153].

8.1.2. NVT ensemble. In the NVT ensemble the system also evolves to equilibrium by changing the relative amounts of liquid and solid phases, in this case to adjust the densities and pressure to their coexistence values. One important difference from the NVE ensemble is that in the NVT the heat released or absorbed by the crystallization or the melting is immediately accommodated by the thermostat and, therefore, it is expected that the system will attain equilibrium faster than in the NVE simulations. Actually, heat transfer is usually the determining rate in the crystallization or melting process, and it has been

seen that the presence of a thermostat in the simulations leads to crystallization rates much higher than those measured experimentally [194]. However, as in the NVE case, the solid is not able to relax in the xy plane and, therefore, the system might be under some stress.

8.1.3. NpH ensemble. A less common approach is to perform the simulations in the isobaric–isoenthalpic NpH ensemble [195], with anisotropic scaling, i.e., the three edges of the simulation box change independently (see, for example, [187]). In this ensemble, the system will also attain equilibrium, in this case by evolving towards the coexistence temperature. One advantage with respect to the previous ensembles is that now the fluctuations of the volume will allow the solid to relax, removing the presence of stress. Moreover, as the volume of the box is allowed to change, the system can adapt more easily to changes in the relative ratio of the amount of solid and liquid phases, especially when the densities of the solid and liquid phases are very different. The problem in this case is that it is not strictly correct to use simulations under constant pressure in the presence of an interface, because, due to the contribution of the interface, the normal and tangential components of the stress tensor are not equal. However, if the system is chosen to be very large in the direction perpendicular to the interface, it is expected that the error introduced by the presence of the interface will be small. Another disadvantage of this ensemble is that, as in the NVE, the transfer of heat is not very efficient and, therefore, long simulations are needed to obtain equilibrium.

8.1.4. NpT ensemble. It is possible to tackle both the problem of having stress in the solid and that of slow heat transfer by performing simulations in the anisotropic NpT ensemble, where each of the edges of the box changes independently. In this case, as the volume is able to fluctuate, the solid can relax to equilibrium and, as the temperature is fixed, the transfer of heat will occur very rapidly. However, as in the NpH ensemble, the use of the NpT ensemble in the presence of an interface is not strictly correct, although, as mentioned before, it is expected that the error is small for a system sufficiently large along the z axis. One important difference of this ensemble from the previous ones is that, as both the pressure and temperature are set, it is not possible to have the interface at equilibrium. The procedure to determine the coexistence properties is as follows. At a given pressure, different simulations are performed at a few temperatures. If the temperature is above the melting temperature the solid will melt (i.e. the total energy of the system will increase), and, vice versa, if the temperature is below the melting temperature the fluid will freeze (i.e. the total energy will decrease). In this way, it is possible to establish a lower and an upper limit to the melting temperature.

8.1.5. Np_zT ensemble. We have mentioned before that, due to the contribution of the interface, the stress tensor has different normal and transversal components and, therefore, it is not correct to perform simulations under constant pressure in the presence of an interface. The correct way would be to allow the size of the box to change only along the axis normal to the surface, i.e. the z axis. We will call such an ensemble Np_zT. The procedure to determine the coexistence properties is completely analogous to the procedure followed in the NpT ensemble. The only difference is that now a new starting configuration with the corresponding bulk lattice parameter at pressure p_z and temperature T must be generated for each simulation at different temperature and/or pressure in order to avoid having stress in the solid. This was not necessary in the NpT ensemble, as the fluctuations along the x and y planes allowed the solid to relax to equilibrium.

Two issues that deserve special attention when implementing the direct coexistence method are the system size and the length of the simulation. As regards the system size, a typical simulation box could have ten molecular diameters in the x and y directions and about 30 in the z direction. Accordingly, studies by direct coexistence used typically 1000–3000 molecules, and these sizes provide results relatively close to the thermodynamic limit [173, 178, 135, 189, 190]. Besides large system sizes, extremely long simulations are also needed (10 million time steps or more may be needed in many systems). Systems without a thermostat (NVE, NpH) may require even longer runs, since heat transfer along the interface may be quite slow.

8.2. Estimating melting points by studying the free surface

It is now commonly accepted that melting starts at the surface and, already at temperatures lower than the bulk melting point, solids exhibit a liquid-like layer at the surface [196–204]. Thus for most substances a liquid layer is present at the surface even at temperatures below the melting point. When the thickness of this layer diverges at the melting point, this is denoted as surface melting. When the thickness of the liquid layer remains finite (or even zero) at the melting point, this is denoted as incomplete surface melting [205–207]. The thickness of the quasi-liquid layer for a certain T depends on the considered material and on the exposed plane (as labeled by the Miller indices). When the size of the liquid layer is sufficiently large either because the system has surface melting or incomplete surface melting (with a significant thickness of the liquid layer) then it is not possible to superheat a solid. This is the reason why experimentally solids usually melt at the melting point (at least one plane of the crystals of the powder presents a large quasi-liquid layer, provoking the melting of the whole sample). For instance, for ice it is not possible to superheat the solid, except for a few nanoseconds [208]. Superheating of solids (over macroscopic times) has been found experimentally only for monocrystals when the exposed planes have no liquid layer at all. Since for most substances a quasi-liquid layer will be present at the melting point, it is expected that for most materials the melting will occur at the melting point (when there is a free surface). That provides a remarkably simple methodology to estimate melting points (at zero pressure). NVT simulations of the solid exhibiting a free surface are performed at different temperatures. A convenient geometry is to locate a slab of solid in the center of an orthorhombic simulation box. The pressure will be essentially zero since no vapor is introduced in the simulation box, and besides

the vapor pressure is typically so small that the sublimation of a molecule from the solid will be a rare event within the typical simulation times. The lattice parameter of the solid in the direction perpendicular to the interface should correspond to the equilibrium values at zero pressure for the studied temperature. At temperatures below the melting point a stable thin liquid layer will be formed at the surface. At temperatures above the melting point the solid will melt. The simulations should be fairly long to allow the system to melt completely. In the case of water, the ice took about 10–20 ns to melt in the presence of a free surface. This technique has been applied successfully to estimate the melting point of the LJ model, water [209] and nitromethane [203, 210]. Notice that the technique will fail, for instance, for NaCl, a substance having no liquid layer on the free surface [183].

9. Consistency checks

Evaluation of free energy and coexistence points requires more effort than performing simple NpT runs. Besides, the possibility of introducing errors in the calculations is relatively high. For this reason it is a good idea to introduce several tests to guarantee the accuracy of the calculations.

9.1. Thermodynamic consistency

In a number of cases it is possible to determine the free energy for two different thermodynamic states. For instance, for a solid the free energy at two different densities along an isotherm can be determined by using Einstein crystal calculations. The free energy difference between these two states (as obtained from free energy calculations) should be identical to that obtained by thermodynamic integration (integrating the EOS along the isotherm). We indeed recommend the implementation of this test before performing any further calculation. Failing the test indicates an error in the free energy calculations. However, passing the test it is not a definite proof of the correctness of the free energy calculations. They could still be wrong by a constant (the constant being identical for the two thermodynamic states). It is clear that other tests should also be introduced to guarantee the correctness of the calculations.

9.2. Consistency in the melting point obtained from different routes

The melting point obtained from free energy calculations should be similar to that obtained from direct coexistence simulations (where the fluid and the solid phases coexist) within the simulation box. Notice that only fluid–solid equilibria can be studied by direct coexistence (it is not obvious how to implement solid–solid equilibria by direct coexistence). This is indeed a useful test. An incorrect prediction of the free energy of the solid phase (the typical source of errors) will provoke an incorrect prediction of the fluid–solid equilibria as compared to the estimate obtained from direct coexistence techniques. Important differences (above 2–3%) in the melting point estimated from free energy calculations and from direct coexistence are not acceptable. The reader may be surprised by the fact that we stated that both melting points should be similar instead of stating that they should be identical. In the thermodynamic limit (for very large system sizes) they should indeed become identical. However, for finite systems some technical aspects may provoke small differences. There are at least two reasons.

(a) *System size effects.* The fluid–solid equilibria may have a strong N dependence. For this reason the coexistence pressure/temperature obtained from free energy calculations for a system of N molecules will not be identical to that obtained from direct coexistence simulations obtained with N^* molecules. The case of HS was illustrated in a previous section. In general, the stability of the solid increases as the system becomes smaller. Since typically $N^* > N$, then the solid will appear slightly more stable in the free energy calculations than in the direct coexistence results (assuming that no FSC corrections were introduced). This is what one may expect when the only difference between both types of calculation is the size of the system.

(b) *Cut-off effects.* This is important when the cut-off used in free energy calculations is different from that used in direct coexistence simulations. The difference in the melting point may just be due to the fact that we are simulating two sightly different potentials. Even if the potentials were truncated at the same distance in both methodologies there may be differences. For instance, in free energy calculations, the potential may be truncated at a distance r_c, but long range corrections can be incorporated in the calculations [130]. In direct coexistence simulations, the potential may have been truncated at the same r_c but in this technique it is difficult to incorporate long range corrections. Therefore, certain differences in the melting point between free energy simulations and direct coexistence calculations can be due to a different implementation of the potential.

Notice that effects (a) and (b) may occur simultaneously. For instance, in the case of water different numbers of particles were used in free energy calculations and in direct coexistence simulations (effect (a)), but also the truncation of the potential (LJ contribution) was different in the free energy simulations (where long range corrections were included) and in the direct coexistence simulations (where they were not included). In any case, for water models we found differences in the melting point as estimated from both techniques of about 1–2% [211, 189].

9.3. Some useful tests involving Gibbs–Duhem integration

Some useful tests that can be performed when using the Gibbs–Duhem technique are the following.

- The coexistence lines should be identical (within statistical uncertainty) when the integration is performed forward (say by increasing T) and when it is performed backward (say by decreasing T).
- If free energy calculations were used to locate an initial coexistence point between phases I–II, I–III and II–III, then the three coexistence lines obtained with Gibbs–Duhem integration should cross at a point (the triple point).

- If the melting point of two models has been determined by free energy calculations then it is also possible to use Hamiltonian Gibbs–Duhem calculations to check that the melting point of model B is obtained starting from the melting point of model A and vice versa.
- If the melting point of models A and B is known, then Hamiltonian Gibbs–Duhem integration could be performed to estimate the melting point of model C. Both integrations (one starting from A and the other starting from B) should provide the same estimate of the melting point of C.
- If two coexistence points between phases I and II are known (either by free energy calculations or by direct coexistence) a Gibbs–Duhem integration starting from one of them should pass through the other one.

9.4. Consistency checks at 0 K

At zero temperature the condition of chemical equilibrium (i.e. the equilibrium pressure p_{eq}) between two phases, labeled as phases I and II, respectively, is given by

$$U_I(p_{eq}, T = 0) + p_{eq}V_I(p_{eq}, T = 0) = U_{II}(p_{eq}, T = 0) + p_{eq}V_{II}(p_{eq}, T = 0). \quad (75)$$

Hence, phase transitions between solid phases at zero temperature occur with zero enthalpy change. This is really useful since it means that phase transitions at 0 K can be estimated without free energy calculations (just computing mechanical properties as densities and internal energies). By performing several NpT simulations where the temperature is reduced to zero it is possible to obtain the EOS (and internal energy) of each solid phase at 0 K. Then by equating the enthalpy it is possible to locate phase transitions (at 0 K). This can be used as a consistency check. By performing free energy calculations it is possible to locate the coexistence pressure between two phases (I and II) at a finite non-zero temperature. Then, by performing Gibbs–Duhem simulations it is possible to determine the coexistence line up to 0 K. The coexistence pressure at 0 K obtained from this long route (free energy calculations + Gibbs–Duhem integration) should be identical to that obtained from the short route (estimating the properties of the system at 0 K). This is again a strong consistency check. Although runs at 0 K enable a check to be made on the consistency of phase diagram calculations, they do not allow us in themselves to draw the phase diagram of a certain model. Gibbs–Duhem simulations cannot be initiated from a known coexistence point at 0 K since both ΔH and T are null so that their ratio ΔS, which within classical statistical thermodynamics is finite even at 0 K, cannot be determined.

10. A worked example. The phase diagram of water for the TIP4P and SPC/E models

We shall now illustrate how the previously described methodology can be applied to determine the phase diagram for two popular water models: SPC/E [212] and TIP4P [213]. We believe that they illustrate quite well the typical difficulties found when determining by computer simulation free energies of solid phases and phase diagram calculations. The SPC/E and TIP4P models are presented in table 2 (along with two other recently proposed models, TIP4P/Ice [214] and TIP4P/2005 [215]). In these models an LJ center is located on the O atom, and positive charges are located on the H atoms. The negative charge is located at a distance d_{OM} from the O along the H–O–H bisector. Let us now describe briefly some of the simulation details.

Table 2. Potential parameters for several water potentials. Notice that the OH bond length and the HOH angle are different for the SPC/E and TIP4P models.

Model	ϵ/k (K)	σ (Å)	q_H (e)	d_{OM} (Å)
SPC/E [212]	78.20	3.1656	0.4238	0
TIP4P [213]	78.0	3.154	0.520	0.150
TIP4P/2005 [215]	93.2	3.1589	0.5564	0.1546
TIP4P/Ice [214]	106.1	3.1668	0.5897	0.1577

10.1. Simulation details

In our Monte Carlo simulations, the LJ potential was truncated for all phases at 8.5 Å. Standard long range corrections to the LJ energy were added. The importance of an adequate treatment of the long range Coulombic forces when dealing with water simulations has been pointed out in recent studies [216–219] and it is likely that this is even more crucial when considering solid phases. In this work, the Ewald summation technique has been employed for the calculation of the long range electrostatic forces. The real space contribution of the Ewald sum was also truncated at 8.5 Å. The screening parameter and the number of vectors of reciprocal space considered had to be carefully selected for each crystal phase [130, 139]. For the fluid phase we used 360 molecules. The number of molecules for each solid phase was chosen so as to fit at least twice the cut-off distance in each direction. Three different types of runs were performed: NpT, NVT Einstein crystal calculations and Gibbs–Duhem integration. The equation of state (EOS) of the fluid was obtained from isotropic NpT runs, whereas anisotropic Monte Carlo simulations (Parrinello–Rahman-like) [124–126] were used for the solid phases. In the NpT runs, about 40 000 cycles were used to obtain averages, after an equilibration period of about 40 000 cycles. However longer runs were used for the fluid phase at low temperatures. A cycle is defined as a trial move per particle plus a trial volume change. To evaluate the free energy of the solid, Einstein crystal (NVT) calculations were performed (with fixed center of mass). Also, the length of the runs was about 40 000 cycles to obtain averages after an equilibration of 40 000 cycles. In the Gibbs–Duhem simulations a fourth order Runge–Kutta was used to integrate the Clapeyron equation. In total about 60 000 cycles were used to pass from a coexistence point to the next one. When using Hamiltonian Gibbs–Duhem integration five to 10 values of λ were used to connect the initial to the final Hamiltonian. In the Gibbs–Duhem simulations, the fluid and the cubic solid were studied with isotropic NpT runs whereas the solid phases were studied with anisotropic NpT runs.

Table 3. Free energy of liquid water ($A_{\rm liquid}$) for the SPC/E and TIP4P models (with $q_{\rm r} = q_{\rm v} = q_{\rm e} = 1$). The residual and ideal contributions to the free energy of the reference LJ fluid are given. The residual term of the LJ fluid as obtained from the EOS of Johnson *et al* [220]. The ideal term was obtained (in $Nk_{\rm B}T$ units) as $\ln(\rho\Lambda^3) - 1$ where $\Lambda = 1$ Å. The difference in free energy between the reference fluid and the water model ΔA is given. Simulations were performed in the NVT ensemble for the density d.

Model	T (K)	p (bar)	d (g cm^{-3})	$A_{\rm liquid}/(Nk_{\rm B}T)$	$A^{\rm res}_{\rm LJ}/(Nk_{\rm B}T)$	$A^{id}_{\rm LJ}/(Nk_{\rm B}T)$	$\Delta A/(Nk_{\rm B}T)$
SPC/E	225	564	1.05	−21.82	2.500	−4.350	−19.97
TIP4P	225	743	1.05	−19.48	2.401	−4.350	−17.52
SPC/E	443	4010	1.05	−9.53	2.856	−4.350	−8.04
TIP4P	443	4280	1.05	−8.58	2.777	−4.350	−7.01

10.2. Free energy of liquid water

The free energy of the liquid is calculated by integrating the free energy along a reversible path in which the water molecules are transformed into Lennard-Jones spheres by switching the charges off. The free energy of the reference Lennard-Jones fluid is reported in the work of Johnson *et al* [220]. The energy (say, for the TIP4P model of water, the treatment for SPC/E being fully equivalent) of the system for a given point of the path, λ, is given by

$$U(\lambda) = \lambda U_{\rm TIP4P} + (1-\lambda)U_{\rm LJ} \tag{76}$$

where λ varies between zero (LJ) and unity (water) along the integration path. Given that $\partial A(\lambda)/\partial\lambda = \langle \partial U(\lambda)/\partial\lambda\rangle_{NVT}$, the free energy difference between liquid water and the Lennard-Jones fluid is given by

$$A_{\rm TIP4P}(N,V,T) - A_{\rm LJ}(N,V,T) = \int_{\lambda=0}^{\lambda=1} \langle U_{\rm TIP4P} - U_{\rm LJ}\rangle_{N,V,T,\lambda}\, {\rm d}\lambda \tag{77}$$

where $\langle U_{\rm TIP4P} - U_{\rm LJ}\rangle_{N,V,T,\lambda}$ is an NVT simulation average computed for a given value of λ. The integral is solved numerically (using Gauss–Legendre quadrature) by calculating the integrand at different values of λ. In practice, we perform the MC runs starting from $\lambda = 1$ and going to $\lambda = 0$. The final configuration of a run was used as the input configuration of the next run. The LJ fluid chosen as a reference state has the same LJ parameters ($\epsilon/k_{\rm B}$ and σ) as the water model. Therefore, the difference $U_{\rm TIP4P} - U_{\rm LJ}$ is just the electrostatic energy. Once the Helmholtz free energy, A, is known, the chemical potential is obtained simply as $\frac{\mu}{k_{\rm B}T} = \frac{A}{Nk_{\rm B}T} + \frac{pV}{Nk_{\rm B}T}$. In this way we have computed the free energy of the liquid at 225 and 443 K (see table 3). In addition to the total free energy we report the free energy difference with respect to the reference LJ fluid (ΔA), the residual free energy for the LJ fluid and the ideal free energy ($Nk_{\rm B}T(\ln(\rho\Lambda^3) - 1)$). In this work, for water, we shall assign the thermal de Broglie wavelength to $\Lambda = 1$ Å both for the liquid and for the solid phases.

Let us now present some consistency checks for the free energies. We shall only discuss it for the TIP4P model. We have computed the free energy at 225 and 443 K for the density $d = 1.05$ g cm^{-3}. The free energy difference between both states is $A_{443\,\rm K}/(Nk_{\rm B}T) - A_{225\,\rm K}/(Nk_{\rm B}T) = -8.58 + 19.48 = 10.90$. Then we calculated the same difference by means of thermodynamic integration along an isochore (equation (7)), obtaining again 10.90 $Nk_{\rm B}T$. Besides, Jorgensen *et al* have estimated the free energy for the TIP4P model at $p = 1$ bar and $T = 298$ K to be $G = -6.1$ kcal mol^{-1} [221]. Starting from the free energy at 225 K and $d = 1.05$ g cm^{-3} and performing thermodynamic integration we obtained −6.09 kcal mol^{-1}, which is in excellent agreement with the value of Jorgensen *et al* [221].

Instead of using the LJ fluid, it is also possible to compute the free energy of the liquid taking the ideal gas as a reference system. We obtain the free energy of TIP4P water at 240 K and 1.0174 g cm^{-3} by two different routes. In the first one the TIP4P is transformed into a LJ model. We obtained for the free energy of TIP4P in this state $A(240\ {\rm K}, 1.0174\ {\rm g\,cm^{-3}})/Nk_{\rm B}T = -20.15$. In the second route, a supercritical isotherm ($T = 900$ K) is used from zero density to 1.0174 g cm^{-3} (obtaining using equation (12) $-4.699NK_{\rm B}T$ for $A/Nk_{\rm B}T$ of this intermediate state). Then we integrate along the isochore up to 240 K (with a free energy change computed by equation (7) of $-15.434\ NK_{\rm B}T$). By adding these two numbers together we obtain $A(240\ {\rm K}, 1.0174\ {\rm g\,cm^{-3}})/Nk_{\rm B}T_2 = -20.13$ from this second route, in very good agreement with that obtained by the first one. The computation of the free energy using the LJ fluid as a reference system is considerably shorter than using the ideal gas (besides, this last route is especially difficult since the parameters of the Ewald sum should be chosen carefully along the supercritical isotherm integration). Values of the free energy of liquid water for other potential models have been reported recently [222].

10.3. Free energy of ice polymorphs

The free energy of the different ice polymorphs is calculated using the Einstein crystal method (with fixed center of mass). The O is used as reference point and the field used is that described by equations (18), (19) and (20). For disordered ices [223–225] (Ih, Ic, III, IV, V, VI, VII, XII) the oxygens form a well defined lattice, but the water molecules can orient in different ways for a given oxygen lattice provided that the Bernal–Fowler ice rules [155] are satisfied. We have generated the disordered solid structures (with almost zero dipole moment) using the algorithm proposed by Buch *et al* [226] (see [227] for another algorithm). For proton disordered ices we calculated the free energy for a particular proton disordered configuration. Due to the fact that there are many configurations compatible with a given oxygen lattice, there is a degenerational contribution to the free energy. The degenerational entropy of ice was estimated by Pauling in 1935 [156] as $S_{\rm deg} = k_{\rm B}\ln\Omega = k_{\rm B}N\ln(3/2)$. Therefore, the disordered ice phases have an extra contribution to the free

Table 4. Free energy of the ice polymorphs for the SPC/E model (with $q_r = q_v = q_e = 1$). The free energy reported in the last column corresponds to the sum of all the terms $(A_0 + \Delta A_1 + \Delta A_2)$ plus the degenerational free energy $(-Nk_BT \ln(3/2))$ for the case of orientationally disordered phases (the typical uncertainty of the resulting solid free energies is about 0.05 Nk_BT). The number of molecules used for each solid phase is indicated in parenthesis just after the Roman numeral of the phase. A finite size correction (Frenkel–Ladd type) has been included in A_0. The thermal de Broglie wavelength Λ was set to $\Lambda = 1$ Å. The residual internal energy of the ice U is reported, so that the entropy of the solid can be obtained easily from the relation $S = (U - A_{sol})/T$. The orientational contribution to A_0 (equation (29)) was computed from the approximate expression given in [48].

Ice	p (bar)	T (K)	d (g cm^{-3})	$\frac{U}{Nk_BT}$	$\frac{\Lambda_E}{k_BT}$ (Å^{-2})	$\frac{A_0}{Nk_BT}$	$\frac{\Delta A_2}{Nk_BT}$	$\frac{\Delta A_1}{Nk_BT}$	$\frac{A_{sol}}{Nk_BT}$
Ih(288)	500	150	0.965	−46.08	25 000	29.46	−16.92	−48.94	−36.84
Ic(216)	2 620	150	0.983	−46.14	25 000	29.45	−16.85	−48.95	−36.80
II(432)	5 000	150	1.269	−46.42	25 000	29.47	−17.27	−49.08	−36.91
III(324)	5 000	150	1.229	−44.89	25 000	29.46	−19.10	−45.66	−35.73
IV(432)	5 000	150	1.353	−43.97	25 000	29.47	−18.23	−45.54	−34.73
V(504)	5 000	150	1.316	−44.39	25 000	29.47	−20.11	−44.17	−35.23
VI(360)	25 000	150	1.492	−43.29	25 000	29.46	−19.78	−42.81	−33.56
VI(360)	25 000	225	1.474	−27.88	25 000	29.46	−19.94	−28.69	−19.60
VII(432)	81 690	443	1.700	−9.79	9 000	26.40	−16.58	−13.81	−4.41
VIII(600)	60 000	225	1.743	−23.92	25 000	29.47	−19.38	−24.68	−14.61
IX(324)	5 000	150	1.244	−46.31	25 000	29.46	−19.10	−46.93	−36.60
XI(360)	500	150	0.971	−46.26	25 000	29.46	−18.01	−48.08	−36.65

energy of $-Nk_BT \ln(3/2)$. Ice III and V present partial proton ordering [228], and this decreases the Pauling estimate a little, but the effect of this change on the phase diagram was found to be small [229, 230]. For this reason we shall also use the Pauling estimate for ices III and V. For ices II, IX, VIII and the antiferroelectric analogue [231] of ice XI the protons are ordered, and there is no degenerational entropy contribution. Generating an initial configuration for proton ordered ices is relatively straightforward.

The free energy calculations were performed in the NVT ensemble using the equilibrium shape of the simulation box obtained in anisotropic NpT runs. The locations of the springs of the ideal Einstein crystal field were chosen to be close to the equilibrium positions/orientations of the molecules. The computed free energy should not depend on the particular choice of the positions and orientations of the ideal Einstein crystal field (provided that they are sufficiently close to the equilibrium position and orientations of the molecules in the absence of the external field). Several strategies are possible. For instance, one could choose the position/orientations of the external field as those obtained from an energy minimization at constant density (using the equilibrium box shape of the system). Another possibility is to use the experimental crystallographic positions (if available) of the atoms of the molecule and modify them slightly to satisfy the bond lengths and angles of the model (the bond lengths may be different in the model and in the real molecule, as for instance in SPC/E water). Also, experimental crystallographic positions (if available) could be used for the reference point (oxygen in the case of water), and the orientations could be optimized from an energy minimization. We have used this last approach for ices. This approach has also been used recently by Wierzchowski and Monson for gas hydrates [68]. To obtain ΔA_2 we used Gaussian integration with 12 points. ΔA_1 was evaluated from runs (200 000 cycles) of the ideal Einstein crystal with fixed center of mass. The value of Λ_E (in $k_BT/(\text{Å})^2$) was identical to the value selected for $\Lambda_{E,a}$ and $\Lambda_{E,b}$ (in k_BT units). The value of Λ_E was chosen so that the computed value of ΔA_1 differs by about $0.02N_BT$ units from the lattice energy of the solid (defined as the intermolecular energy of the system when the molecules occupy the positions and orientations of the external Einstein field).

Coexistence between phases at 150, 225 and 443 K was investigated. Therefore, the free energy calculations have been performed at these temperatures. In tables 4 and 5 we report the free energy $(A_{sol}/(Nk_BT))$ calculated for different ice phases for SPC/E and TIP4P respectively. The different contributions to the free energy (A_0, ΔA_1, ΔA_2) are given. The term A_0 is the sum of $A^{CM}_{Eins\text{-}id}$ plus ΔA_3 plus a finite size correction (Frenkel–Ladd type, $(2/N) \ln N$). For proton disordered ices the value of A_{sol} is the sum of A_0, ΔA_1, ΔA_2 and the Pauling degeneracy entropy $-Nk_BT \ln(3/2)$. For proton ordered ices (XI, II, IX, VIII) the total value of A is just the sum of A_0, ΔA_1, ΔA_2. The lattice energy $U_{lattice}/Nk_BT$ is the energy of the solid when all water molecules remain fixed on the position/orientations of the Einstein crystal field (the value of $\Delta A_1/(Nk_BT)$ being quite close to $U_{lattice}/Nk_BT$). The free energies of the SPC/E model are lower than those of the TIP4P (this is consistent with their lower internal energies).

As a consistency check we determined via Einstein crystal calculations the free energy of ice VI at two different thermodynamic conditions for SPC/E and TIP4P. Let us discuss the results for TIP4P. For TIP4P (ice VI) we obtained from free energy calculations $A_1(225 \text{ K}, 1.480 \text{ g cm}^{-3}) = -17.67\ Nk_BT$ and $A_2(150 \text{ K}, 1.498 \text{ g cm}^{-3}) = -30.65\ Nk_BT$ (both states having a pressure of 25 000 bar). Starting from the value of A_1 and performing thermodynamic integration we estimated $A_2(150 \text{ K}, 1.498 \text{ g cm}^{-3}) = -30.66\ Nk_BT$, in excellent agreement with the value obtained from Einstein crystal calculations.

10.4. Determining the initial coexistence points

Once the free energy of each phase is known, it is possible to find the points in the pressure–temperature plane at which two

Table 5. The same as table 4 for the TIP4P model.

Ice	p (bar)	T (K)	d (g cm^{-3})	$\frac{U}{Nk_BT}$	$\frac{\Delta_E}{k_BT}$ (Å^{-2})	$\frac{A_0}{Nk_BT}$	$\frac{\Delta A_2}{Nk_BT}$	$\frac{\Delta A_1}{Nk_BT}$	$\frac{A_{sol}}{Nk_BT}$
Ih(288)	1365	150	0.966	−42.50	25 000	29.46	−16.92	−45.55	−33.45
Ic(216)	500	150	0.958	−42.50	25 000	29.45	−16.96	−45.52	−33.47
II(432)	8230	150	1.269	−41.80	25 000	29.46	−16.98	−44.75	−32.28
III(324)	5000	150	1.237	−41.43	25 000	29.46	−18.82	−42.63	−32.39
IV(432)	5000	150	1.353	−40.86	25 000	29.47	−18.18	−42.60	−31.74
V(504)	5000	150	1.315	−41.13	25 000	29.47	−19.62	−41.56	−32.11
VI(360)	25 000	150	1.498	−40.26	25 000	29.46	−19.20	−40.48	−30.65
VI(360)	25 000	225	1.480	−25.91	25 000	29.46	−19.58	−27.12	−17.67
VII(432)	78350	443	1.700	−8.66	9 000	26.40	−16.76	−12.85	−3.63
VIII(600)	60000	225	1.743	−21.97	25 000	29.47	−19.11	−23.24	−12.90
IX(324)	5000	150	1.238	−42.25	25 000	29.46	−18.85	−42.56	−31.98
XI(360)	500	150	0.959	−42.53	25 000	29.46	−17.03	−45.50	−33.09
XII(540)	5000	150	1.358	−40.94	25 000	29.47	−18.80	−42.20	−31.94

Table 6. Coexistence points for TIP4P and SPC/E models from free energy calculations (and thermodynamic integration).

Model	Phases	T (K)	p (bar)
SPC/E	Ih–II	150	−444
SPC/E	II–VI	150	25 270
SPC/E	liquid–II	250	5 000
SPC/E	liquid–VI	225	20 690
SPC/E	VI–VIII	225	57 860
SPC/E	liquid–VIII	225	57 500
SPC/E	liquid–VII	443	103 520
SPC/E	liquid–Ih	211	500
SPC/E	liquid–Ic	210	500
SPC/E	liquid–XI	187	500
TIP4P	liquid–Ih	228.8	500
TIP4P	Ih–II	150	3 041
TIP4P	II–VI	150	6 215
TIP4P	II–V	152.6	5 000
TIP4P	II–III	180.3	5 000
TIP4P	liquid–III	196.6	5 000
TIP4P	liquid–V	204.1	5 000
TIP4P	liquid–VI	225	8 940
TIP4P	VI–VIII	225	57 290
TIP4P	liquid–VII	443	91 940
TIP4P	liquid–Ic	228.8	500
TIP4P	liquid–XI	192	500
TIP4P	liquid–XII	205.0	5 000

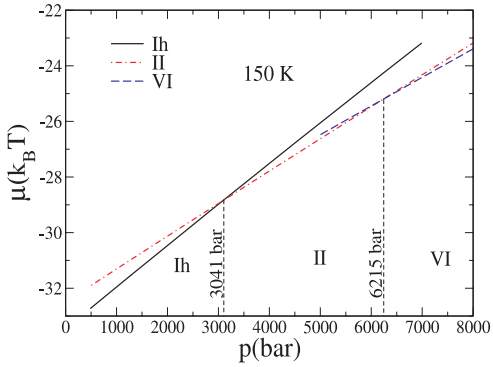

Figure 5. Chemical potential as a function of pressure at 150 K for ices Ih, II and VI modeled with TIP4P.

phases have the same chemical potential, i.e. the coexistence points. Given that most of the free energies and equations of state were obtained either at temperatures of 150 or 225 K and at pressures of 500 or 5000 bar, we focus the search for the coexistence points at these temperatures and pressures.

Figure 5 shows the chemical potential as a function of the pressure at 150 K for ices Ih, II, and VI. For a given pressure, the phase of lowest chemical potential is the most stable one. Ice Ih is the stable phase up to 3041 bar. At this pressure, ices Ih and II coexist. Beyond 3041 bar, ice II is the stable phase up to 6215 bar, where the chemical potentials of ices II and VI are equal. For higher pressures ice VI is the stable phase. By performing similar plots, coexistence points between different phases could be determined. In table 6 these coexistence points are presented (for TIP4P and SPC/E). The relative stability between ices Ih and Ic (or between ices V and XII) could not be determined, since the free energy difference between these solids was smaller than the typical uncertainty of our free energy calculations (0.05 Nk_BT). As to the stability of ices Ih(Ic) with respect to ice XI (we used the antiferroelectric version of ice XI of Davidson and Morokuma [231] rather than the true ferroelectric version), we found that the XI–Ih transition occurs at 84 K for SPC/E and 18 K for TIP4P (the proton ordered ice XI being the stable phase at low temperatures).

The region of the phase diagram corresponding to 5000 bar (figure 6) is the most problematic given that there are as many as seven phases competing; namely, ices II, III, IV, V, IX and XII and the liquid. For SPC/E, ice II is clearly the most stable phase among the solid polymorphs. The liquid is again the stable phase at high temperatures (beyond 250 K). For the case of TIP4P, ices V and XII are the solid phases of lower chemical potential. The free energy difference between both polymorphs (0.008 Nk_BT) is smaller than the error bar (0.05 Nk_BT), so we could not determine which one is the most stable. Liquid water coexists either with ice XII or with ice V at 205 K and 5000 bar.

10.5. The phase diagram of water

Once an initial coexistence point has been determined, by using Gibbs–Duhem integration (either $\mathrm{d}p/\mathrm{d}T$ or $\mathrm{d}T/\mathrm{d}p$)

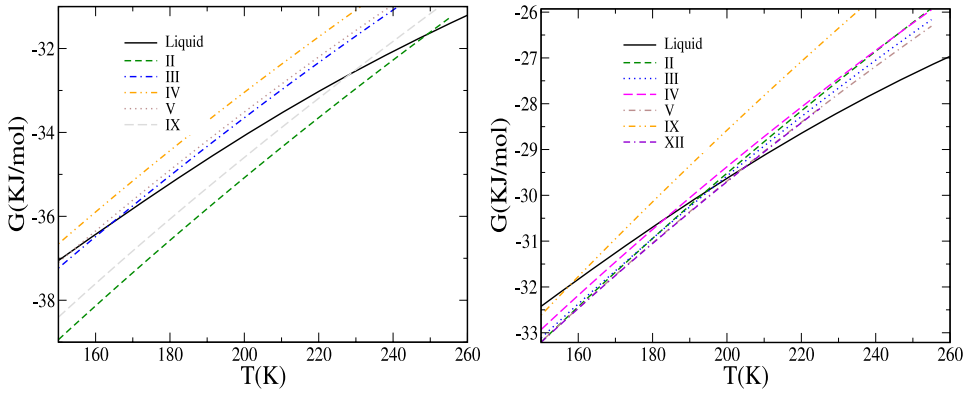

Figure 6. Gibbs free energy versus temperature at 5000 bar for different phases of SPC/E (left) and TIP4P (right).

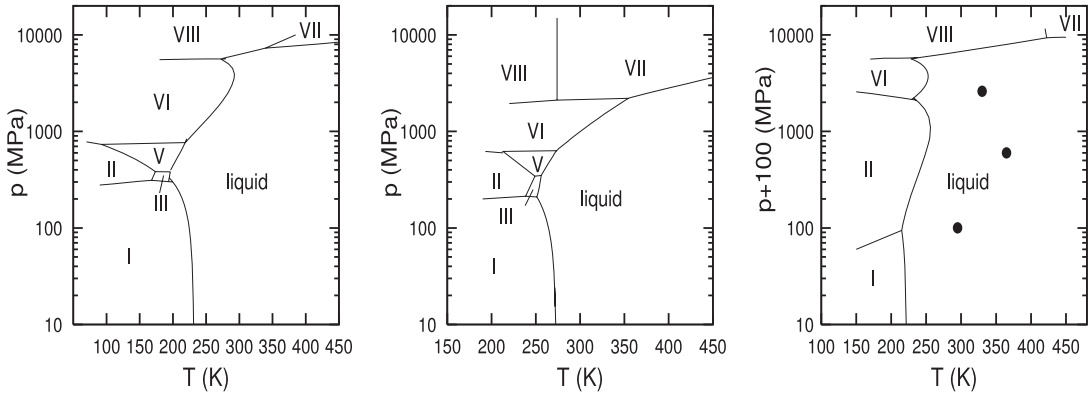

Figure 7. Phase diagram of water as obtained from experiment (center) and from computer simulations for the TIP4P model (left) and for the SPC/E model (right). The filled circles on the right panel indicate the stability limit of the solid phases in NpT simulations (without interfaces). Notice the shift of 100 MPa in the right panel.

it is then possible to draw the complete phase diagram. In certain cases the point where two coexistence lines met (triple point) was used as the origin of the third coexistence line emerging from the triple point. The complete phase diagram of SPC/E and TIP4P is presented in figure 7. As can be seen SPC/E fails in reproducing the phase diagram of water (notice for instance that ice Ih is stable for this model only at negative pressures), whereas TIP4P provides a qualitatively correct description of the phase diagram (except for the high pressure region of the phase diagram). The reason for the failure of SPC/E and success of TIP4P has been identified recently. The low quadrupole moment of SPC/E and the high value of the ratio dipole/quadrupole of this model is the cause of the failure [112, 114]. In fact, TIP4P provides a quadrupole moment and a dipole/quadrupole ratio in much better agreement with experiment. The effect of a quadrupole moment on the vapor–liquid equilibria of molecular models is well known [232–234]. However it seems that the role of the quadrupole in water properties has been overlooked, in spite of some warnings about its importance [235–237, 218, 238, 239]. Figure 7 illustrates how the evaluation of the phase diagram of water by computer simulation is indeed possible.

10.6. Hamiltonian Gibbs–Duhem simulations for water

The liquid–Ih solid coexistence temperatures at $p = 1$ bar for TIP4P and SPC/E have been estimated from free energy calculations to be $T = 232 \pm 5$ and 215 ± 5 K, respectively. These numbers are in relatively good agreement with estimates from other authors for TIP4P [22, 23, 187] and for SPC/E [185, 186, 240, 101]. An interesting question is whether these two values (for TIP4P and SPC/E) are mutually consistent. Starting from the SPC/E model and performing constant pressure Hamiltonian Gibbs–Duhem simulations (integrating the generalized Clapeyron equation as described previously) one should recover the melting temperature of the TIP4P. In fact starting from the SPC/E ice Ih melting point we obtain $T = 232.3$ K for TIP4P (see figure 8), in very good agreement with the result obtained through free energy calculations.

Once the melting points of ice Ih for TIP4P and SPC/E seem to be firmly established one could use these values to estimate (by using Hamiltonian Gibbs–Duhem simulations) the melting point of another water model, for instance TIP5P [241]. Obviously, the properties of the final model should be independent of the reference model. When the starting model is SPC/E we obtain $T = 275$ K for TIP5P, whereas the calculated result using the TIP4P model as a

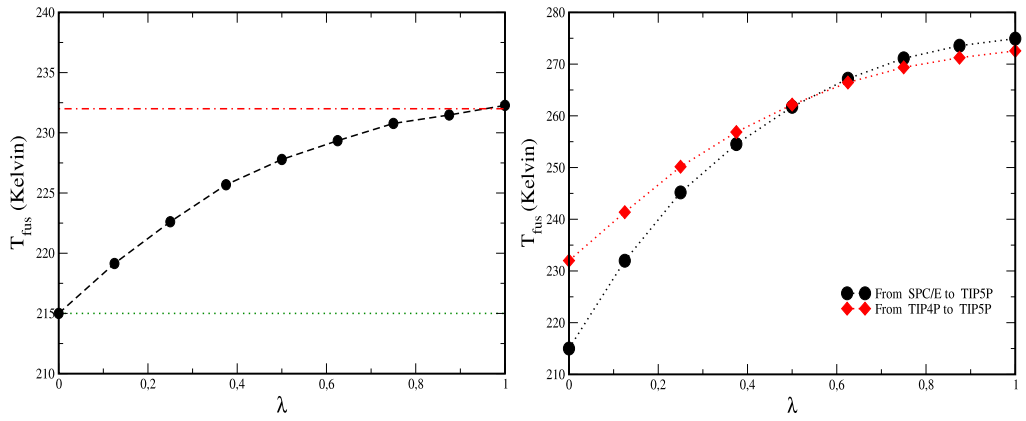

Figure 8. Hamiltonian Gibbs–Duhem integration results. Left: melting temperature of ice Ih as a function of the parameter λ connecting the models SPC/E (λ = 0) and TIP4P (λ = 1). The points were obtained by using Hamiltonian Gibbs–Duhem integration. The dashed line is a guide to the eye. The horizontal lines correspond to the melting temperatures of SPC/E (dotted line) and TIP4P (dashed–dotted line) as obtained from free energy calculations. Right: melting temperature of ice Ih for the TIP5P model (λ = 1) obtained from Hamiltonian Gibbs–Duhem integration starting from SPC/E or TIP4P models. When connecting two water models by Hamiltonian Gibbs–Duhem integration, the position of the oxygen atom and of the HOH bisector was the same in both models.

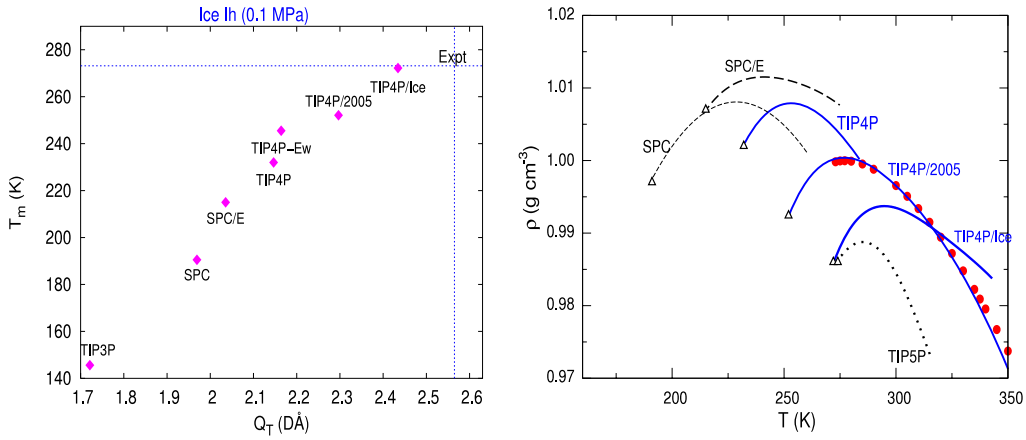

Figure 9. Left: melting temperature of ice Ih at 1 bar plotted as a function of the quadrupole moment Q_T (taken from [112]). Q_T is defined as the value of $(Q_{xx} - Q_{yy})/2$ of the quadrupolar tensor, where the x axis joins the two H atoms and the y axis is perpendicular to the molecular plane. Right: density of water at room pressure as a function of temperature as obtained from experiment (filled circles) and from computer simulations of several water models (lines). The open triangles indicate the melting point of ice Ih for each model.

reference is $T = 273$ K. The agreement between both estimates is satisfactory taking into account that the error of the Gibbs–Duhem integration is about 3 K. This is is further illustrated in the right panel of figure 8, which shows the results of the integration. By using Hamiltonian Gibbs–Duhem integration the melting points of ice Ih for other models of water were determined. They are presented in table 7. Notice that most of the water models tend to give low melting points.

For models with three charges (SPC, SPC/E, TIP3P, TIP4P, TIP4P/Ew, TIP4P/Ice, TIP4P/2005) a correlation between the melting point and the quadrupole moment has been found. This is illustrated in figure 9. It is seen that models with rather low quadrupole moment (TIP3P, SPC, SPC/E) provide rather low melting points. The melting temperature of TIP4P is closer to the experimental value. Motivated by this we have proposed a new modified TIP4P model, with a higher quadrupole moment, able to reproduce the experimental melting point of water. We have denoted this new model as TIP4P/Ice [214]. A second finding was that for three charge models the temperature at which the maximum in density occurs at room pressure (TMD) is about 20–25 K

Table 7. Melting points obtained from free energy calculations (TIP4P and SPC/E), Hamiltonian Gibbs–Duhem integration (rest of the models) [215, 211, 242, 214] and direct fluid–solid coexistence. The last column is the value of T_s (see text) obtained from simulations of ice Ih with a free interface. TIP4P-Ew is a water model proposed by Horn *et al* [243] and NvdE is a six site model proposed by Nada and van der Eerden [244].

Model	Free energy	Direct coexistence	Free surface
TIP4P/Ice	272(6)	268(2)	271(1)
TIP4P/2005	252(6)	249(2)	249(3)
TIP4P-Ew	245.5(6)	242(2)	243(2)
TIP4P	232(4)	229(2)	230(2)
TIP5P	274(6)	271(2)	—
SPC/E	215(4)	213(2)	217(2)
NvdE	290(3)	288(3)	—

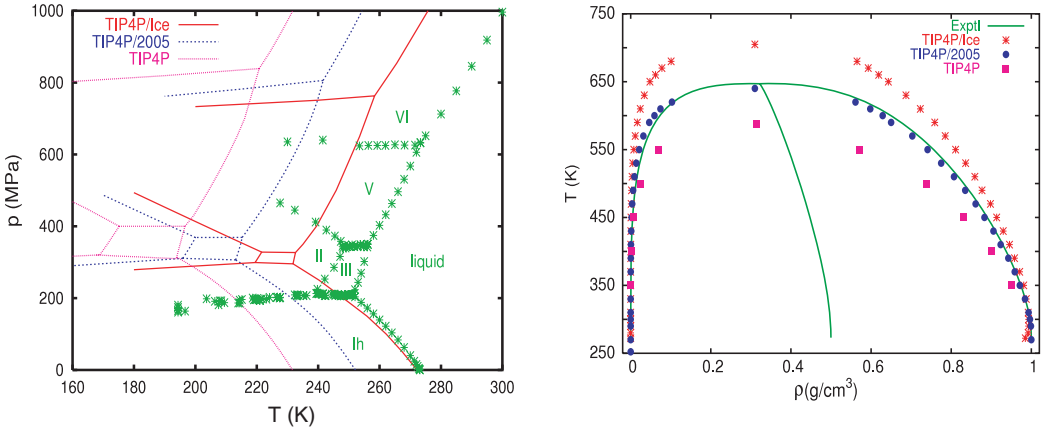

Figure 10. Phase diagram for the TIP4P family. (a) Left panel: fluid–solid equilibria (the lines show the predictions for several TIP4P-like models and the symbols represent the experimental data). (b) Right panel: vapor–liquid equilibria (the symbols show the predictions for TIP4P-like models and the lines represent the experimental data).

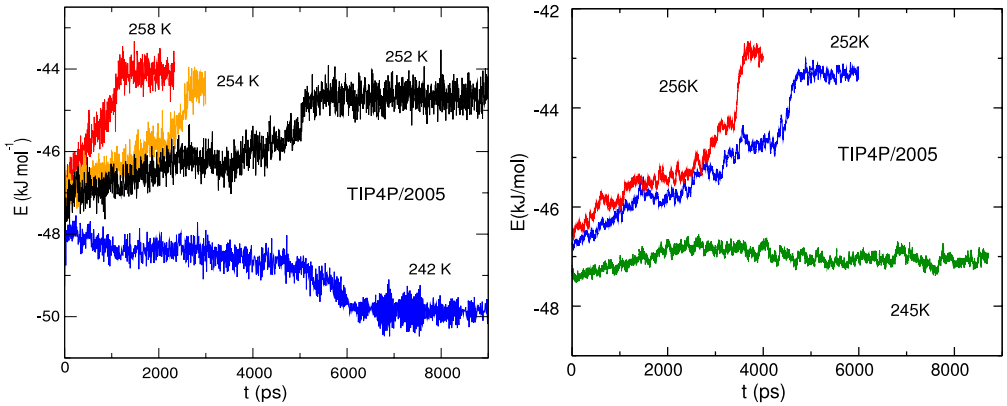

Figure 11. Left panel: evolution of the total energy (per mole of molecules) in NpT MD simulations of a box containing ice and liquid water at 1 bar for the TIP4P/2005 model. Right panel: total energy as a function of time obtained at several temperatures by performing MD simulations of TIP4P/2005 for a block of ice I_h with a free surface.

above the melting temperature [242, 245]. Experimentally, for water the maximum in density occurs 4° above the melting point. Therefore it is impossible with three charge models to reproduce simultaneously the melting point and the TMD. It is likely that the inclusion of quantum effects and/or polarizability [246–252] may be needed to reproduce these two properties simultaneously. For this reason we have proposed the TIP4P/2005, which reproduces the TMD of real water better than any other water model proposed so far (see figure 9(b)). An interesting question is to analyze whether these new models still predict correctly the phase diagram of water. By using Hamiltonian Gibbs–Duhem integration it is possible to estimate the phase diagram of a certain water model, starting from the phase diagram of another reference model. Thus, by using TIP4P as reference, we have estimated the complete phase diagrams for TIP4P/Ice and TIP4P/2005. The obtained phase diagrams are presented in figure 10. As can be seen these models predict quite well the fluid–solid equilibria of water, improving the predictions of TIP4P. TIP4P/2005 yields also an excellent prediction of the vapor–liquid equilibria.

10.7. Direct coexistence simulations

To estimate the melting point of ice Ih for several water models by direct coexistence, NpT simulations were performed with 870 molecules and the MD program Gromacs [253, 254]. In the initial configuration half of them formed ice, and the other half were in the liquid state. Both phases were in contact, so that these are direct coexistence simulations.

The evolution of the energy for the TIP4P/2005 model with time is presented in figure 11. As can be seen, the energy increases with time for $T = 252, 254, 256$ K, reaching a plateau (the plateau indicates the complete melting of the ice). The energy decreases for $T = 242$ K, reaching a plateau (the plateau indicates the complete freezing of the water). Snapshots of these final configurations can be found in [189]. At a temperature of 249 K the energy does not change with time, and the interface is stable after 10 ns. Therefore, this is the estimate of the melting point by direct coexistence for TIP4P/2005. Similar runs were performed for other water models. In table 7 the melting points of different water models as estimated from direct coexistence are compared to those obtained from free energy calculations.

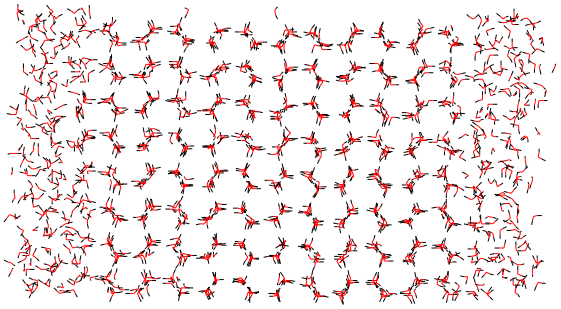

Figure 12. Instantaneous configuration of the TIP4P/Ice system at $T = 268$ K at the end of a 8 ns run. Although the temperature is well below the melting point of the model, a quasi-liquid layer is clearly present in the ice–vacuum interface.

The agreement between both techniques is quite good. Direct interface simulations have been used by several authors to estimate melting points or ice growth rates for different water models [92, 255, 194, 256, 187, 192].

10.8. Melting point as estimated from simulations of the free surface

In figure 11 the evolution of the total energy of ice Ih (having a free surface) with time is presented [209]. At high temperatures, the total energy of the system increases continuously and then reaches a plateau (that corresponds to the complete melting of the solid). The behavior at low temperatures is different. At the beginning (first 1–2 ns) there is an increase of the energy, but after this the energy remains approximately constant, apart from the thermal fluctuations. The analysis of the configurations of the TIP4P/2005 at $T = 245$ K shows that the increase of energy during the first 1 ns is due to the formation of a thin liquid layer at the surface of ice, which may indicate the onset of surface melting, mentioned already in the introduction, and first proposed by Faraday [257]. The formation of a quasi-liquid layer on the surface of ice below T_m has been found both in experiment (see [258–262] and references therein) and in computer simulation for several potential models of water [263–266, 92], and it has been explained by several theoretical treatments [258, 260]. By repeating the simulation at several temperatures it is possible to determine the lowest temperature at which the block of ice melts T_+, and the highest temperature at which it does not melt T_-. By taking the average of these two temperatures we obtain what we call $T_s = 1/2(T_+ + T_-)$. T_s provides an estimate of the melting point. The values of T_s obtained for water models are presented in table 7. As can be seen, T_s is identical to T_m, within the error bar. Thus for ice Ih the presence of a free surface suppresses superheating and ice melts at the equilibrium melting temperature (although runs of about 10 ns or longer may be needed). In figure 12 the final configuration (after a 8 ns run) obtained for TIP4P/Ice at a temperature well below the melting point of the model ($T = 264$ K) is shown. As can be seen, a quasi-liquid layer is already present in the system.

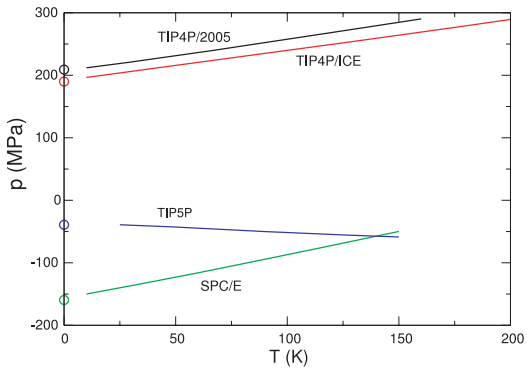

Figure 13. Coexistence lines between ices Ih and II as obtained from Gibbs–Duhem simulations for TIP4P/2005, TIP4P/Ice, SPC/E and TIP5P models (solid lines). The symbols represent the coexistence pressures as obtained from the properties of the systems at zero temperature. For each water model, ice Ih is the stable phase below the coexistence line (low pressures) and ice II is the stable phase above the coexistence line (high pressures).

Table 8. Residual internal energy (in kcal mol^{-1}) of several ice polymorphs at $T = 0$ K and $p = 0$ for popular water models. The results for the most stable phase of each model are presented in bold.

Ice	TIP4P/Ice	TIP4P/2005	SPC/E	TIP5P
Ih	**−16.465**	**−15.059**	−14.691	−14.128
II	−16.268	−14.847	**−14.854**	**−14.162**
III	−16.140	−14.741	−14.348	−13.320
V	−16.049	−14.644	−14.169	−13.101
VI	−15.917	−14.513	−13.946	−12.859

10.9. Properties at 0 K

In table 8 the residual internal energies at zero T and p are given for the TIP4P/Ice, TIP4P/2005, SPC/E and TIP5P models. For TIP4P/Ice and TIP4P/2005, ice Ih is the structure with the lowest energy (probably ice XI, which is a proton ordered version of ice Ih, would have an slightly lower energy, but it was not considered for this study). However, for SPC/E and TIP5P the lowest internal energy corresponds to ice II. Thus, for TIP4P/2005 and TIP4P/Ice ice Ih is the stable phase at zero pressure and temperature whereas for SPC/E and TIP5P the stable phase is ice II. From the properties at 0 K it is simple to locate the Ih–II transition pressure at 0 K (see [267]). In figure 13 the predicted pressures using the calculations at 0 K are presented (circles). The lines represent the results obtained from free energy calculations (used to obtain an initial coexistence point at 150 K) and Gibbs–Duhem integration. It may be seen that both sets of calculations agree quite well so both sets of results are mutually consistent (i.e., the estimated coexistence pressure at 0 K is the same). It is clear that ice II is more stable than ice Ih at zero temperature and pressure for the SPC/E and TIP5P models. This example illustrates how 0 K properties can be used to test for self-consistency in phase diagram predictions. They are also quite useful to test the performance of water models [268, 89, 90, 269, 267].

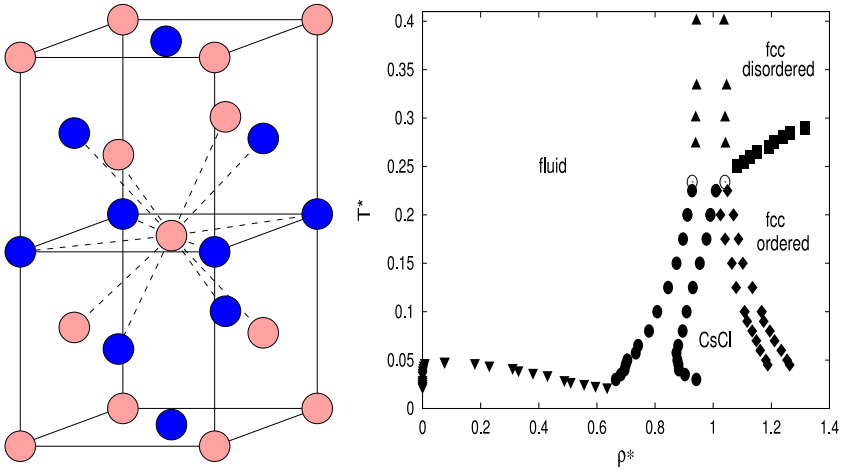

Figure 14. Left: tetragonal ordered structure of the RPM model. The atoms form an fcc structure, but the ions are ordered. Right: phase diagram of the RPM model showing the equilibria between vapor and liquid (inverted triangles), fluid and CsCl-like structure (filled circles), CsCl-like structure and tetragonal (fcc ordered) phase (rhombs), fluid and tetragonal structure (open circles), fluid and fcc disordered structure (triangles) and ordered–disordered fcc phases (squares).

11. Phase diagram for a primitive model of electrolytes

Let us now present another example of a phase diagram calculation for a completely different model, the restricted primitive model (RPM). The restricted primitive model (RPM) is one of the simplest models of electrolytes. It this model the cations are represented by hard spheres of diameter σ having a charge $+q$ and anions represented by hard spheres of diameter σ having a charge $-q$. The model is quite simple and for this reason it can also be studied theoretically [270, 271]. The system has vapor–liquid equilibrium [272–274] (in spite of the absence of dispersive forces). Several solid structures can be considered [275], the simplest being the CsCl-like structure (a bcc type of structure with the anions occupying the vertices of a cube and the cations occupying the center of the unit cell). Another possible structure is the fcc disordered structure. In this structure the ions occupy an fcc lattice, but with positional disorder (cations and anions occupy the lattice points in a disordered way). At low temperatures it is possible to conceive a solid structure with an fcc arrangements of the ions, but with positional order. The symmetry of the phase is tetragonal. This phase will be labeled as the tetragonal phase [49]. It is presented in figure 14. Free energy calculations (Einstein crystal) were performed to determine the free energy of the CsCl and tetragonal structures. Due to the presence of partial disorder the Einstein crystal method can not be applied directly (to a snapshot) to get the free energy of the fcc disordered structure (although one may suspect that a strategy similar in spirit to that proposed for the plastic crystal phases can also be successful here if the external field is able to lead the system from disordered configurations to an ordered solid without crossing first order transitions). The RPM system becomes a hard sphere at infinitely high T for which the free energy is known (a trivial mixing contribution should be added). For this reason the free energy of the fluid and of the fcc disordered solid can be obtained by thermodynamic integration. Exchange moves (where a cation and an anion exchange their positions) were used to sample correctly the disorder, both in the fluid and in the fcc disordered structure.

After computing the free energies, some initial coexistence points were determined, and then by using Gibbs–Duhem integration the complete phase diagram was computed. The resulting phase diagram [276, 277, 49, 50] is presented in figure 14. At high temperatures, freezing leads to the substitutionally disordered close-packed structure. By decreasing the temperature this solid structure undergoes an order–disorder transition transforming into the tetragonal solid. At low temperatures freezing leads to the cesium chloride structure (CsCl), which undergoes a phase transition to the tetragonal structure at high pressures. The tetragonal solid is the stable solid phase at low temperatures and high densities. In a narrow range of temperatures coexistence between the fluid and the tetragonal solid is observed. Three triple points are found for the model considered: the usual vapor–liquid–CsCl, the fluid–CsCl–tetragonal and the fluid–fcc disordered–tetragonal triple point (notice in figure 14 the narrow range of the fluid–tetragonal solid coexistence line).

Although initially conceived to describe electrolytes and ionic salts, the RPM has been found to be quite useful to describe certain colloidal mixtures, consisting in equimolar mixtures of colloidal particles of equal size, but with charges of different sign. Thus a colloidal version of the RPM exists [278]. For these colloidal mixtures, three different solid phases have been found experimentally, the fcc disordered solid, the CsCl solid and an fcc ordered structure [279, 280]. The fcc ordered structure was found to be of CuAu type, rather than the tetragonal structure of figure 14. This difference with the RPM phase diagram seems to be due to the fact that in colloidal mixtures the interaction between charged particles is of Yukawa type rather than being purely Coulombic. This is so because the interaction between charged particles is screened by the presence of an ionic atmosphere due to the counter-ions of the colloids. In fact, when this screening is incorporated in

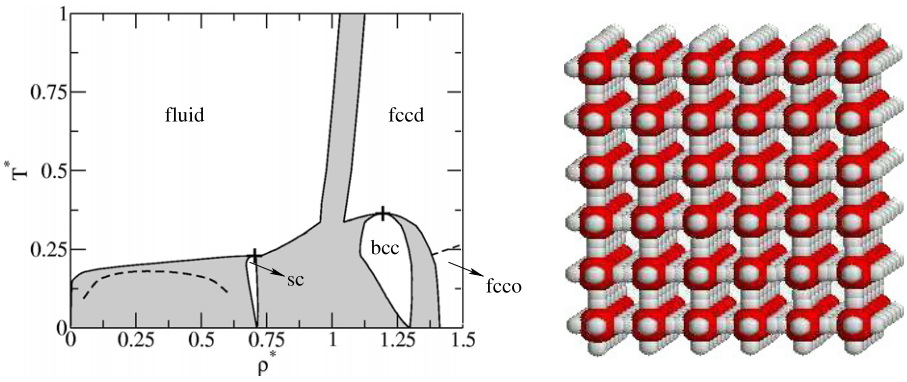

Figure 15. Left: phase diagram of the octahedral six patch model. Labels show the region of stability of each phase. The dashed line in the fluid–sc coexistence region signals the expected fluid–fluid binodal (see [57] for more details). Right: structure of the low density sc solid for the octahedral anisotropic model.

the potential with a Yukawa type model, the CuAu structure was found to be stable in a thermodynamic region between the CsCl and the tetragonal structure [56, 281].

In summary, the RPM has proved to be quite useful in the description of mixtures of charged colloidal particles. It would be of interest to determine the phase diagram for a model where the two spheres of the model present different sizes. This is usually called the primitive model. In fact the primitive model (where cations and anions have different sizes) may indeed be a more general model than RPM, since in real ionic fluids the size of the ions is usually different. A colloidal realization of the PM model has been obtained experimentally [279]. Finally, there is an increasing interest in determining the properties of ionic liquids. It would be of interest to determine the factors affecting the melting point of ionic liquids [282] which are regarded as new solvents [283]. Work in this direction has appeared recently [284].

12. Phase diagram of a simplified model of globular proteins

A final example of the application of the techniques described here is provided by the calculation of the phase diagram of a simple model of globular proteins. During the last few years there has been an increasing number of studies of the phase behavior of globular proteins using very simplified models. The first studies have been performed using short ranged isotropic potentials and, even with these very simple models, it was already possible to reproduce some of the features of the phase diagram of proteins, e.g. the existence of a metastable critical point [285]. However, proteins are known to form very low density crystals, with densities below those of the close-packed crystals typically formed by isotropic potentials, which is indicative of highly directional interactions [286]. Further evidence of the importance of anisotropy in the interactions among proteins has been recently obtained in a theoretical study of the fluid–fluid equilibria. This study has shown that a quantitative agreement with experiments is obtained by the introduction of anisotropy [287], as opposed to isotropic models, that only provided a qualitative description. Moreover, theoretical studies of the phase behavior of anisotropic models are also acquiring much interest due to the fact that several experimental groups have recently been able to produce colloids that are anisotropic either in shape or in their interactions [288–291]. So far there have been already a few theoretical studies of the phase behavior of simple anisotropic models [48, 292–295, 58, 296, 297], although most of them were concerned with the fluid–fluid equilibria rather than with the solid–fluid and solid–solid equilibria.

We have used a very simplified model, which consists of a repulsive core (the Lennard-Jones repulsive core), plus an attractive tail modulated by Gaussian functions located at some given positions or patches, which will be specified by some vectors. The total energy between two interacting particles will be given by [298, 299, 57]:

$$V(\mathbf{r}_{ij}, \mathbf{\Omega}_i, \mathbf{\Omega}_j) = \begin{cases} V_{\mathrm{LJ}}(r_{ij}) & r_{ij} < \sigma_{\mathrm{LJ}} \\ V_{\mathrm{LJ}}(r_{ij}) V_{\mathrm{ang}}(\hat{\mathbf{r}}_{ij}, \mathbf{\Omega}_i, \mathbf{\Omega}_j) & r_{ij} \geqslant \sigma_{\mathrm{LJ}} \end{cases} \tag{78}$$

$$V_{\mathrm{ang}}(\hat{r}_{ij}, \mathbf{\Omega}_i, \mathbf{\Omega}_j) = \exp\left(-\frac{\theta^2_{k_{\min},ij}}{2\sigma^2_{\mathrm{patchy}}}\right) \exp\left(-\frac{\theta^2_{l_{\min},ji}}{2\sigma^2_{\mathrm{patchy}}}\right), \tag{79}$$

where V_{LJ} is the Lennard-Jones potential, σ_{patchy} is the standard deviation of the Gaussian, $\theta_{k,ij}$ ($\theta_{l,ji}$) is the angle formed between patches k (l) on atom i (j) and the interparticle vector $\mathbf{r}_{ij}$ ($\mathbf{r}_{ji}$) and $k_{\min}$ ($l_{\min}$) is the patch that minimizes the magnitude of this angle. The interaction is a maximum when both patches are pointing at each other along the interparticle vector $\mathbf{r}_{ij}$ and it will decrease as the particles deviate further from this equilibrium orientation. We have chosen to study a model with six patches distributed in an octahedral symmetry, and a relatively narrow width of the patches ($\sigma_{\mathrm{patchy}} = 0.3$ rad), for which it is expected that the low density simple cubic (sc) crystal becomes stable.

Besides the sc crystal, in which each of a particle's patches is pointing at one of its six nearest neighbors (see figure 15), there are other three solid phases that might be formed with this model and at this patch width, $\sigma_{\mathrm{patchy}} = 0.3$ rad. The first structure is a body centered cubic (bcc) solid, in which each patch is aligned with the second neighbors. This structure can

be also seen as two interpenetrating sc lattices that almost do not interact between each other (similar to the behavior of high density ice polymorphs). Therefore, a higher density crystal is obtained with a low penalty in the energy. At high pressures it is expected that a close packed face centered cubic (fcco) structure will also appear. In this case the patches will also be pointing to the second neighbors. This structure exhibits a much higher energy than both the sc and the bcc solids. Finally, at high temperatures, it is expected that a plastic phase will also appear (fccd), i.e. a solid where the center of mass of each particle is located at the lattice positions of a fcc structure, but that is orientationally disordered.

Following the procedure described before, the coexistence point between two phases was computed by imposing the conditions of equal temperature, pressure and chemical potential. The free energy of the fluid was computed by thermodynamic integration. In the case of the fluid, the equation of state was integrated to very low densities, where the fluid can be considered to behave as an ideal gas. The free energy of the solid was computed by Einstein crystal calculations. Once a coexistence point is known all the coexistence lines can be traced using the Gibbs–Duhem method.

The resulting phase diagram is plotted in figure 15. At high temperatures the fluid freezes into the orientationally disordered plastic crystal phase (fccd), at intermediate temperatures into the bcc solid and at low temperatures into the sc crystal. The sc structure is destabilized at high pressure by the bcc solid and, at even higher pressures, the ordered fcc solid becomes stable (fcco). This fcco ordered solid transforms into a plastic crystal fccd as the temperature increases. There are three triple points in the phase diagram: the fluid–sc–bcc, fluid–fccd–bcc and bcc–fccd–fcco. Finally, it is also worth noting that in the neighborhood of the fluid–sc–bcc and fluid–fccd–bcc triple points re-entrant melting occurs. Coexistence points from free energy calculations were found to be in agreement with those found from direct coexistence calculations.

In summary, even for a relatively simple model potential, we have obtained a complex phase diagram with many solid phases and unusual behavior such as re-entrant melting. But the most interesting finding is that, even with a very simple model such as the one described here, it is possible to reproduce two important features of the phase diagram of globular proteins, namely, the existence of a metastable critical point and the stabilization of a low density crystal. Similar behavior has been found for a primitive model of water [146, 48, 300]. Studies of nucleation of these models can be very relevant to understand the crystallization of globular proteins.

13. Conclusions

In this work we have reviewed the methodology of free energy calculations and given examples of recent work on the determination of fluid–solid and solid–solid equilibria by computer simulations. Free energy calculations are used to compute initial coexistence points between phases, and then Gibbs–Duhem integration is used to compute coexistence lines. Other procedures to estimate fluid–solid equilibria such as direct coexistence and simulations of the free surface of the solid have been discussed. The Einstein crystal methodology and the Einstein molecule approach have been presented in a rather comprehensive way. Both methodologies yield identical values of the free energy. It is shown that the free energy presents a strong N dependence, and that finite size corrections are needed to estimate properties of solids in the thermodynamic limit. The issue of the symmetry of the orientational field in Einstein crystal calculations for molecular fluids has been discussed. We do hope that the extensive discussion of all these aspects helps other researchers in the area to perform free energy calculations and phase diagram determination. In fact there are at least six areas where one can predict intense activity in the future. The first one is the determination of the phase diagram of molecular fluids. In this work, the procedure to obtain free energies for water is presented. Besides, free energies and coexistence points for SPC/E and TIP4P models of water are presented for the first time. These results lead to the determination of the full phase diagram for water, performed recently by our group [110]. The example of water illustrates clearly that phase diagram calculations for molecular fluids is indeed feasible nowadays and that it can help to improve current models. In fact these free energy calculations led to the proposal of an improved version of TIP4P denoted as TIP4P/2005. This model is able to describe correctly the phase diagram of water, the maximum in density of water, the density of the ice polymorphs including the methane hydrate [301–303], the vapor–liquid equilibria [304], the surface tension [305], the diffusion coefficient and the structure of water [215, 306] over a wide range of temperatures and pressures. The determination of the phase diagram of TIP4P was a crucial step in the development of TIP4P/2005. We do not see any difficulty in performing similar studies to improve potential models for other molecular fluids. The work on water shows that melting points obtained from free energy calculations, direct coexistence simulations and free surface simulations are almost identical (taking into account the statistical uncertainties and the slightly different implementations of the potential). The second area where phase diagram calculations can be useful is in the study of ionic systems. Here we reviewed the phase diagram of the RPM model, but it is clear that the determination of the phase diagram of PM models and of other models of salts (including probably ionic liquids, which are becoming increasingly important from a technological point of view) would be of great interest. Some ionic systems can also be used to describe charged colloids.

The third area is the area of crystallization of proteins. It is now clear that models with short range anisotropic forces can be regarded as primitive models of proteins. In such models the liquid–liquid separation is metastable with respect to freezing, and the competition between phase separation and crystallization is of great interest to understand the presence or absence of crystallization in proteins. The fourth area is the study of freezing under confinement due to the interest in understanding fluid–solid equilibria on the nanometer

scale [307–309]. The fifth area is the study of the solubility of salts (or solids in general) in water (or solvents in general), where the knowledge of the chemical potential of the solute in the solid phase is required. Very little effort has been devoted to this problem [143, 147]. Finally, studies on nucleation [120] should benefit from the knowledge of the equilibrium melting temperatures. In summary, the study of fluid–solid and solid–solid equilibria of molecular and complex systems by computer simulation is now feasible, and the procedures to do it seem well established. The study of fluid–solid and solid–solid equilibria by computer simulation can play a central role in developing potential models for condensed phases and for providing molecular understanding of a number of phenomena involving solid and liquid phases. The enormous sensitivity of phase diagrams to interaction potentials allows us to test the performance of the different potentials available for a certain substance, and offers a unique opportunity for their improvement.

Acknowledgments

One of us (CV) would like to thank Peter Monson (Amherst, USA) for introducing him, during his post-doctoral stay in 1991–1992, into the fascinating world of fluid–solid equilibria, and Daan Frenkel for teaching him the first steps in computer simulation. It is a pleasure to acknowledge L G MacDowell, C McBride and R G Fernandez for many helpful discussions and for their contribution to different parts of this work. The same is true for the younger members of our group, M M Conde and J L Aragones. Discussions with E de Miguel (Huelva), A Patrykiejew (Lublin), I Nezbeda (Prague), F Bresme (London), A A Louis and J P K Doye (Oxford) are also gratefully acknowledged. This work was funded by grants FIS2007-66079-C02-01 from the DGI (Spain), S-0505/ESP/0229 from the CAM, MTKD-CT-2004-509249 from the European Union and 910570 from the UCM. We would like to thank Francesco Sciortino for the invitation to write this review. EGN wishes to thank the Ministerio de Educación y Ciencia and the Universidad Complutense de Madrid for a Juan de la Cierva fellowship.

Appendix A. Partition function of the Einstein crystal with fixed center of mass

The translational contribution to the partition function of an Einstein crystal with fixed center of mass is

$$Q^{\mathrm{CM}}_{\mathrm{Ein,t}} = \frac{1}{h^{3(N-1)}} \int \exp\left[-\beta \sum_{i=1}^{N} \frac{\mathbf{p}_i^2}{2m_i}\right] \times \delta\left(\sum_{i=1}^{N} \mathbf{p}_i\right) \mathrm{d}\mathbf{p}_1 \ldots \mathrm{d}\mathbf{p}_N \times \int \exp\left[-\beta\Lambda_E \sum_{i=1}^{N} (\mathbf{r}_i - \mathbf{r}_{i0})^2\right] \times \delta\left(\sum_{i=1}^{N} \mu_i (\mathbf{r}_i - \mathbf{r}_{i0})\right) \mathrm{d}\mathbf{r}_1 \ldots \mathrm{d}\mathbf{r}_N. \quad (80)$$

The integral over the space of momenta is not relevant to compute the free energy and, therefore, we will leave aside this contribution, that we will include simply as a factor P^{CM}:

$$P^{\mathrm{CM}} = \frac{1}{h^{3(N-1)}} \int \exp\left[-\beta \sum_{i=1}^{N} \frac{\mathbf{p}_i^2}{2m_i}\right] \times \delta\left(\sum_{i=1}^{N} \mathbf{p}_i\right) \mathrm{d}\mathbf{p}_1 \ldots \mathrm{d}\mathbf{p}_N. \quad (81)$$

We will focus on the integral over the configurational space:

$$Z^{\mathrm{CM}}_{\mathrm{Ein,t}} = \int \exp\left[-\beta\Lambda_E \sum_{i=1}^{N} (\mathbf{r}_i - \mathbf{r}_{i0})^2\right] \times \delta\left(\sum_{i=1}^{N} \mu_i (\mathbf{r}_i - \mathbf{r}_{i0})\right) \mathrm{d}\mathbf{r}_1 \ldots \mathrm{d}\mathbf{r}_N. \quad (82)$$

This integral can be expressed in a simpler way by defining a change of variable, $\mathbf{r}_i - \mathbf{r}_{i0} = \mathbf{r}'_i$. The Jacobian of this change of variable is unity, and the configurational integral can be written as

$$Z^{\mathrm{CM}}_{\mathrm{Ein,t}} = \int \exp\left[-\beta\Lambda_E \sum_{i=1}^{N} (\mathbf{r}'_i)^2\right] \times \delta\left(\sum_{i=1}^{N} \mu_i \mathbf{r}'_i\right) \mathrm{d}\mathbf{r}'_1 \ldots \mathrm{d}\mathbf{r}'_N. \quad (83)$$

The Dirac delta function can be written [310] as

$$\delta\left(\sum_{i=1}^{N} \mu_i \mathbf{r}'_i\right) = \frac{1}{(2\pi)^3} \int \exp\left[\mathrm{i}\mathbf{k}\left(\sum_{i=1}^{N} \mu_i \mathbf{r}'_i\right)\right] \mathrm{d}\mathbf{k}; \quad (84)$$

the configurational integral can be written as

$$Z^{\mathrm{CM}}_{\mathrm{Ein,t}} = \frac{1}{(2\pi)^3} \int \exp\left[-\beta\Lambda_E \sum_{i=1}^{N} \left((\mathbf{r}'_i)^2 - \frac{i\mathbf{k}}{\beta\Lambda_E} \mu_i \mathbf{r}'_i\right)\right] \times \mathrm{d}\mathbf{k}\, \mathrm{d}\mathbf{r}'_1 \ldots \mathrm{d}\mathbf{r}'_N. \quad (85)$$

Each term in the summation can be rewritten in a more convenient form:

$$(\mathbf{r}'_i)^2 - \frac{\mathrm{i}\mathbf{k}}{\beta\Lambda_E} \mu_i \mathbf{r}'_i = (\mathbf{r}'_i)^2 - \frac{2\mathrm{i}\mathbf{k}}{2\beta\Lambda_E} \mu_i \mathbf{r}'_i + \frac{\mathrm{i}^2 k^2 \mu_i^2}{4\beta^2\Lambda_E^2} - \frac{\mathrm{i}^2 k^2 \mu_i^2}{4\beta^2\Lambda_E^2} \quad (86)$$

$$= \left(\mathbf{r}'_i - \frac{\mathrm{i}\mathbf{k}\mu_i}{2\beta\Lambda_E}\right)^2 + \frac{k^2\mu_i^2}{4\beta^2\Lambda_E^2}. \quad (87)$$

Notice that in equations (84)–(86) there is an implicit scalar product between the vector $\mathbf{k}$ and the accompanying vector. The integral can then be expressed as

$$Z^{\mathrm{CM}}_{\mathrm{ein},t} = \frac{1}{(2\pi)^3} \times \int \exp\left[-\beta\Lambda_E \sum_{i=1}^{N} \left(\left(\mathbf{r}'_i - \frac{\mathrm{i}\mathbf{k}\mu_i}{2\beta\Lambda_E}\right)^2 + \frac{k^2\mu_i^2}{4\beta^2\Lambda_E^2}\right)\right] \times \mathrm{d}\mathbf{k}\, \mathrm{d}\mathbf{r}'_1 \ldots \mathrm{d}\mathbf{r}'_N. \quad (88)$$

It is now convenient to do another change of variable:

$$\mathbf{r}''_i = \mathbf{r}'_i - \frac{\mathrm{i}\mathbf{k}\mu_i}{2\beta\Lambda_E}. \quad (89)$$

To compute the Jacobian associated with this transformation, we will consider the simple case of a system in one dimension and with two particles. The Jacobian J is given by the following determinant:

$$J = \begin{vmatrix} \frac{\partial \mathbf{r}_1'}{\partial \mathbf{r}_1''} & \frac{\partial \mathbf{r}_1'}{\partial \mathbf{r}_2''} & \frac{\partial \mathbf{r}_1'}{\partial \mathbf{k}} \\ \frac{\partial \mathbf{r}_2'}{\partial \mathbf{r}_1''} & \frac{\partial \mathbf{r}_2'}{\partial \mathbf{r}_2''} & \frac{\partial \mathbf{r}_2'}{\partial \mathbf{k}} \\ \frac{\partial \mathbf{k}}{\partial \mathbf{r}_1''} & \frac{\partial \mathbf{k}}{\partial \mathbf{r}_2''} & \frac{\partial \mathbf{k}}{\partial \mathbf{k}} \end{vmatrix} \tag{90}$$

$$J = \begin{vmatrix} 1 & 0 & \frac{2\beta\Lambda_E}{\mathrm{i}\mu_i} \\ 0 & 1 & \frac{2\beta\Lambda_E}{\mathrm{i}\mu_i} \\ 0 & 0 & 1 \end{vmatrix} = 1 \tag{91}$$

After applying the change of variable, the integral can be expressed as

$$Z_{\mathrm{Ein,t}}^{\mathrm{CM}} = \frac{1}{(2\pi)^3} \int \exp\left[-\beta\Lambda_E \sum_{i=1}^{N} \left((\mathbf{r}_i'')^2 + \frac{k^2\mu_i^2}{4\beta^2\Lambda_E^2} \right) \right] \times \mathrm{d}\mathbf{k}\, \mathrm{d}\mathbf{r}_1'' \ldots \mathrm{d}\mathbf{r}_N''. \tag{92}$$

This integral can be split into two Gaussian integrals:

$$Z_{\mathrm{Ein,t}}^{\mathrm{CM}} = \frac{1}{(2\pi)^3} \int \exp\left[-\beta\Lambda_E \sum_{i=1}^{N} (\mathbf{r}_i'')^2\right] \mathrm{d}\mathbf{r}_1'' \ldots \mathrm{d}\mathbf{r}_N'' \times \int \exp\left[-\frac{k^2 \sum_{i=1}^{N} \mu_i^2}{4\beta\Lambda_E}\right] \mathrm{d}\mathbf{k} \tag{93}$$

whose solution is

$$Z_{\mathrm{Ein,t}}^{\mathrm{CM}} = \frac{1}{(2\pi)^3} \left(\frac{\pi}{\beta\Lambda_E}\right)^{N3/2} \left(\frac{4\beta\pi\Lambda_E}{\sum_{i=1}^{N}\mu_i^2}\right)^{3/2}. \tag{94}$$

Doing a bit of algebra it can be shown that

$$Z_{\mathrm{Ein,t}}^{\mathrm{CM}} = \left(\frac{\beta\Lambda_E}{\pi}\right)^{3/2} \left(\frac{\pi}{\beta\Lambda_E}\right)^{N3/2} \left(\sum_{i=1}^{N}\mu_i^2\right)^{-3/2} \tag{95}$$

or, more simply,

$$Z_{\mathrm{Ein,t}}^{\mathrm{CM}} = \left(\frac{\pi}{\beta\Lambda_E}\right)^{3(N-1)/2} \left(\sum_{i=1}^{N}\mu_i^2\right)^{-3/2}. \tag{96}$$

Summarizing, we have obtained that the partition function of an Einstein crystal with fixed center of mass is given by

$$Q_{\mathrm{Ein,t}}^{\mathrm{CM}} = P^{\mathrm{CM}} \left(\frac{\pi}{\beta\Lambda_E}\right)^{3(N-1)/2} \left(\sum_{i=1}^{N}\mu_i^2\right)^{-3/2}. \tag{97}$$

When all molecules are identical the reduced mass μ_i is simply $1/N$. Therefore, the previous equation can be simplified to

$$Q_{\mathrm{Ein,t}}^{\mathrm{CM}} = P^{\mathrm{CM}} \left(\frac{\pi}{\beta\Lambda_E}\right)^{3(N-1)/2} (N)^{3/2}. \tag{98}$$

which is the final expression for the free energy of an ideal Einstein crystal with fixed center of mass. An explicit expression for P^{CM} is not needed to get the free energy of the solid since it cancels out with a similar term in equation (46). However, it is not difficult to obtain P^{CM} by realizing that equation (81) is formally identical to equation (82) (with $\mu_i = 1$ and $\Lambda_E = 1/(2m_i)$ and omitting the prefactor $h^{3(N-1)}$). A derivation similar to that used to get equation (96) from equation (82) leads to

$$P^{\mathrm{CM}} = \frac{1}{\Lambda^{3(N-1)}} N^{-3/2} \tag{99}$$

to be compared with

$$P = \frac{1}{\Lambda^{3N}} \tag{100}$$

so that the ratio P^{CM}/P adopts the value $\Lambda^3 N^{-3/2}$. If equation (99) is replaced into equation (98) one obtains

$$Q_{\mathrm{Ein,t}}^{\mathrm{CM}} = \frac{1}{\Lambda^{3(N-1)}} \left(\frac{\pi}{\beta\Lambda_E}\right)^{3(N-1)/2} \tag{101}$$

which is dimensionless as it should be.

Appendix B. Computing $U_{\mathrm{Ein}}^{\mathrm{CM}}$ within a Monte Carlo program

The condition of fixing the center of mass of the reference points is quite useful since it eliminates any divergence of the integrand of equation (39). A displacement $\vec{d}$ of a given molecule must be accompanied by a displacement $(-\vec{d}/(N))$ of all the molecules of the system (assuming all particles are identical), so that the center of mass remains in its original position. In practice, this is not very convenient. It is more convenient to perform a simulation without the restriction over the center of mass but keeping track of the position of the center of mass [139]. Let us denote as $\mathbf{r}_{i0}$ the initial position of the reference point of molecule i in the perfect lattice, and $\Delta\mathbf{R}_{\mathrm{CM}}$ is the difference between the present position of the center of mass and its initial position. Let us denote by $\mathbf{r}_i^U$ the actual position in the simulation (without the restriction in the center of mass) of the reference atom of molecule i. Let us define $\Delta\mathbf{r}_i = \mathbf{r}_i^U - \mathbf{r}_{i0} - \Delta\mathbf{R}_{\mathrm{CM}}$. Let us compute the energy change when, in a trial move, the random displacement of molecule is $\boldsymbol{\Delta}_i$. The energy of the old (prefix *old*) and new (prefix *new*) configurations is given by

$$U_{\mathrm{Eins}}^{\mathrm{CM,old}}/\Lambda_E = (\Delta\mathbf{r}_i^{\mathrm{old}})^2 + \sum_{j\neq i} (\Delta\mathbf{r}_j^{\mathrm{old}})^2$$

$$U_{\mathrm{Eins}}^{\mathrm{CM,new}}/\Lambda_E = \left(\mathbf{r}_i^{\mathrm{U,old}} + \boldsymbol{\Delta}_i - \mathbf{r}_{i0} - \Delta\mathbf{R}_{\mathrm{CM}}^{\mathrm{old}} - \frac{\boldsymbol{\Delta}_i}{N}\right)^2 + \sum_{j\neq i} \left(\mathbf{r}_j^{\mathrm{U,old}} - \mathbf{r}_{jo} - \Delta\mathbf{R}_{\mathrm{CM}}^{\mathrm{old}} - \frac{\boldsymbol{\Delta}_i}{N}\right)^2 = \left(\Delta\mathbf{r}_i^{\mathrm{old}} + \boldsymbol{\Delta}_i - \frac{\boldsymbol{\Delta}_i}{N}\right)^2 + \sum_{j\neq i} \left(\Delta\mathbf{r}_j^{\mathrm{old}} - \frac{\boldsymbol{\Delta}_i}{N}\right)^2. \tag{102}$$

We have assumed that all particles have the same mass, so that a displacement $\boldsymbol{\Delta}_i$ of one of them leads to a displacement $\boldsymbol{\Delta}_i/N$ of the center of mass. We have not included the orientational contribution since it cancels out when computing the energy change (i.e., the orientational energy is not affected

by the translation of molecule i). Therefore, the potential energy change will be given by

$$\Delta U^{\rm CM}_{\rm Eins}/\Lambda_E = 2\Delta \mathbf{r}_i^{\rm old}\cdot\boldsymbol{\Delta}_i - 2\Delta\mathbf{r}_i^{\rm old}\cdot\frac{\boldsymbol{\Delta}_i}{N} + \left(\frac{N\boldsymbol{\Delta}_i-\boldsymbol{\Delta}_i}{N}\right)^2 + \sum_{j\neq i}\left[\left(\frac{\boldsymbol{\Delta}_i}{N}\right)^2 - 2\Delta\mathbf{r}_j^{\rm old}\frac{\boldsymbol{\Delta}_i}{N}\right]. \quad (103)$$

This equation can be simplified since, as the center of mass is constrained, it holds that $\sum_{i=1}^{N}\Delta\mathbf{r}_i = 0$ (in the right-hand side, the second and last terms cancel out):

$$\Delta U^{\rm CM}_{\rm Eins}/\Lambda_E = 2\Delta\mathbf{r}_i^{\rm old}\cdot\boldsymbol{\Delta}_i + \left(\frac{N\boldsymbol{\Delta}_i-\boldsymbol{\Delta}_i}{N}\right)^2 + \sum_{j\neq i}\left(\frac{\boldsymbol{\Delta}_i}{N}\right)^2. \quad (104)$$

It is easy to show that this expression can also be written as

$$\Delta U^{\rm CM}_{\rm Eins}/\Lambda_E = 2\Delta\mathbf{r}_i^{\rm old}\cdot\boldsymbol{\Delta}_i + \boldsymbol{\Delta}_i^2\left(\frac{N-1}{N}\right). \quad (105)$$

In this way, it is possible to perform an MC simulation without keeping the center of mass fixed, but including this constraint through the Monte Carlo acceptance rule.

Appendix C. The Frenkel–Ladd expression

In 1984 Frenkel and Ladd derived an expression for the free energy of a solid. It is not the same as that given by Polson *et al* [142] and also presented in this paper. The reason for this difference is the following.

- 1. The expression used for ΔA_3 by Frenkel and Ladd was $(1/N)\ln N$ (in $Nk_{\rm B}T$ units) lower than the correct one.
- 2. The expression used for $A^{\rm CM}_{\rm Ein-id}$ by Frenkel and Ladd was $(3/N)\ln N$ (in $Nk_{\rm B}T$ units) higher than the correct one.

Taking into account both contributions it turns out that the Frenkel–Ladd expression gives an energy (in $Nk_{\rm B}T$ units) $(2/N)\ln N$ higher than the correct one. Let us describe briefly the source of these two discrepancies. For ΔA_3 Frenkel and Ladd used

$$\Delta A_3^{\rm FL} = A_{\rm sol} - A^{\rm CM}_{\rm sol} = k_{\rm B}T(\ln(P^{\rm CM}/P) - \ln(V)) \quad (106)$$

instead of

$$\Delta A_3 = A_{\rm sol} - A^{\rm CM}_{\rm sol} = k_{\rm B}T(\ln(P^{\rm CM}/P) - \ln(V/N)) \quad (107)$$

which is the expression to be used when all permutations, $N!$, are included in the reference ideal Einstein crystal. The second discrepancy is due to the fact that the constraint of fixing the center of mass was implemented by Frenkel and Ladd as

$$\sum_{i=1}^{N}(\mathbf{r}_i - \mathbf{r}_{i0}) = 0 \quad (108)$$

instead of:

$$\sum_{i=1}^{N}\mu_i(\mathbf{r}_i - \mathbf{r}_{i0}) = 0 \quad (109)$$

with $\mu_i = 1/N$. One can simply say that to fix the center of mass Frenkel and Ladd used $\mu_i = 1$ instead of $\mu_i = 1/N$. It is simple to analyze the mathematical consequences of this. It is just enough to look at appendix A, and to see what happens in the final expression (equation (97)) when $\mu_i = 1$ is used instead of $\mu_i = 1/N$. Then one obtains

$$Q^{\rm CM}_{\rm Ein,t} = P^{\rm CM}\left(\frac{\pi}{\beta\Lambda_E}\right)^{3(N-1)/2}(N)^{-3/2}. \quad (110)$$

By comparing equation (110) (Frenkel–Ladd) with equation (98) it is simple to see how the Frenkel–Ladd expression for $Q^{\rm CM}_{\rm Ein,t}$ gives a contribution (in $Nk_{\rm B}T$ units) $(3/N)\ln N$ higher than the correct one.

In summary, when all factors are considered, the Frenkel–Ladd expression gives an energy (in $Nk_{\rm B}T$ units) $(2/N)\ln N$ higher than the correct one.

References

[1] Wood W W and Jacobson J D 1957 *J. Chem. Phys.* **27** 1207
[2] Alder B J and Wainwright T E 1957 *J. Chem. Phys.* **27** 1208
[3] Hoover W G and Ree F H 1968 *J. Chem. Phys.* **49** 3609
[4] Pusey P N and van Megen W 1986 *Nature* **320** 340
[5] Monson P A and Kofke D A 2000 *Advances in Chemical Physics* vol 115, ed I Prigogine and S A Rice (New York: Wiley) p 113
[6] Panagiotopoulos A Z 1987 *Mol. Phys.* **61** 813
[7] Panagiotopoulos A Z, Quirke N, Stapleton M R and Tildesley D J 1988 *Mol. Phys.* **63** 527
[8] Chen B, Siepmann J I, Karaborni S and Klein M L 2003 *J. Phys. Chem.* B **107** 12320
[9] Bruce A D, Wilding N B and Ackland G J 1997 *Phys. Rev. Lett.* **79** 3002
[10] Bruce A D and Wilding N B 2003 *Adv. Chem. Phys.* **127** 1
[11] Bruce A D, Jackson A N, Ackland G J and Wilding N B 2000 *Phys. Rev.* E **61** 906
[12] Wilding N B and Bruce A D 2000 *Phys. Rev. Lett.* **85** 5138
[13] Wilding N B 2002 *Comput. Phys. Commun.* **146** 99
[14] Errington J R 2004 *J. Chem. Phys.* **120** 3130
[15] McNeil-Watson G C and Wilding N B 2006 *J. Chem. Phys.* **124** 064504
[16] Grochola G 2004 *J. Chem. Phys.* **120** 2122
[17] Lovett R 1994 Can a solid be turned into a gas without passing through a first order phase transition? *NATO ASI Series C* vol 460 (Dordrecht: Kluwer–Academic) p 641
[18] Grochola G 2005 *J. Chem. Phys.* **122** 046101
[19] Eike D M, Brennecke J F and Maginn E J 2005 *J. Chem. Phys.* **122** 014115
[20] Eike D M and Maginn E J 2006 *J. Chem. Phys.* **124** 164503
[21] Born M and Huang K 1954 *Dynamical Theory of Crystal Lattices* (Oxford: Clarendon)
[22] Gao G T, Zeng X C and Tanaka H 2000 *J. Chem. Phys.* **112** 8534
[23] Koyama Y, Tanaka H, Gao G and Zeng X C 2004 *J. Chem. Phys.* **121** 7926
[24] Hoover W G and Ree F H 1967 *J. Chem. Phys.* **47** 4873
[25] Hansen J P and Verlet L 1969 *Phys. Rev.* **184** 151
[26] Hansen J P and McDonald I R 1986 *Theory of Simple Liquids* (London: Academic)
[27] Frenkel D and Ladd A J C 1984 *J. Chem. Phys.* **81** 3188

[28] Frenkel D and Mulder B M 1985 *Mol. Phys.* **55** 1171
[29] de Miguel E and Vega C 2002 *J. Chem. Phys.* **117** 6313
[30] Prestipino S and Saija F 2007 *J. Chem. Phys.* **126** 194902
[31] Singer S J and Mumaugh R 1990 *J. Chem. Phys.* **93** 1278
[32] Vega C, Paras E P A and Monson P A 1992 *J. Chem. Phys.* **96** 9060
[33] Vega C, Paras E P A and Monson P A 1992 *J. Chem. Phys.* **97** 8543
[34] Gay S C, Beale P D and Rainwater J C 1998 *J. Chem. Phys.* **109** 6820
[35] McGrother S C, Williamson D C and Jackson G 1996 *J. Chem. Phys.* **104** 6755
[36] Bolhuis P and Frenkel D 1997 *J. Chem. Phys.* **106** 666
[37] Vega C and Monson P A 1997 *J. Chem. Phys.* **107** 2696
[38] Vega C, McBride C, de Miguel E, Blas F J and Galindo A 2003 *J. Chem. Phys.* **118** 10696
[39] Galbraith A L and Hall C K 2007 *Fluid Phase Equilibr.* **262** 1
[40] Lisal M and Vacek V 1997 *Mol. Simul.* **19** 43
[41] Vega C and Monson P A 1995 *J. Chem. Phys.* **102** 1361
[42] Malanoski A P and Monson P A 1997 *J. Chem. Phys.* **107** 6899
[43] Malanoski A P and Monson P A 1999 *J. Chem. Phys.* **110** 664
[44] Blas F J, Sanz E, Vega C and Galindo A 2003 *J. Chem. Phys.* **119** 10958
[45] Galindo A, Vega C, Sanz E, MacDowell L G, de Miguel E and Blas F J 2004 *J. Chem. Phys.* **120** 3957
[46] Cao M and Monson P A 2005 *J. Chem. Phys.* **122** 054505
[47] Sese L M 2007 *J. Chem. Phys.* **126** 164508
[48] Vega C and Monson P A 1998 *J. Chem. Phys.* **109** 9938
[49] Bresme F, Vega C and Abascal J L F 2000 *Phys. Rev. Lett.* **85** 3217
[50] Vega C, Abascal J L F, McBride C and Bresme F 2003 *J. Chem. Phys.* **119** 964
[51] Schroer J W and Monson P A 2000 *J. Chem. Phys.* **112** 8950
[52] Schroer J W and Monson P A 2001 *J. Chem. Phys.* **114** 4124
[53] Shen W N and Monson P A 1995 *J. Chem. Phys.* **103** 9756
[54] Hagen M H J and Frenkel D 1994 *J. Chem. Phys.* **101** 4093
[55] Almarza N G and Lomba E 1994 *J. Chem. Phys.* **100** 8367
[56] Hynninen A P, Leunissen M E, van Blaaderen A and Dijkstra M 2006 *Phys. Rev. Lett.* **96** 018303
[57] Noya E G, Vega C, Doye J P K and Louis A A 2007 *J. Chem. Phys.* **127** 054501
[58] Chang J, Lenhoff A M and Sandler S I 2004 *J. Chem. Phys.* **120** 3003
[59] Meijer E J, Frenkel D, Lesar R A and Ladd A J C 1990 *J. Chem. Phys.* **92** 7570
[60] Polson J M and Frenkel D 1999 *J. Chem. Phys.* **111** 1501
[61] Hagen M H J, Meijer E J, Mooij G C A M, Frenkel D and Lekkerkerker H N W 1993 *Nature* **365** 425
[62] Anwar J, Frenkel D and Noro M G 2003 *J. Chem. Phys.* **118** 728
[63] Rodrigues P C R and Fernandez F M S S 2007 *J. Chem. Phys.* **126** 024503
[64] Ghiringhelli L M, Los J H, Meijer E J, Fasolino A and Frenkel D 2005 *Phys. Rev. Lett.* **94** 145701
[65] Kaczmarski M, Bedoya-Martinez O N and Hernandez E R 2005 *Phys. Rev. Lett.* **94** 095701
[66] Saika-Voivod I, Sciortino F, Grande T and Poole P H 2004 *Phys. Rev.* E **70** 061507
[67] Ford M H, Auerbach S M and Monson P A 2007 *J. Chem. Phys.* **126** 144701
[68] Wierzchowski S J and Monson P A 2007 *J. Phys. Chem.* B **111** 7274
[69] Finney J L 2004 *Phil. Trans. R. Soc.* B **359** 1145
[70] Barker J A and Watts R O 1969 *Chem. Phys. Lett.* **3** 144
[71] Rahman A and Stillinger F H 1971 *J. Chem. Phys.* **55** 3336
[72] Poole P H, Sciortino F, Essmann U and Stanley H E 1992 *Nature* **360** 324
[73] Harrington S, Zhang R, Poole P H, Sciortino F and Stanley H E 1997 *Phys. Rev. Lett.* **78** 2409
[74] Mishima O and Stanley H E 1998 *Nature* **396** 329
[75] Debenedetti P G 2003 *J. Phys.: Condens. Matter* **15** R1669
[76] Paschek D and Geiger A 2005 *Preprint* cond-mat/0512199
[77] Brovchenko I, Geiger A and Oleinikova A 2005 *J. Chem. Phys.* **123** 44515
[78] Marques M I 2007 *Phys. Rev.* E **76** 021503
[79] Loerting T and Giovambattista N 2006 *J. Phys.: Condens. Matter* **18** R919
[80] Morse M D and Rice S A 1982 *J. Chem. Phys.* **76** 650
[81] Impey R W, Klein M L and Tse J S 1984 *J. Chem. Phys.* **81** 6406
[82] Svishchev I and Kusalik P G 1994 *Phys. Rev. Lett.* **73** 975
[83] Matsumoto M, Saito S and Ohmine I 2002 *Nature* **416** 409
[84] Gay S C, Smith E J and Haymet A D J 2002 *J. Chem. Phys.* **116** 8876
[85] Ayala R B and Tchijov V 2003 *Can. J. Phys.* **81** 11
[86] Tanaka H 1998 *J. Chem. Phys.* **108** 4887
[87] Fennell C J and Gezelter J D 2005 *J. Chem. Theory Comput.* **1** 662
[88] Rick S W 2005 *J. Chem. Phys.* **122** 094504
[89] Baranyai A, Bartok A and Chialvo A A 2005 *J. Chem. Phys.* **123** 54502
[90] Baranyai A, Bartok A and Chialvo A A 2006 *J. Chem. Phys.* **124** 074507
[91] Vrbka L and Jungwirth P 2005 *Phys. Rev. Lett.* **95** 148501
[92] Carignano M A, Shepson P B and Szleifer I 2005 *Mol. Phys.* **103** 2957
[93] Slovak J and Tanaka H 2005 *J. Chem. Phys.* **122** 204512
[94] Buch V, Martoňák R and Parrinello M 2006 *J. Chem. Phys.* **124** 204705
[95] Picaud S 2006 *J. Chem. Phys.* **125** 174712
[96] Jedlovszky P, Partay L, Hoang P N M, Picaud S, von Hessberg P and Crowley J N. 2006 *J. Am. Chem. Soc.* **128** 15300
[97] Tribello G A and Slater B 2006 *Chem. Phys. Lett.* **425** 246
[98] Tribello G A, Slater B and Salzmann C G 2006 *J. Am. Chem. Soc.* **128** 12594
[99] Sharma M, Resta R and Car R 2007 *Phys. Rev. Lett.* **98** 247401
[100] Sizov V V and Piotrovskaya E M 2007 *J. Phys. Chem.* B **111** 2886
[101] Brodskaya E N 2007 *Mol. Phys.* **105** 2211
[102] Jiang H, Jordan K D and Taylor C E 2007 *J. Phys. Chem.* B **111** 6486
[103] Wang J W, Kalinichev A G and Kirkpatrick R J. 2006 *Geochim. Cosmochim. Acta* **70** 562
[104] Wissner-Gross A D and Kaxiras E 2007 *Phys. Rev.* E **76** 020501
[105] Baez L A and Clancy P 1995 *J. Chem. Phys.* **103** 9744
[106] Baez L A and Clancy P 1995 *Mol. Phys.* **86** 385
[107] Vlot M J, Huinink J and van der Eerden J P 1999 *J. Chem. Phys.* **110** 55
[108] Karim O A and Haymet A D J 1988 *J. Chem. Phys.* **89** 6889
[109] Karim O A, Kay P A and Haymet A D J 1990 *J. Chem. Phys.* **92** 4643
[110] Sanz E, Vega C, Abascal J L F and MacDowell L G 2004 *Phys. Rev. Lett.* **92** 255701
[111] Sanz E, Vega C, Abascal J L F and MacDowell L G 2004 *J. Chem. Phys.* **121** 1165
[112] Abascal J L F and Vega C 2007 *Phys. Chem. Chem. Phys.* **9** 2775
[113] Abascal J L F and Vega C 2007 *Phys. Rev. Lett.* **98** 237801
[114] Abascal J L F and Vega C 2007 *J. Phys. Chem.* C **111** 15811
[115] Guillot B 2002 *J. Mol. Liq.* **101** 219
[116] Jorgensen W L and Tirado-Rives J 2005 *Proc. Am. Acad. Sci. Arts* **102** 6665
[117] Auer S and Frenkel D 2001 *Nature* **409** 1020
[118] tenWolde P R, RuizMontero M J and Frenkel D 1996 *J. Chem. Phys.* **104** 9932

[119] Radhakrishnan R and Trout B L 2002 *J. Chem. Phys.* **117** 1786
[120] Radhakrishnan R and Trout B 2003 *J. Am. Chem. Soc.* **125** 7743
[121] Auer S and Frenkel D 2005 *Adv. Comput. Simul. Approaches Soft Matter Sci.* I **173** 149
[122] McQuarrie D A 1976 *Statistical Mechanics* (New York: Harper and Row)
[123] Gray C G and Gubbins K E 1984 *Theory of Molecular Fluids* (Oxford: Clarendon)
[124] Parrinello M and Rahman A 1980 *Phys. Rev. Lett.* **45** 1196
[125] Parrinello M and Rahman A 1981 *J. Appl. Phys.* **52** 7182
[126] Yashonath S and Rao C N R 1985 *Mol. Phys.* **54** 245
[127] Najafabadi P and Yip S 1983 *Scr. Metall.* **17** 1199
[128] Debenedetti P G 1996 *Metastable Liquids: Concepts and Principles* (Princeton, NJ: Princeton University Press)
[129] Bridgman P W 1912 *Proc. Am. Acad. Arts Sci.* **XLVII** 441
[130] Allen M P and Tildesley D J 1987 *Computer Simulation of Liquids* (New York: Oxford University Press)
[131] Stegailov V 2005 *Comput. Phys. Commun.* **169** 247
[132] McBride C, Vega C, Sanz E, MacDowell L G and Abascal J L F 2005 *Mol. Phys.* **103** 1
[133] McBride C, Vega C, Sanz E and Abascal J L F 2004 *J. Chem. Phys.* **121** 11907
[134] Zheng L, Luo S N and Thompson D L 2006 *J. Chem. Phys.* **124** 154504
[135] Agrawal P M, Rice B M and Thompson D L 2003 *J. Chem. Phys.* **119** 9617
[136] Alavi S and Thompson D L 2006 *Mol. Simul.* **32** 999
[137] Norman G E and Stegailov V V 2002 *Dokl. Phys.* **47** 667
[138] Norman G E and Stegailov V V 2004 *Mol. Simul.* **30** 397
[139] Frenkel D and Smit B 2002 *Understanding Molecular Simulation* (London: Academic)
[140] Widom B 1963 *J. Chem. Phys.* **39** 2808
[141] Lu N D, Singh J K and Kofke D A 2003 *J. Chem. Phys.* **118** 2977
[142] Polson J M, Trizac E, Pronk S and Frenkel D 2000 *J. Chem. Phys.* **112** 5339
[143] Ferrario M, Ciccotti G, Spohr E, Cartailler T and Turq P 2002 *J. Chem. Phys.* **117** 4947
[144] Barroso M A and Ferreira A L 2002 *J. Chem. Phys.* **116** 7145
[145] Vega C and Noya E G 2007 *J. Chem. Phys.* **127** 154113
[146] Kolafa J and Nezbeda I 1987 *Mol. Phys.* **61** 161
[147] Sanz E and Vega C 2007 *J. Chem. Phys.* **126** 014507
[148] Press W H, Flannery B P, Teukosky S A and Vetterling W T 1990 *Numerical Recipes: The Art of Scientific Computing* (Cambridge: Cambridge University Press)
[149] Chang J and Sandler S I 2003 *J. Chem. Phys.* **118** 8390
[150] Almarza N G 2007 *J. Chem. Phys.* **126** 211103
[151] de Miguel E, Marguta R G and del Rio E M 2007 *J. Chem. Phys.* **127** 154512
[152] Speedy R J 1997 *J. Phys.: Condens. Matter* **9** 8591
[153] Davidchack R L and Laird B B 1998 *J. Chem. Phys.* **108** 9452
[154] Sweatman M B 2005 *Phys. Rev.* E **72** 016711
[155] Bernal J D and Fowler R H 1933 *J. Chem. Phys.* **1** 515
[156] Pauling L 1935 *J. Am. Chem. Soc.* **57** 2680
[157] Berg B A and Yang W 2007 *J. Chem. Phys.* **127** 224502
[158] Wojciechowski K W 1987 *Phys. Lett.* A **122** 377
[159] Wojciechowski K W, Frenkel D and Brańka A C 1991 *Phys. Rev. Lett.* **66** 3168
[160] Vega C, MacDowell L G, McBride C, Blas F J, Galindo A and Sanz E 2004 *J. Mol. Liq.* **113** 37
[161] Nagle J 1966 *J. Math. Phys.* **7** 1484
[162] Flory P J 1941 *J. Chem. Phys.* **9** 660
[163] Huggins M L 1941 *J. Chem. Phys.* **9** 440
[164] Kofke D A 1993 *Mol. Phys.* **78** 1331
[165] Kofke D A 1993 *J. Chem. Phys.* **98** 4149
[166] Kofke D A 1998 *Monte Carlo Methods in Chemical Physics* vol 105, ed D M Ferguson, J I Siepmann and D G Truhlar (New York: Wiley) p 405
[167] Agrawal R and Kofke D A 1995 *Mol. Phys.* **85** 43
[168] Sturgeon J B and Laird B B 2000 *Phys. Rev.* B **62** 14720
[169] Ladd A J C and Woodcock L 1977 *Chem. Phys. Lett.* **51** 155
[170] Ladd A J C and Woodcock L 1978 *Mol. Phys.* **36** 611
[171] Cape J and Woodcock L 1977 *Chem. Phys. Lett.* **59** 271
[172] Broughton J Q and Gilmer G H 1986 *J. Chem. Phys.* **84** 5749
[173] Morris J R and Song X 2002 *J. Chem. Phys.* **116** 9352
[174] Mori A, Manabe R and Nishioka K 1995 *Phys. Rev.* E **51** 3831
[175] Kyrlidis A and Brown R A 1995 *Phys. Rev.* E **51** 5832
[176] Sibug-Aga R and Laird B B 2002 *J. Chem. Phys.* **116** 3410
[177] Belonoshko A B, Ahuja R and Johansson B 2000 *Phys. Rev. Lett.* **84** 3638
[178] Morris J R, Wang C Z, Ho K M and Chan C T 1994 *Phys. Rev.* B **49** 3109
[179] Jesson B J and Madden P A 2000 *J. Chem. Phys.* **113** 5935
[180] Alfe D 2003 *Phys. Rev.* B **68** 064423
[181] Yoo S, Zeng X C and Morris J R 2004 *J. Chem. Phys.* **120** 1654
[182] Lanning O J, Shellswell S and Madden P A 2004 *Mol. Phys.* **102** 839
[183] Zykova-Timan T, Ceresoli D, Tartaglino U and Tosatti E 2005 *J. Chem. Phys.* **123** 164701
[184] Mu Y and Song X Y 2006 *Phys. Rev.* E **74** 031611
[185] Bryk T and Haymet A D J 2002 *J. Chem. Phys.* **117** 10258
[186] Bryk T and Haymet A D J 2004 *Mol. Simul.* **30** 131
[187] Wang J, Yoo S, Bai J, Morris J R and Zeng X C 2005 *J. Chem. Phys.* **123** 036101
[188] Vatamanu J and Kusalik P G 2006 *J. Phys. Chem.* B **110** 15896
[189] Fernandez R G, Abascal J L F and Vega C 2006 *J. Chem. Phys.* **124** 144506
[190] Abascal J L F, Fernandez R G, Vega C and Carignano M A 2006 *J. Chem. Phys.* **125** 166101
[191] Frankcombe T J and Kroes G J 2007 *J. Phys. Chem.* C **111** 13044
[192] Wang J, Tang Y W and Zeng X C 2007 *J. Chem. Theory Comput.* **3** 1494
[193] Luo S N, Strachan A and Swift D C 2005 *Modelling Simul. Mater. Sci. Eng.* **13** 321
[194] Nada H, van der Eerden J and Furukawa Y 2004 *J. Cryst. Growth* **266** 297
[195] Andersen H C 1980 *J. Chem. Phys.* **72** 2384
[196] Abraham F F 1981 *Phys. Rep.* **80** 339
[197] Dash J G 1989 *Contemp. Phys.* **30** 89
[198] Bienfait M 1992 *Surf. Sci.* **272** 1
[199] Broughton J Q and Gilmer G H 1983 *J. Chem. Phys.* **79** 5119
[200] Nenov D 1984 *Cryst. Growth Charact.* **9** 185
[201] Frenken J W M and van der Veen J F 1985 *Phys. Rev. Lett.* **54** 134
[202] Frenken J W M, Maree P M J and vanderveen J F 1986 *Phys. Rev.* B **34** 7506
[203] Siavosh-Haghighi A and Thompson D L 2007 *J. Phys. Chem.* C **111** 7980
[204] Delogu F 2006 *J. Phys. Chem.* B **110** 12645
[205] Carnevali P, Ercolessi F and Tosatti E 1987 *Phys. Rev.* B **36** 6701
[206] Pluis B, van der Gon A W D, Frenken J W M and van der Veen J F 1987 *Phys. Rev. Lett.* **59** 2678
[207] Tartaglino U, Zykova-Timan T, Ercolessi F and Tosatti E 2005 *Phys. Rep.* **411** 291
[208] Iglev H, Schmeisser M, Simeonidis K, Thaller A and Laubereau A 2006 *Nature* **439** 183
[209] Vega C, Martin-Conde M and Patrykiejew A 2006 *Mol. Phys.* **104** 3583
[210] Siavosh-Haghighi A and Thompson D L 2006 *J. Chem. Phys.* **125** 184711
[211] Vega C, Sanz E and Abascal J L F 2005 *J. Chem. Phys.* **122** 114507

[212] Berendsen H J C, Grigera J R and Straatsma T P 1987 *J. Phys. Chem.* **91** 6269
[213] Jorgensen W L, Chandrasekhar J, Madura J D, Impey R W and Klein M L 1983 *J. Chem. Phys.* **79** 926
[214] Abascal J L F, Sanz E, Fernández R G and Vega C 2005 *J. Chem. Phys.* **122** 234511
[215] Abascal J L F and Vega C 2005 *J. Chem. Phys.* **123** 234505
[216] van der Spoel D, van Maaren P J and Berendsen H J C 1998 *J. Chem. Phys.* **108** 10220
[217] Lísal M, Kolafa J and Nezbeda I 2002 *J. Chem. Phys.* **117** 8892
[218] Rick S W 2004 *J. Chem. Phys.* **120** 6085
[219] Yonetani Y 2006 *J. Chem. Phys.* **124** 204501
[220] Johnson J K, Zollweg J A and Gubbins K E 1993 *Mol. Phys.* **78** 591
[221] Jorgensen W, Blake J and Buckner J 1989 *Chem. Phys.* **129** 193
[222] Henchman R H 2007 *J. Chem. Phys.* **126** 064504
[223] Petrenko V F and Whitworth R W 1999 *Physics of Ice* (Oxford: Oxford University Press)
[224] Eisenberg D and Kauzmann W 1969 *The Structure and Properties of Water* (London: Oxford University Press)
[225] Lobban C, Finney J L and Kuhs W F 1998 *Nature* **391** 268
[226] Buch V, Sandler P and Sadlej J 1998 *J. Phys. Chem.* B **102** 8641
[227] Hayward J A and Reimers J R 1997 *J. Chem. Phys.* **106** 1518
[228] Lobban C, Finney J L and Kuhs W F 2000 *J. Chem. Phys.* **112** 7169
[229] MacDowell L G, Sanz E, Vega C and Abascal L F 2004 *J. Chem. Phys.* **121** 10145
[230] Berg B A, Muguruma C and Okamoto Y 2007 *Phys. Rev.* B **75** 092202
[231] Davidson E R and Morokuma K 1984 *J. Chem. Phys.* **81** 3741
[232] Garzon B, Lago S, Vega C, de Miguel E and Rull L F 1994 *J. Chem. Phys.* **101** 4166
[233] Boublik T 1991 *Mol. Phys.* **73** 417
[234] Stoll J, Vrabec J, Hasse H and Fischer J 2001 *Fluid Phase Equilibr.* **179** 339
[235] Patey G N and Valleau J P 1976 *J. Chem. Phys.* **64** 170
[236] Carnie S L and Patey G N 1982 *Mol. Phys.* **47** 1129
[237] Finney J L, Quinn J E and Baum J O 1985 *Water Science Reviews 1* ed F Franks (Cambridge: Cambridge University Press)
[238] Carlevaro C M, Blum L and Vericat F 2003 *J. Chem. Phys.* **119** 5198
[239] Ichiye T and Tan M L 2006 *J. Chem. Phys.* **124** 134504
[240] Vrbka L and Jungwirth P 2007 *J. Mol. Liq.* **134** 64
[241] Mahoney M W and Jorgensen W L 2000 *J. Chem. Phys.* **112** 8910
[242] Vega C and Abascal J L F 2005 *J. Chem. Phys.* **123** 144504
[243] Horn H W, Swope W C, Pitera J W, Madura J D, Dick T J, Hura G L and Head-Gordon T 2004 *J. Chem. Phys.* **120** 9665
[244] Nada H and van der Eerden J P J M 2003 *J. Chem. Phys.* **118** 7401
[245] Paschek D 2004 *J. Chem. Phys.* **120** 6674
[246] Jedlovszky P 2003 *Phys. Rev.* E **67** 011201
[247] Nicholson B F, Clancy P and Rick S W 2006 *J. Cryst. Growth* **293** 78
[248] Li J, Zhou Z and Sadus R J 2007 *J. Chem. Phys.* **127** 154509
[249] Paricaud P, Predota M, Chialvo A A and Cummings P T 2005 *J. Chem. Phys.* **122** 244511
[250] Rivera J L, Predota M, Chialvo A A and Cummings P T 2002 *Chem. Phys. Lett.* **357** 189
[251] Yu H and van Gunsteren W F 2004 *J. Chem. Phys.* **121** 9549
[252] Moucka F, Rouha M and Nezbeda I 2007 *J. Chem. Phys.* **126** 224106
[253] Lindahl E, Hess B and van der Spoel D 2001 *J. Mol. Modeling* **7** 306
[254] van der Spoel D, Lindahl E, Hess B, Groenhof G, Mark A E and Berendsen H J C 2005 *J. Comput. Chem.* **26** 1701
[255] Carignano M A 2007 *J. Phys. Chem.* C **111** 501
[256] Nada H and Furukawa Y 2005 *J. Cryst. Growth* **283** 242
[257] Rosenberg R 2005 *Phys. Today* **58** 50
[258] Dash J G, Fu H and Wettlaufer J S 1995 *Rep. Prog. Phys.* **58** 115
[259] Dash J G, Rempel A W and Wettlaufer J S 2006 *Rev. Mod. Phys.* **78** 695
[260] Henson B F, Voss L F, Wilson K R and Robinson J M 2005 *J. Chem. Phys.* **123** 144707
[261] Suter M T, Andersson P U and Pettersson J B C 2006 *J. Chem. Phys.* **125** 174704
[262] Engemann S, Reichert H, Dosch H, Bilgram J, Honkimaki V and Snigirev A 2004 *Phys. Rev. Lett.* **92** 205701
[263] Kroes G J 1992 *Surf. Sci.* **275** 365
[264] Furukawa Y and Nada H 1997 *J. Phys. Chem.* B **101** 6167
[265] Nada H and Furukawa Y 2000 *Surf. Sci.* **446** 1
[266] Ikeda-Fukazawa T and Kawamura K 2004 *J. Chem. Phys.* **120** 1395
[267] Aragones J L, Noya E G, Abascal J L F and Vega C 2007 *J. Chem. Phys.* **127** 154518
[268] Whalley E 1984 *J. Chem. Phys.* **81** 4087
[269] Hulme A T and Price S L 2007 *J. Chem. Theory Comput.* **3** 1597
[270] Ciach A and Patsahan O 2006 *Phys. Rev.* E **74** 021508
[271] Ciach A and Stell G 2001 *J. Chem. Phys.* **114** 3617
[272] Chasovskikh B P and Vorontsov-Vel'yaminov P N 1976 *High. Temp. (USSR)* **14** 174
[273] Orkoulas G and Panagiotopoulos A Z 1994 *J. Chem. Phys.* **101** 1452
[274] Panagiotopoulos A Z 2002 *J. Chem. Phys.* **116** 3007
[275] Stillinger F H and Lovett R 1968 *J. Chem. Phys.* **48** 3858
[276] Smit B, Esselink K and Frenkel D 1996 *Mol. Phys.* **87** 159
[277] Vega C, Bresme F and Abascal J L F 1996 *Phys. Rev.* E **54** 2746
[278] Caballero J B, Puertas A M, Fernandez-Barbero A and de las Nieves F J 2004 *J. Chem. Phys.* **121** 2428
[279] Leunissen M E, Christova C G, Hynninen A P, Royall C P, Campbell A I, Imhof A, Dijkstra M, van Roij R and van Blaaderen A 2005 *Nature* **437** 235
[280] Bartlett P and Campbell A I 2005 *Phys. Rev. Lett.* **95** 128302
[281] Caballero J B, Noya E G and Vega C 2007 *J. Chem. Phys.* **127** 244910
[282] Rogers R D and Seddon K R 2003 *Science* **302** 792
[283] Rogers R D and Seddon K R 2003 *Ionic Liquids as Green Solvents: Progress and Prospects* (Washington, DC: American Chemical Society)
[284] Jayaraman S and Maginn E J 2007 *J. Chem. Phys.* **127** 214504
[285] ten Wolde P R and Frenkel D 1997 *Science* **277** 1975
[286] Matthews B W 1968 *J. Mol. Biol.* **33** 491
[287] Liu H, Kumar S K and Sciortino F 2007 *J. Chem. Phys.* **127** 084902
[288] Manoharan V N, Elsesser M T and Pine D J 2003 *Science* **301** 483
[289] van Blaaderen A 2006 *Nature* **439** 545
[290] Levy R 2006 *ChemBioChem* **7** 1141
[291] Roh K H, Martin D C and Lahann J 2006 *J. Am. Chem. Soc.* **128** 6796
[292] Sear R P 1999 *J. Chem. Phys.* **111** 4800
[293] Song X Y 2002 *Phys. Rev.* E **66** 011909
[294] Dixit N M and Zukoski C F 2002 *J. Chem. Phys.* **117** 8540
[295] Kern N and Frenkel D 2003 *J. Chem. Phys.* **118** 9882
[296] Chang J, Lenhoff A M and Sandler S I 2005 *J. Phys. Chem.* B **109** 19507

[297] Talanquer V 2005 *J. Chem. Phys.* **122** 084704
[298] Doye J P K, Louis A A, Lin I-C, Allen L R, Noya E G, Wilber A W, Kok H C and Lyus R 2007 *Phys. Chem. Chem. Phys.* **9** 2197
[299] Wilber A W, Doye J P K, Louis A A, Noya E G, Miller M A and Wong P 2007 *J. Chem. Phys.* **127** 085106
[300] Romano F, Tartaglia P and Sciortino F 2007 *J. Phys.: Condens. Matter* **19** 322101
[301] Sloan E D 2003 *Nature* **426** 353
[302] Docherty H, Galindo A, Vega C and Sanz E 2006 *J. Chem. Phys.* **125** 074510
[303] Docherty H, Galindo A, Sanz E and Vega C 2007 *J. Phys. Chem.* B **111** 8993
[304] Vega C, Abascal J L F and Nezbeda I 2006 *J. Chem. Phys.* **125** 034503
[305] Vega C and de Miguel E 2007 *J. Chem. Phys.* **126** 154707
[306] Soper A K 2000 *Chem. Phys.* **258** 121
[307] Koga K, Gao G T, Tanaka H and Zeng X C 2001 *Nature* **412** 802
[308] Hirunsit P and Balbuena P B 2007 *J. Phys. Chem.* C **111** 1709
[309] Alba-Simionesco C, Coasne B, Dosseh G, Dudziak G, Gubbins K E, Radhakrishnan R and Sliwinska-Bartkowiak M 2006 *J. Phys.: Condens. Matter* **18** R15
[310] Eldridge M D, Madden P A and Frenkel D 1993 *Mol. Phys.* **79** 105